科技部補助

大專學生研究計畫研究成果報告

計畫名稱：	單股DNA結合蛋白質(SSB)的結晶結構與其抑制劑之開發與機制探討

執行計畫學生：陳冠霖
學生計畫編號：MOST 107-2813-C-040-030-B
研究期間：107年07月01日至108年02月28日止，計8個月
指導教授：黃晟洋

處理方式：本計畫涉及專利或其他智慧財產權，2年後可公開查詢

執行單位：中山醫學大學生物醫學科學學系（所）

中華民國　108年03月30日

目錄

研究計畫摘要

在DNA代謝的過程中，單股DNA結合蛋白質 (SSB) 參與了所有相關的程序，包括DNA複製、修復、重組與DNA複製重啟(DNA replication restart)。在DNA複製重啟程序中，SSB 需與 PriA 解旋酶所引導的引子合成體 (PriA-directed primosome) 進行蛋白質交互作用並啟動後續多個蛋白質結合反應，以便重新喚回DNA聚合酶 (polymerase) 並重啟複製作用。並且，此細菌重啟DNA複製的機制並未發現於人類，因此據此 SSB/PriA-directed primosome 程序所設計出的抑制劑可能可以是一種新型的抗生素，也較不傷人體。在此科技部大專生研究計畫”**單股DNA結合蛋白質(SSB)的結晶結構與其抑制劑之開發與機制探討**(107-2813-C-040-030-B)”的執行，我們以抗藥性十分嚴重的金黃色葡萄球菌、綠膿桿菌與沙門氏菌為研究模型，欲找到以細菌的 SSB/PriA-directed primosome 反應機制與結構為基礎的抑制劑 (mechanism and structure-based inhibitor) 並探討其結合模式。我們首先選殖、表現與純化出SSB與相關引子合成體蛋白質如 DnaT 等蛋白質，接著透過篩選條件來晶體成長並得到各種蛋白質晶體，欲藉由結晶結構了解各項分子層次的機制。另外，我們也對這些蛋白質做了各種基本性質研究，包括突變分析與DNA結合能力以及活化PriA解旋酶活性等。為了瞭解天然物中是否有抑制此 SSB/PriA-directed

primosome 化合物，我們利用高壓液相層析儀分離豬籠草萃取的化合物，並發現數個化合物具明顯抑制 SSB的活性並已將這些化合物與 SSB 進行共結晶 (co-crystallization) 希望能得到複合結晶並解出其複合結構(complex structure)。透過這些結構與功能性分析，我們已初步了解這些化合物是如何的抑制SSB。目前此計畫執行結果已獲2篇 SCI 科學期刊接受刊登，本人皆為第一作者 [**(1) Chen KL (陳冠霖)**, Cheng JH, Lin CY, Huang YH, Huang CY (2018) Characterization of single-stranded DNA-binding protein SsbB from *Staphylococcus aureus*: SsbB cannot stimulate PriA helicase. ***RSC Adv***., 8, 28367-28375. **(2) Chen KL (陳冠霖)**, Huang YH, Liao JF, Lee WC, Huang CY (2019) Crystal structure of the C-terminal domain of the primosomal DnaT protein: Insights into a new oligomerization mechanism. ***Biochem. Biophys. Res. Commun.***, 511, 1-6.]。此兩論文解釋了單股DNA結合蛋白質與刺激PriA解旋酶活性的分子機制、如何結合單股DNA，以及另一單股DNA結合蛋白質 DnaT 是如何以強的結構之變化 (a strong structural change) 來結合單股DNA。其他已經完成、仍待發表之結果包括不同的單股DNA結合複合結構、單股DNA與抑制劑myc-SSB三重複合結晶結構已經解出並上傳至PDB等待論文發表後釋出以及各種功能性DNA結合分析與突變研究。希望此計畫的執行結果包括解

出這些SSB與抑制劑的複合結晶結構將可清楚地提供後續抑制劑結合方式與藥物研發的分子資訊。

第一章：緒論

1-1 研究背景與動機

具有抗藥性之病原菌造成嚴重感染性問題，一直是全球所關注的棘手公共衛生議題，同時也造成醫療上需要花費更多的資源來延緩其所造成的危害，包括嚴重的群落感染 [1]。最早於印度被報導的超級細菌，即 NDM-1 腸道菌感染症 [2]，帶有 NDM-1 基因的克雷白氏菌、綠膿桿菌與大腸桿菌目前正逐步流行至全球各地 [3]。這些細菌所引發的感染症第一線治療用藥均是使用 β-lactam 類抗生素治療，然而這些細菌已經經由突變或是交換基因等方式發展出對抗這些傳統抗生素的能力，尤其是 β-lactam 及 aminoglycoside 類抗生素，具有多重抗藥性的細菌不斷被發現與報導，像是綠膿桿菌已被發現至少超過 120 種以上的 β-lactamases [4-6]，因此在臨床治療中不得不選用具有較多副作用的後線抗生素或甚至面臨無藥可醫的情況。因此若能開發出新的攻擊標靶，也許對此棘手的問題將可能有所幫助。本計畫提出不同於傳統細菌細胞壁、核醣體為標靶的細菌 DNA 複製與重啟系統作為新型抗生素研發標的 [7, 8]。細菌 DNA 複製與重啟對於細菌本身為必需之程序 [9-11]，但人類 [12] 並不使用這套系統來進行 DNA 複製與 DNA 複製重啟 [13, 14]。本計劃的主要標的細菌 SSB 是一個單股 DNA 結合蛋白質 [15]，同時也可以結合許多其他蛋白質 [16]，例

如引子合成體蛋白質群中的 PriA [17, 18]與 PriB [19]，而這些活性已被證明絕對必需要於細菌各 DNA 複製程序 [20]。因此，若能透過詳細的研究出這些病原菌的 DNA 複製機制是可以如何的被抑制，可能有助於這類新型抗生素的研發。我們希望以結晶結構來分析 SSB 是如何結合 DNA 以及了解抑制劑的結合機制。這些結果預期在學術上可發表論文外，在臨床應用上我們亦希望能具體結論出數個化合物對於細菌 SSB 活性可明顯抑制之。其他引子合成體具單股 DNA 結合活性的蛋白質如 DnaT 亦希望一同研究之。

1-2 SSB 功能介紹與作用

1-2-1 SSB 主要功能

單股 DNA 結合蛋白質(SSB)參與了 DNA 代謝過程中所有相關的程序，包括 DNA 複製、修復、重組與 DNA 複製之重啟 (DNA replication restart)。SSB 是細菌 DNA 複製的必要因子，可保護脆弱的單股 DNA 包括避免受到 nucleases 的攻擊以及各種物質的化學修飾與氧化作用 [21]。SSB 具有高度保留性的寡核苷酸摺疊(OB-fold) [22, 23]的 N 端區域作為單股 DNA 的結合 [24, 25]，以及高度不規則結構的 C 端區域 [26-28]，作為多重蛋白質-蛋白質的交互作用區，例如與 PriA 解旋酶和 RecG 解旋酶。目前至少超過 10 個以上的蛋白質已被報導會與 SSB 作用，藉之以調控各種核酸代謝程序 [29]。

1-2-2 SSB在複製再啟動中的作用

大腸桿菌重新啟動複製叉的引子合成體蛋白質包括PriA、PriB、PriC、DnaT、DnaC、DnaB 與DnaG [30-32]，其中其組裝機制早已研究清楚，主要是這些蛋白質是以換手機制 (hand-off mechanism)一個接著一個的進入PriA 所結合的複製叉 [33-35]。PriA雖然是一個解旋酶，但是其活性必須經由SSB 的結合而刺激數十倍 [36, 37]，但同時我們實驗室也發現，並非每一個SSB 都能夠刺激 PriA 解旋酶活性 [7, 38]。這種結果可能與每種細菌所含有的引子合成體蛋白質種類有關。在此計畫執行結果 [39] 我們亦發現到金黃色葡萄球菌的單股DNA結合蛋白質 SsbB 也無法刺激 PriA 解旋酶活性，並進一步發現可能與 SSB 高變異的C端有關。

1-3 DnaT功能介紹與作用

1-3-1 DnaT主要功能

DnaT一開始由諾貝爾獎得主Arthur Kornberg發現並被稱為蛋白質i (protein i) [40]，是在PriA為首之引子合成體組裝中的第三個關鍵蛋白質，而第二個結合蛋白質 PriB 則會促進 DnaT 與 PriA 的結合 [41-43]。DnaT 是一種含有179個氨基酸的單股DNA結合蛋白質 [34]，分子量約為20 kDa [44]，DnaT的C端區域會參與ssDNA的結合 [45]。

DnaT的N端區域則會與 PriB 上的 Asp66-Glu76 區域相互作用[46]。與使用 OB-fold 結合單股DNA 的 PriB 不同[47, 48]，DnaT 則是以三螺旋狀與單股DNA結合 [45]。DnaT的C端區域如DnaT84-153蛋白質會以二聚體的形式存在，但在與單股DNA結合時會形成五聚體[45]。此計畫結果我們亦發現此不同聚體在DNA結合前後的分子結構變化 [49]，若能進一步找到如何卡住此結構改變亦可能有助於抑制劑之研發。

1-3-2 DnaT 寡聚化 (oligomerization) 作用

寡聚化是蛋白質的共同特性 [50]，在生物系統中擁有至少35%的蛋白質呈現寡聚化的現象。有些蛋白質會形成一種寡聚狀態才具有特定的活性，例如nicotinic acetylcholine receptor僅在形成五聚體時才會有活化狀態 [51]。有些蛋白質的寡聚化會根據不同 pH 而有不一樣的狀態 [52, 53]。至於 DnaT 會在具有不同活性的幾種狀態之間，處於一種動態的寡聚化平衡，包括可以形成單體、二聚體、三聚體、四聚體或五聚體這五種不同的形態 [41, 43, 54]。此計畫執行結果亦以明顯的分子證據解釋了如何透過 DnaT 的R146胺基酸來完成結構改變 [49]。

第二章：材料與方法

本計畫須從基因轉殖開始嘗試獲得蛋白質晶體，以便有機會解出結構。雖然理論上所有化學分子都能有其最佳熱力學堆疊狀態發生，然而我們未必有機會找到此結晶條件，因此必須從不同、多個細菌的 SSB 與其引子合成體蛋白質群的選殖開始嘗試獲得重組蛋白質與蛋白質晶體。另外，若獲得結構，亦須進行相關功能性分析如 DNA 結合與抑制劑的抑制效果分析。以下茲對相關步驟進行說明：

2-1 蛋白質純化及相關技術

2-1-1 抽取質體 DNA

1. 將轉型後大腸桿菌在恆溫培養箱（37℃）中培養至濃度OD_{600}：1.0
2. 待濃度到達後，將其批次取至 eppendorf 中並用高速微量離心機（設定時間1 min, 轉速12000 rpm）離心後倒除上清液留下pellet
3. 加入solution I 250μl 將pellet回溶，並放置冰上約1 min
4. 再加入solution II 250μl ，並緩慢搖晃均勻，並放置室溫約1 min
5. 最後加入solution III 250μl，並緩慢混和均勻，並放置室溫約1 min，再使用高速微量離心機（設定時間10 min, 轉速12000 rpm）離心
6. 離心後再用pipette小心吸取上清液（注意不能吸到白色沉澱）
7. 將上清液取至spin column中，並放置室溫約1 min

8. 待時間到後再使用高速微量離心機（設定時間1 min, 轉速12000 rpm）離心，離心後倒除collection tube中液體
9. 加入500 µl wash buffer至spin column中，再使用高速微量離心機（設定時間1 min, 轉速12000 rpm)離心，離心後倒除collection tube中液體（此步驟需重複兩次）
10. 再打開spin column上蓋，再使用高速微量離心機（設定時間1 min 轉速12000 rpm）離心使其空轉（確保wash buffer中酒精都揮發移除）
11. 最後加入50 µl 滅菌過之 ddH_2O 至 spin column中，再使用高速微量離心機（設定時間1 min, 轉速12000 rpm）離心，離心後取得的即為實驗所需之質體DNA

2-1-2 轉型至勝任細胞

1. 開啟乾浴機（溫度設定42℃）
2. 自-80℃冰箱拿出勝任細胞（須放置於冰上）
3. 待勝任細胞微溶後取10 µl至eppendorf中
4. 取1 µl 質體DNA加至eppendorf中與勝任細胞反應
5. 將含有質體與勝任細胞之eppendorf放置乾浴機中（42℃）約45秒進行heat shock反應

6. 反應45秒後立刻eppendorf插置冰上，完成heat shock反應
7. 準備培養皿（含有抗生素）並將塗菌棒浸泡至95%酒精後，點燃酒精燈並將塗菌棒過火（約過火3次）
8. 待塗菌棒降溫至常溫後，將轉型後之勝任細胞加至培養皿（含有抗生素）中，並用塗菌棒塗抹均勻
9. 在培養皿上註明名稱後，將其放置於37℃恆溫培養箱內overnight培養至產生colony，便可將其挑出培養進行後續實驗

2-1-3 表現測試與菌體儲存

1. 將轉型後含勝任細胞之plate自恆溫培養箱取出
2. 挑選出單一菌落群並用tips將其挑起並放入含4 μl 100 mg/ml LB中，再將整管放置恆溫培養箱（37℃）內，使其在恆溫培養箱內搖晃反應至濃度OD_{600}：1.0
3. 待濃度到達後，取200 μl菌液至eppendorf中做為表現前之sample，之後加入4 μl 1M IPTG ，並在恆溫培養箱（37℃）內搖晃反應4 hours
4. 加入4 μl 1M IPTG反應4 hours後，取200 μl菌液至eppendorf中做為表現後之sample
5. 將先前準備之表現前（後）sample 用高速微量離心機（設定時間1 min, 轉速12000 rpm）

6. 倒除上清液，並各加入10μl 4X dye，同時將pellet回溶

7. 使用乾浴機（98°C）加熱20mins （加熱完後須冷卻完才能跑膠）

8. 製備SDS-PAGE（15％ or 12％），使用power supply 跑膠（設定70V 120 mins，待marker跑至下膠可將電壓調至120V）

9. 跑膠完後將膠片放入Coomassie Blue中染大約30分鐘（放置在shaker上搖晃）

10. 染完後膠後（染色至可看到band）再用退染液（或者水中但時間較久）退染至清楚看見band，並可分析目標蛋白是否有成功表現

2-1-4 蛋白質純化（放大培養）

1. 從-80冰箱拿出冰存的菌液，放置冰桶中退冰

2. 準備100 mg/ml LB(4c.c.)，加入4μl 0.1g/ml ampicillin(加ampicillin前要過火）

3. 從退完冰的菌液中取15～20μl至小管LB液中

4. 之後拿到恆溫培養箱（設定溫度37°C 轉速200 rpm）約4小時（至OD_{600}約1～1.6）

5. 準備大錐形瓶並加入500 ml ddH_2O 和12.5 g的100 mg/ml LB，再用鋁箔紙將瓶口覆蓋並貼上滅菌膠帶

6. 放入滅菌鍋(需先加水過底盤，確認鎖緊蓋子)(用濕滅 15mins）約等待1小時

7. 滅菌結束後，確認大瓶LB冷卻至室溫（可用冰浴）

8. 加入 200 µl, 0.1g/ml ampicillin 至大瓶LB（加入前要在瓶口處過火），之後再小瓶菌液倒入大瓶中（要注意到入時避免讓菌液碰到瓶壁）

9. 將大瓶放入恆溫培養箱（設定溫度37°C　轉速200rpm）約6～7小時（至O.D大於1）後加入125 µl 1M IPTG ，再放入恆溫培養箱中約12小時（設定溫度25°C 轉速200rpm）進行誘導表現目標蛋白

2-1-5 蛋白質純化（高速低溫離心）

1. 待誘導表現後，準備將菌液倒入（beckman）離心瓶並將其秤重平衡（確認每瓶離心瓶重量為300.00 g）
2. 將離心瓶拿至貴儀中心，使用高速離心機低溫離心（設定時間20 mins 轉速12000 rpm　溫度4°C），離心結束後將上清液到至廢液桶

2-1-6 蛋白質純化（破菌&管柱層析）

1. 準備binding buffer（5 mM imidazole, 500 mM NaCl, pH 7.4）倒入40 c.c至離心瓶中將pellet回溶
2. 回溶完後將菌液倒回tube，準備冰桶（防止過熱造成蛋白質斷裂）將tube插置其中並使用超音波震盪機來震菌（震碎細胞壁）機器

設定為震盪5秒、休息5秒、50個cycle（循環次數需觀察菌液的顏色由米黃色變至稍微灰黑色）

3. 震菌完後拿至低溫高速離心機離心(設定時間20 mins, 轉速12000 rpm, 溫度4°C），離心完後將上清液收集至乾淨tube
4. 準備HisTrap™ HP column 並使用蠕動幫浦儀器依序以 ddH_2O、硫酸鎳、ddH_2O、binding buffer （5 mM imidazole, 500 mM NaCl, pH 7.4）至HisTrap™ HP column中
5. 將經過高速低溫離心之上清蛋白質溶液通至HisTrap™ HP column（使帶有His-tag的蛋白與column裡的Ni^{2+}結合）（要先取20 µl作為sample）
6. 通完上清後依序以（5 mM、60 mM、100 mM、200 mM、500 mM imidazole, 500 mM NaCl, pH 7.4）溶液通入column中（依序各收集50 c.c.、50 c.c.、30 c.c.、30 c.c.、30 c.c.的溶液），在5 mM、60 mM、100 mM imidazole, 500 mM NaCl, pH 7.4溶液進行wash將非目標蛋白移除，同時在200 mM、500 mM imidazole, 500 mM NaCl, pH 7.4溶液進行elute純化出目標蛋白
7. 準備8個eppendorf依序收集上清、沉澱（ddH_2O 20µl混合一點pellet）、過濾、5 mM、60 mM、100 mM、200 mM、500 mM各20 µl作為sample

8. 之後各加入10 µl 4X dye ，再用乾浴機（98°C）加熱20分鐘（加熱完後須冷卻完才能跑膠）
9. 配置protein assay dye（比例為800 µl ddH_2O + 200 µl protein assay dye）至 cuvette中並用石臘膜蓋上搖晃使其均勻混和
10. 利用分光光度計OD_{600}先將含有protein assay dye之cuvette進行blank（作為測定之背景值）
11. 取1 µl 蛋白質溶液至cuvette中，搖晃均勻使其與protein assay dye反應後，再利用分光光度計OD_{600}進行濃度測定，並記錄下濃度數值
12. 將收集下來含有目標蛋白的溶液加入100％甘油（加入溶液體積的10％）
13. 拿至-80°C的冰箱中保存，待下次實驗使用

2-1-7 蛋白質電泳分析（SDS-PAGE）

1. 製備SDS-PAGE（15％ or 12％）
2. 使用power supply 跑膠（設定70V 120mins，待 marker 跑至下膠可將電壓調至120V）
3. 跑膠完後將膠片放入Coomassie Blue中染大約30分鐘
4. 染完後再用退染液（或者水中但時間較久）退染（退至清楚看見band）

5. 退染完乾後再用玻璃紙封膠，待它風乾

2-1-6 蛋白質濃縮

1. 將存放於-80°C的蛋白拿出並放置於冰桶上退冰
2. 將spin column用酒精及ddH_2O清洗
3. 裝入ddH_2O拿至離心機離心（設定轉速3000rpm 時間10mins），將膜內酒精去除並測漏
4. 離心後將水倒除後將imidazole溶液加入spin column潤洗內膜
5. 倒除imidazole溶液後，加入需濃縮之蛋白質溶液
6. 秤重平衡後拿至離心機離心（3000 rpm, 10mins）至體積剩餘1 c.c
7. 將濃縮後之蛋白質溶液取至eppendorf，並配置protein assay dye（比例為800 µl ddH_2O + 200 µl protein assay dye）至 cuvette中並用石臘膜蓋上搖晃使其均勻混和
8. 利用分光光度計OD_{600}先將含有protein assay dye之cuvette進行blank（作為測定之背景值）
9. 取1 µl 蛋白質溶液至cuvette中，搖晃均勻使其與protein assay dye反應後，再利用分光光度計OD_{600}進行濃度測定
10. 記錄下所測定之OD值後便可將其保存或後續之實驗進行

2-1-9 蛋白質透析（降低鹽濃度）

1. 將 buffer（40 mM Tris-HCL、400 mM NaCl）緩慢加入濃縮後的蛋白中（使 NaCl 的濃度下降至接近 400 mM），再將其加入 spin column 中，並拿至離心機離心（轉速設定 3000 rpm、時間 10mins），再使其離心後體積降至 1 c.c.
2. 重複上述動作再將另一 buffer（40 mM Tris-HCL、300 mM NaCl）緩慢加入濃縮後的蛋白中重複上述步驟離心至 1 c.c.
3. 最後再以 buffer（40 mM Tris-HCL、200 mM NaCl）緩慢加入濃縮後的蛋白中重複上述步驟離心降至 1 c.c.
4. 離心完後再將其收集至 eppendorf 中，此時蛋白質溶液環境為 40 mM Tris-HCL、200 mM NaCl
5. 配置protein assay dye（比例為800 µl ddH_2O + 200 µl protein assay dye）至 cuvette中並用石臘膜蓋上搖晃使其均勻混和
6. 利用分光光度計OD_{600}先將含有protein assay dye之cuvette進行blank（作為測定之背景值）
7. 取1 µl 蛋白質溶液至cuvette中，搖晃均勻使其與protein assay dye反應後，再利用分光光度計OD_{600}進行濃度測定，並記錄下濃度數值，便可提供後續實驗進行

2-1-10 蛋白質點晶（懸吊法）

1. 準備架膠台、點晶膠帶、24 well 之養晶盒及 kit buffer

2. 取kit buffer各250 µl 加入養晶盒之well中

3. 將點晶膠帶拉至合適長度，拉平貼至架膠台上

4. 確認膠帶拉平後，將其割下

5. 從各well中取1 µl buffer至點晶膠帶上（從A1至D6）

6. 再將透析後的蛋白質溶液1 µl 到drop中（從A1至D6）

7. 完成後將膠帶貼平至養晶盒上，用拭鏡紙確認是否貼平，並將膠帶割下

8. 紀錄完相關資訊後再放回櫃子等待晶體形成

9. 待晶體形成後再透過光學顯微鏡進行晶體觀察與記錄

2-2-11 結晶結構（X 光繞射實驗）

蛋白質分子整齊排列而成的晶體，經由 X-ray 繞射後產生的繞射圖形與其他獲取數據時的系統參數，藉由傅立葉轉換 (Fourier transform) 等數學運算後，獲得蛋白質在晶體狀態下靜態結構的電子雲密度圖。

1. 利用光學顯微鏡觀察並選定好要撈起的蛋白質晶體

2. 選擇適當大小的loop在顯微鏡下判斷是否能包覆住晶體

3. 選定好晶體位置及loop後將點晶膠帶割下並用攝子取下

4. 將割下的膠帶固定好再用顯微鏡確認晶體位置

5. 使用loop將晶體撈起後迅速放置液態氮中

6. 在液態氮中用金屬夾將loop取下(記得皆須在液態氮液面下進行，以免冰晶產生影響繞射結果)

7. 之後用金屬夾將loop架到X光繞射儀器上

8. 透過電腦軟體（Blue ice）來調整X光繞射儀器距離、角度等數值

9. 將收集的繞射數據使用HKL2000軟體數值的計算Space group等相關資訊並儲存所計算的繞射數據，以供後續結構解析所需的晶體繞射資訊

第三章：結果與討論

相關結果在此報告以綠膿桿菌 SSB (PaSSB), 金黃色葡萄球菌 SSB (SaSsbB)以及沙門氏菌的 DnaT (StyDnaT)為主，包括我們已經發表的兩篇論文之內容[39, 49]。

3-1 **PaSSB** 相關實驗結果

3-1-1 PaSSB 純化（SDS-PAGE）

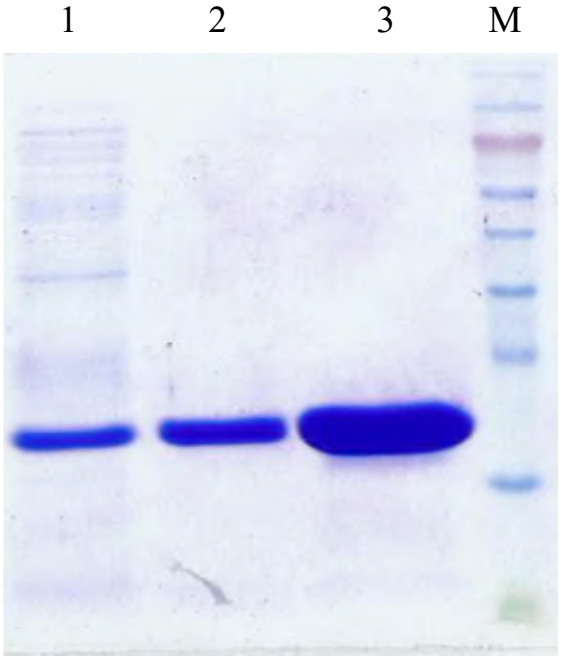

- 蛋白質表現與純化。利用轉型大腸桿菌來大量表達重組蛋白質，經由放大培養後，再透過IPTG 誘導表現目標蛋白，經過高速低溫離心、超音波破菌後，利用Ni-NTA column，透過金屬親和性管柱層析法進行蛋白質純化，我們利用內含200 mM imidazole,

500 mM NaCl, pH 7.4 溶液純化出綠膿桿菌SSB (PaSSB) (lane 3)，從SDS-PAGE可以得知綠膿桿菌SSB (PaSSB)分子量約為20 kDa。

3-1-2 PaSSB 晶體形成（懸吊法）

- **PaSSB 晶體成長 1**

PaSSB: (1-1)

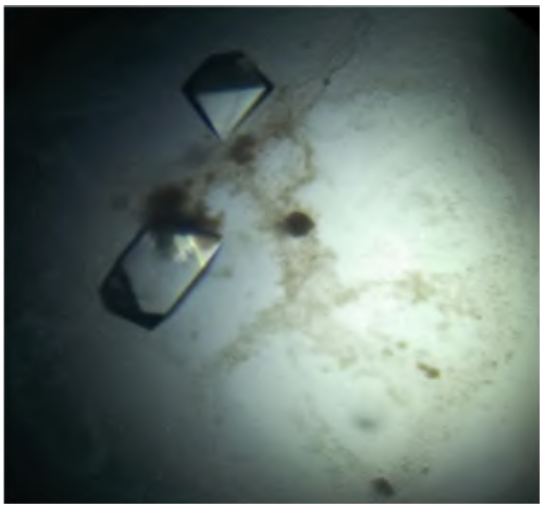

PaSSB: (1-2)

PaSSB: (1-3)

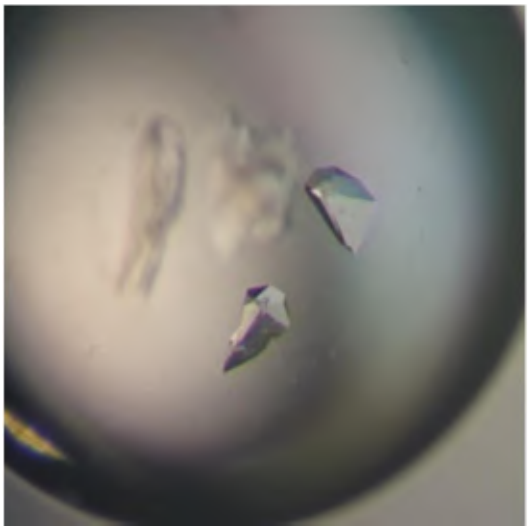

PaSSB: (1-4)

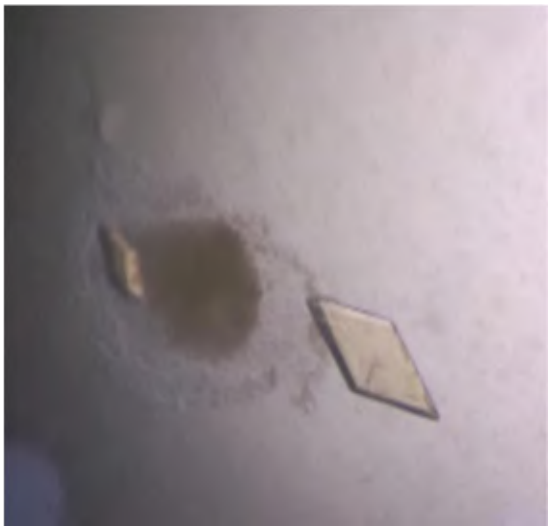

晶體名稱	長晶條件
PaSSB: (1-1)	**28%PEG 400、100mM HEPES ,pH7.5、**

	200mM Calcium chloride
PaSSB: (1-2)	**30% PEG 1000、100 mM Tris-HCL ,pH 8.5**
PaSSB: (1-3)	**20% PEG 8000、100 mM MES ,pH 6.5、200 mM Magnesium acetate**
PaSSB: (1-4)	**16% PEG 4000、100mMTris-HCL ,pH 8.5、200 mM Sodium acetate**

- **PaSSB+ssDNA 晶體成長 2**

PaSSB: (2-1)

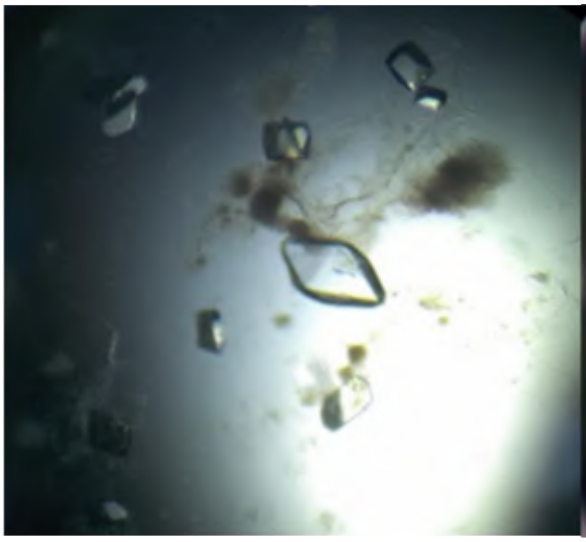

PaSSB: (2-2)

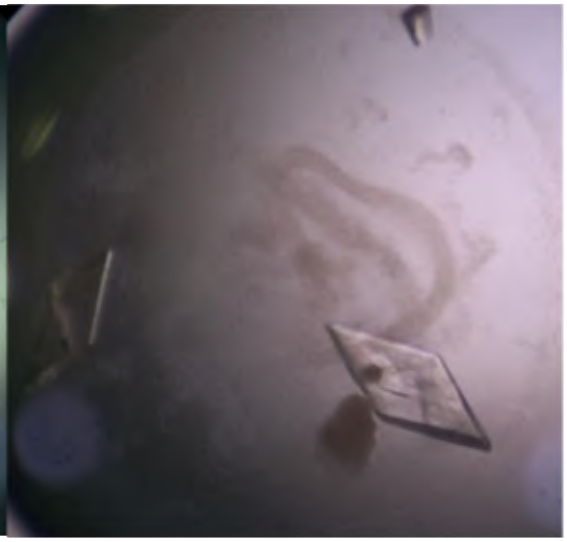

PaSSB: (2-3)

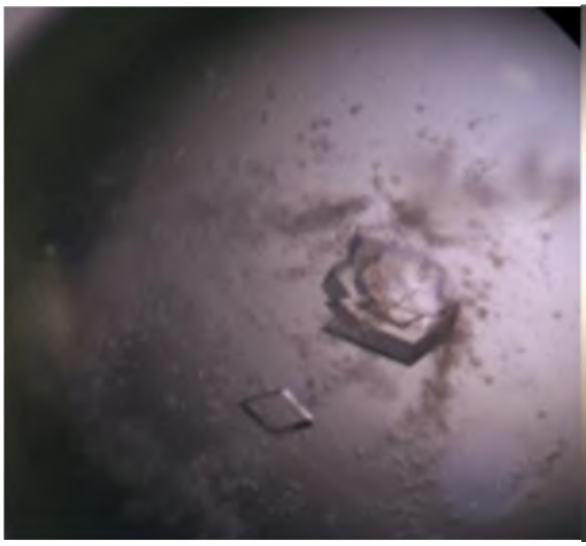

PaSSB: (2-4)

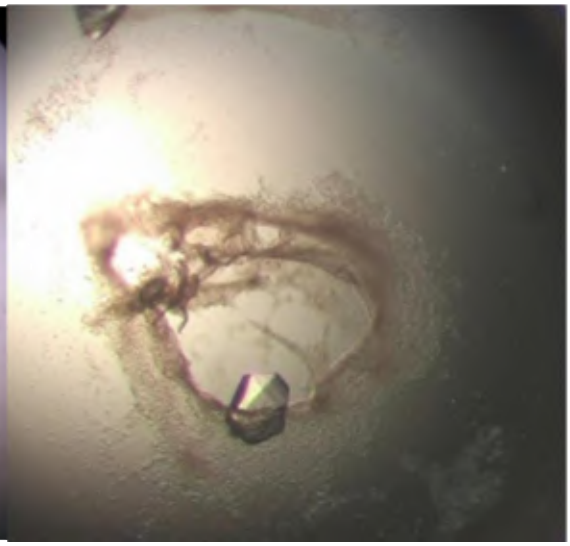

晶體名稱	長晶條件
PaSSB: (2-1)	**28 % PEG 400、100 mM HEPES ,pH 7.5、200mM Calcium chloride**
PaSSB: (2-2)	**30% PEG 1000、100 mM Tris-HCL ,pH 8.5**
PaSSB: (2-3)	**10% PEG 8000、100 mM HEPES ,pH 7.5、10% Ethylene glycol**
PaSSB: (2-4)	**10% PEG 8000、200 mM Magnesium acetate**

- **PaSSB+ssDNA 晶體成長 3**

PaSSB: (3-1)

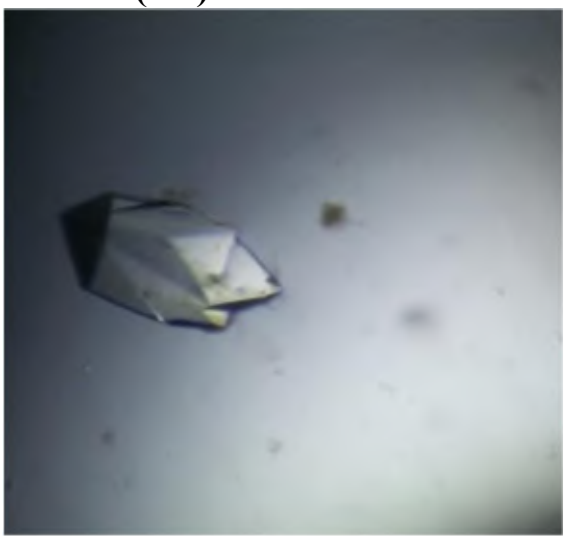

PaSSB: (3-2)

PaSSB: (3-3)

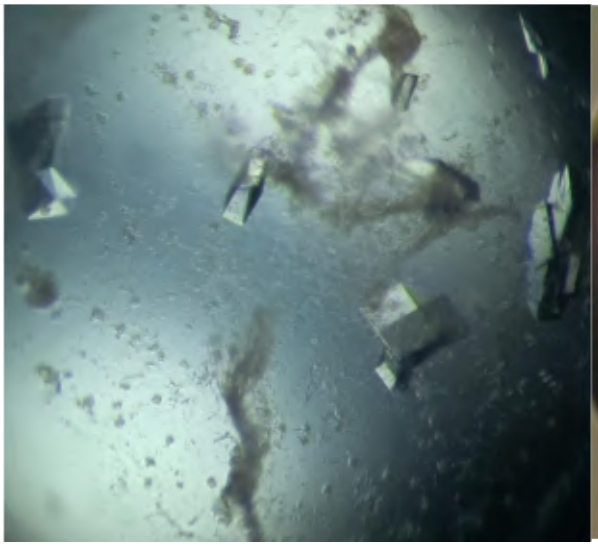

PaSSB: (3-4)

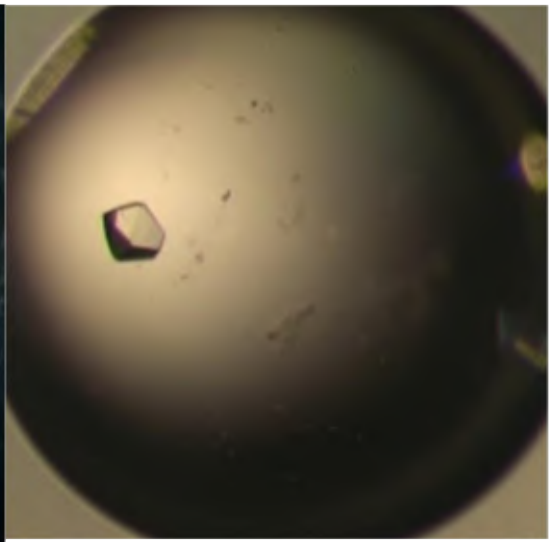

晶體名稱	長晶條件
PaSSB: (3-1)	**28 % PEG400、100 mM HEPES ,pH 7.5、200mM Calcium chloride**
PaSSB: (3-2)	**30%PEG5000MME 、 100 mM MES ,pH6.5、200 mM Ammonium sulfate**
PaSSB: (3-3)	**10%PEG8000、100mM HEPES,pH 7.5、10%Ethylene glycol**
PaSSB: (3-4)	**30%PEG400、100 mM MES,pH 6.5、100 mM Magnesium chloride**

- **PaSSB+ssDNA 晶體成長 4**

PaSSB: (4-1)

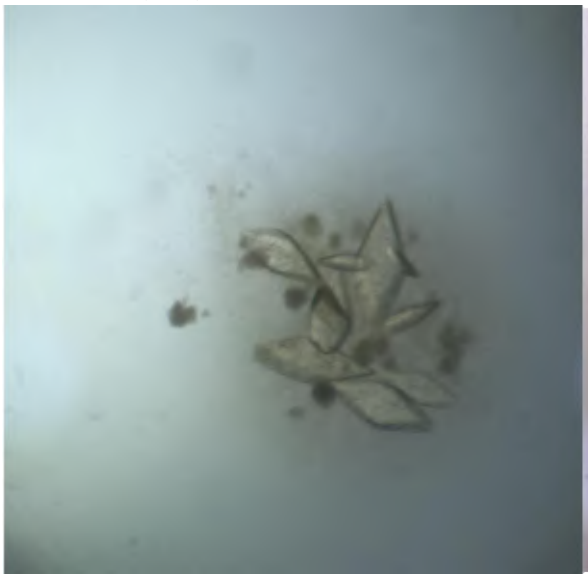

PaSSB: (4-2)

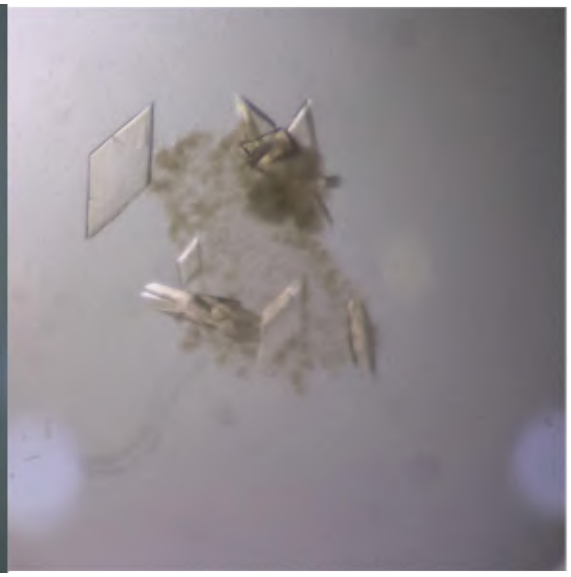

PaSSB: (4-3)

PaSSB: (4-4)

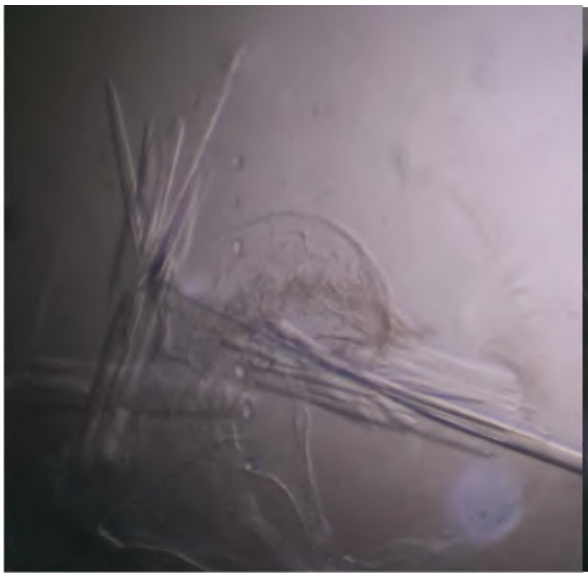


晶體名稱	長晶條件
PaSSB: (4-1)	**20% PEG 1500、100 mM HEPES ,pH 7.5**
PaSSB: (4-2)	**22% PEG 4000、100 mM HEPES ,pH 7.5 、100 mM Sodium acetate**
PaSSB: (4-3)	**20% PEG 4000、100 mM Sodium citrate 、5% 2-Propanol**
PaSSB: (4-4)	**20% PEG 4000、100 mM Sodium citrate 、5% 2-Propanol**

- **PaSSB+ssDNA 晶體成長 5**

PaSSB: (5-1) **PaSSB: (5-2)**

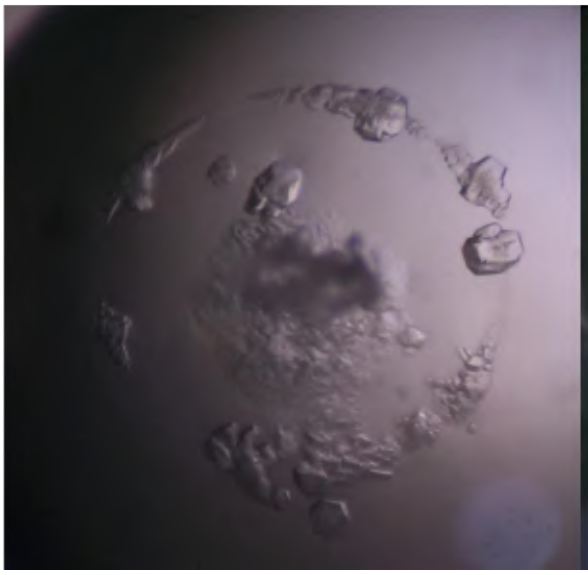
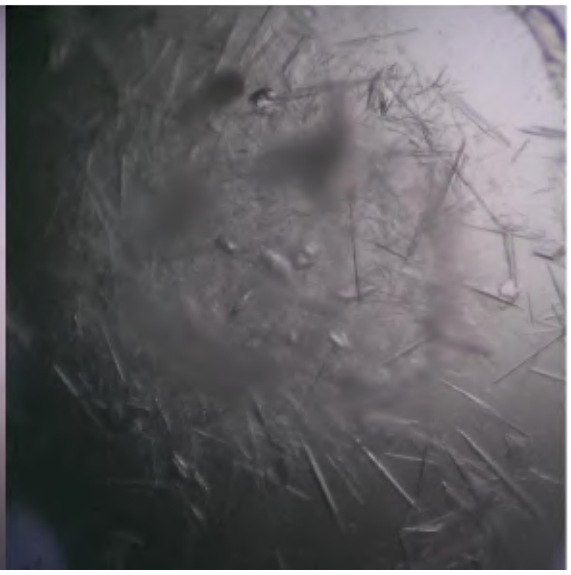

PaSSB: (5-3) **PaSSB: (5-4)**

晶體名稱	長晶條件
PaSSB: (5-1)	**32% PEG 4000、100 mM Tris-HCL ,pH 7.5、800 mM Lithium chloride**
PaSSB: (5-2)	**22% PEG 4000、100 mM HEPES ,pH 7.5 、100 mM Sodium acetate**
PaSSB: (5-3)	**10% PEG 8000 、50 mM Magnesium acetate、100 mM Sodium acetate**
PaSSB: (5-4)	**10% PEG 8000 、50 mM Magnesium acetate、100 mM Sodium acetate**

- **PaSSB+ssDNA 晶體成長 6**

PaSSB: (6-1) **PaSSB: (6-2)**

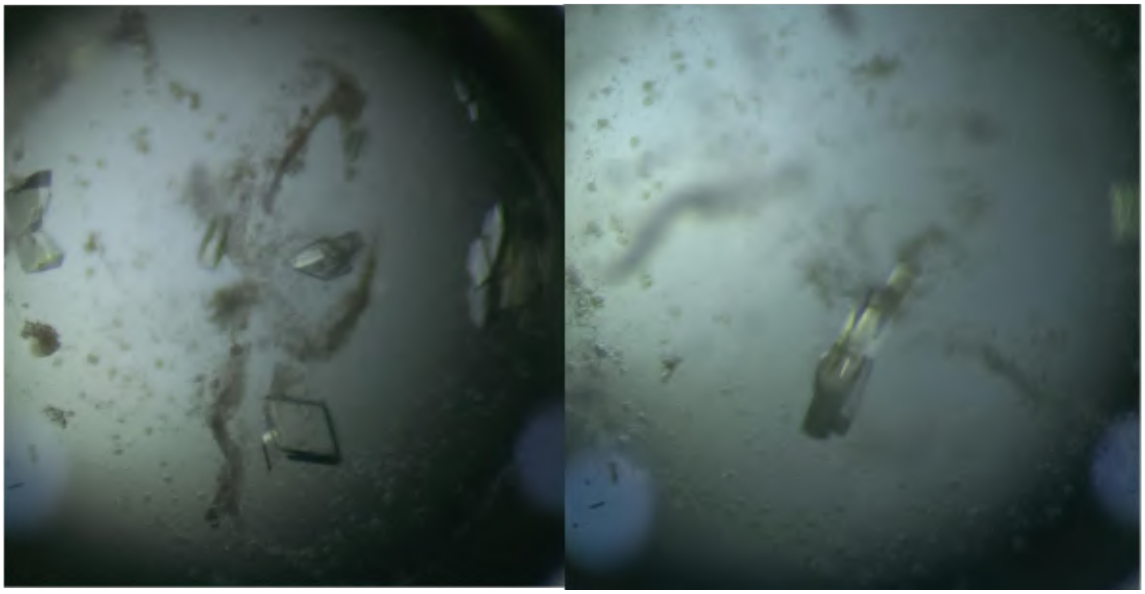

PaSSB: (6-3) **PaSSB: (6-4)**

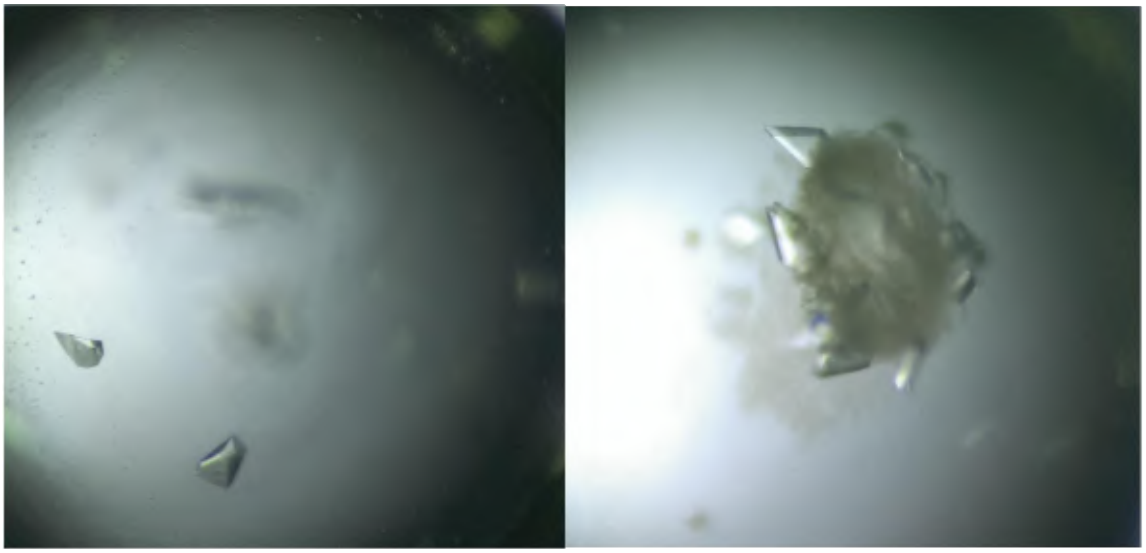

晶體名稱	長晶條件
PaSSB: (6-1)	**10% PEG 8000、100 mM HEPES ,pH 7.5 、10% Ethylene glycol**
PaSSB: (6-2)	**10% PEG 8000、100 mM HEPES ,pH 7.5 、10% Ethylene glycol**
PaSSB: (6-3)	**20% PEG 8000、100 mM MES ,pH 6.5、 200 mM Magnesium acetate**
PaSSB: (6-4)	**30% PEG 10000、100 mM Tris-HCL ,pH 8.5**

- **PaSSB+ssDNA 晶體成長 7**

PaSSB: (7-1) **PaSSB: (7-2)**

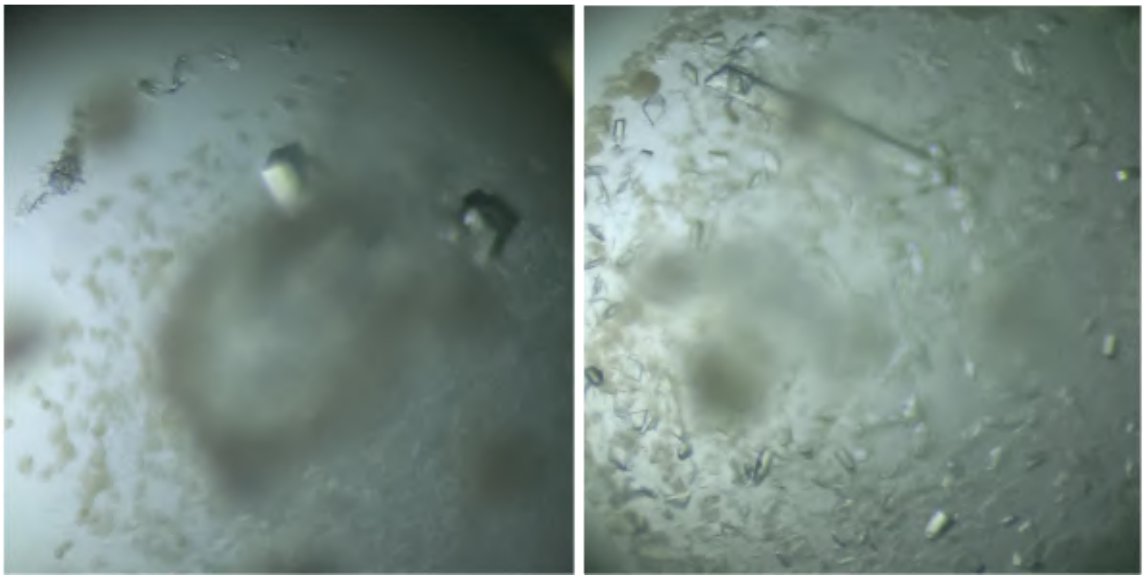

PaSSB: (7-3) **PaSSB: (7-4)**

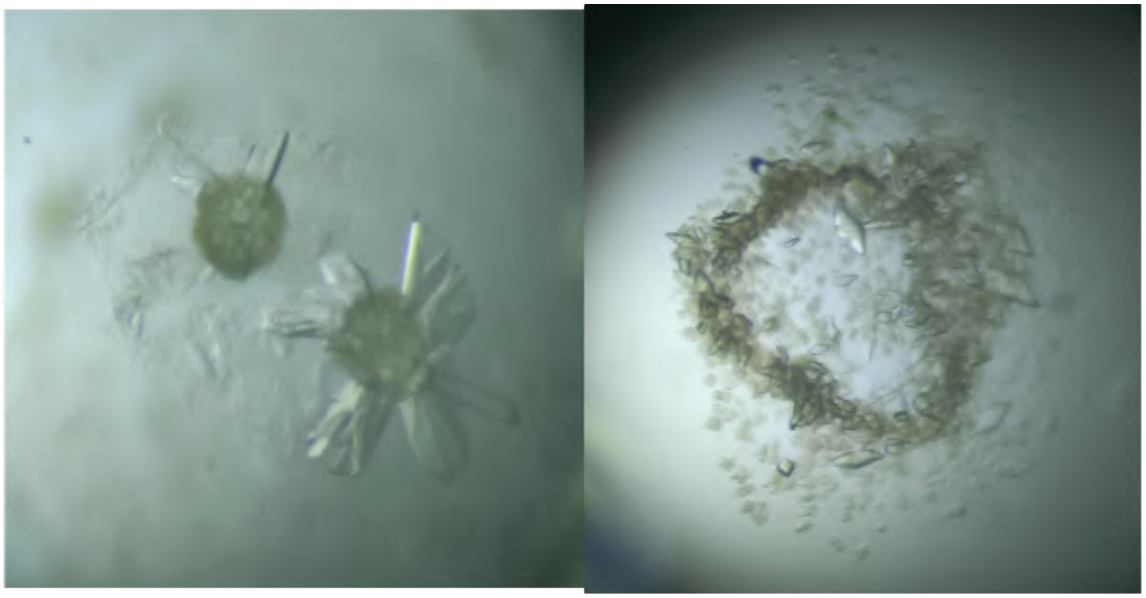

晶體名稱	長晶條件
PaSSB: (7-1)	**17% PEG 20000、100 mM MES ,pH 6.5**
PaSSB: (7-2)	**17% PEG 20000、100 mM MES ,pH 6.5**
PaSSB: (7-3)	**17% PEG 20000、100 mM MES ,pH 6.5**
PaSSB: (7-4)	**30% PEG 10000、100 mM Tris-HCL ,pH 8.5**

- **PaSSB+ssDNA 晶體成長 8**

PaSSB: (8-1) **PaSSB: (8-2)**

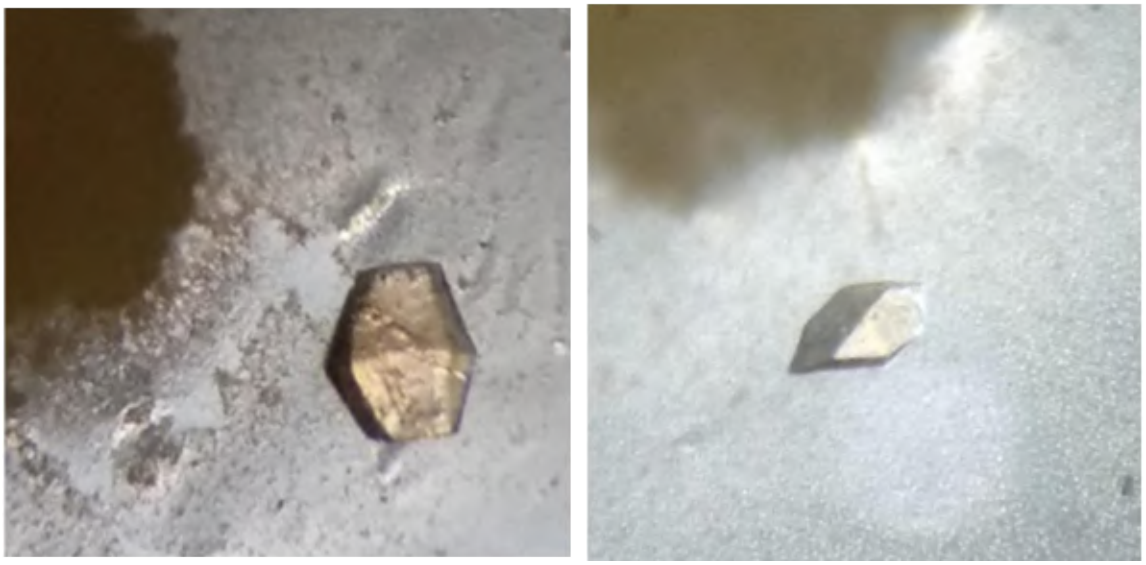

PaSSB: (8-3) **PaSSB: (8-4)**

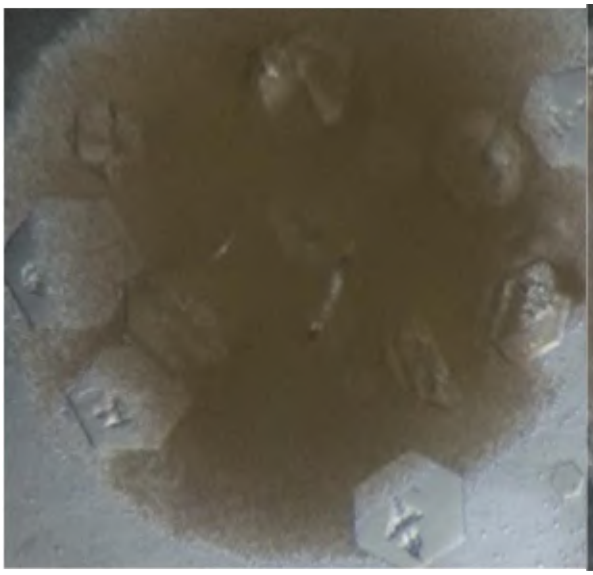
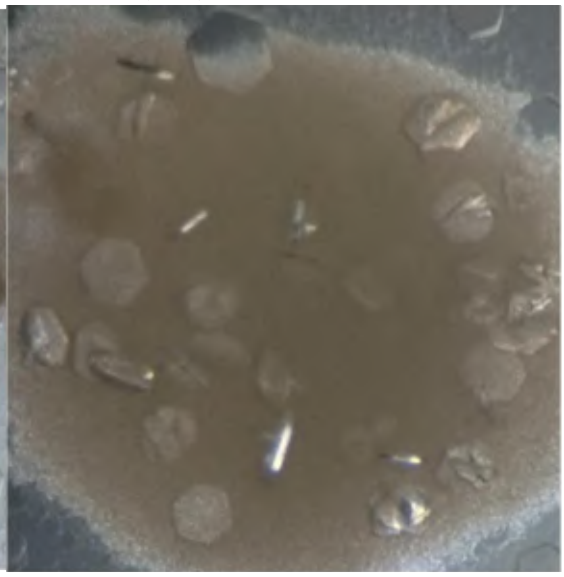

晶體名稱	長晶條件
PaSSB: (8-1)	**10%PEG 8000、100mM HEPES, pH 7.5、200mM Calcium acetate**
PaSSB: (8-2)	**10%PEG 8000、100mM HEPES, pH 7.5、200mM Calcium acetate**
PaSSB: (8-3)	**10% PEG 8000、50 mM Magnesium acetate、100 mM Sodium acetate**
PaSSB: (8-4)	**10% PEG 8000、50 mM Magnesium acetate、100 mM Sodium acetate**

- **PaSSB+inhibitor 晶體成長 9**

PaSSB: (9-1) **PaSSB: (9-2)**

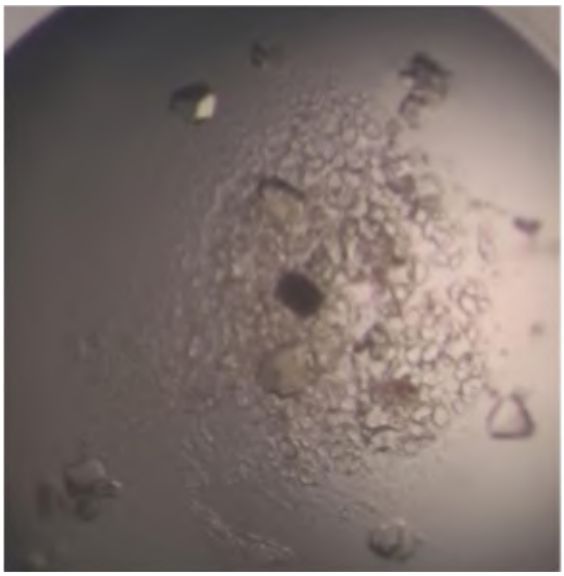
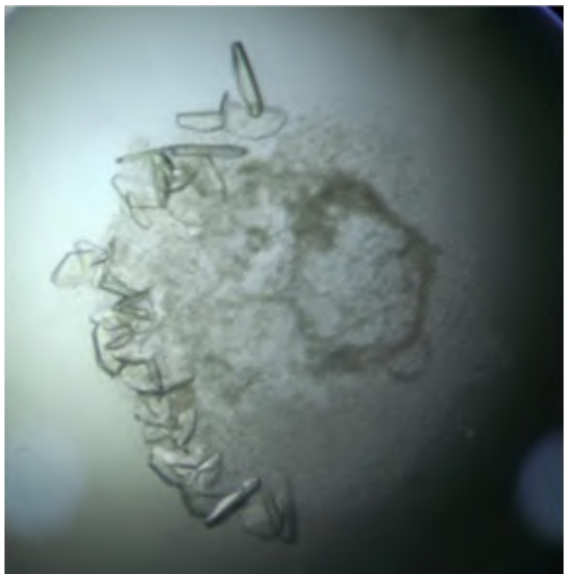

PaSSB: (9-3) **PaSSB: (9-4)**

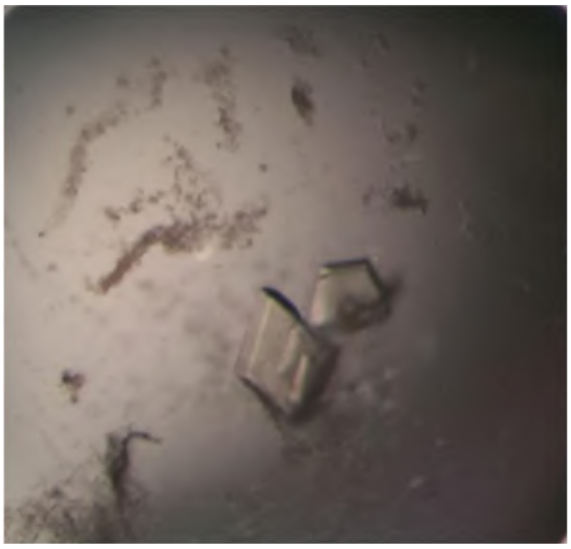
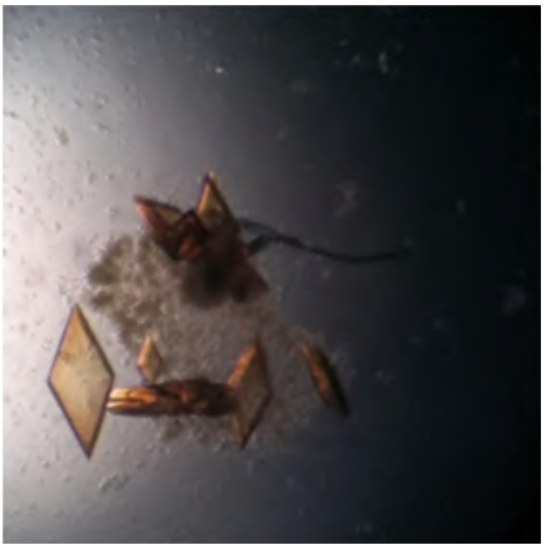

晶體名稱	長晶條件
PaSSB: (9-1)	**10 % PEG 8000、100 mM Sodium acetate、50mM Magnesium acetate**
PaSSB: (9-2)	**12% MPD、100 mMTris-HCL , pH8.5、50 mM Magnesium chloride**
PaSSB: (9-3)	**25% PEG 4000、100 mM MES ,pH 6.5、200 mM Magnesium chloride**
PaSSB: (9-4)	**30% PEG 3000、100 mM Tris-HCL ,pH 8.5、200 mM Lithium sulfate**

- **PaSSB+inhibitor 晶體成長 10**

PaSSB: (10-1) **PaSSB: (10-2)**

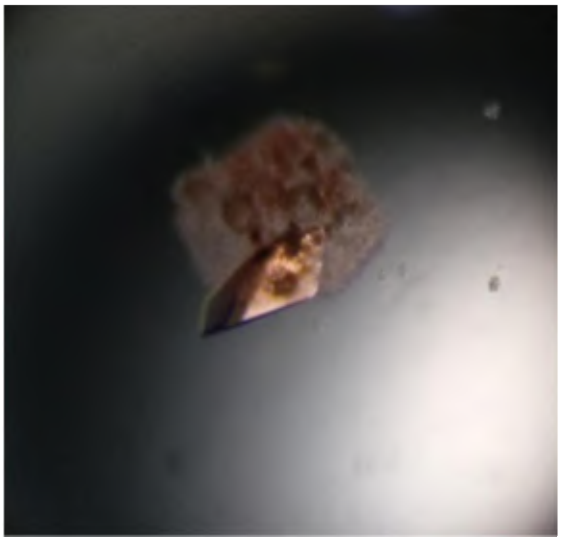
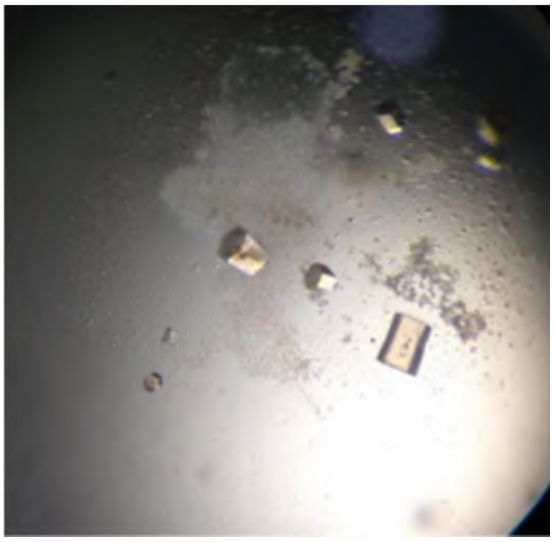

PaSSB: (10-3) **PaSSB: (10-4)**

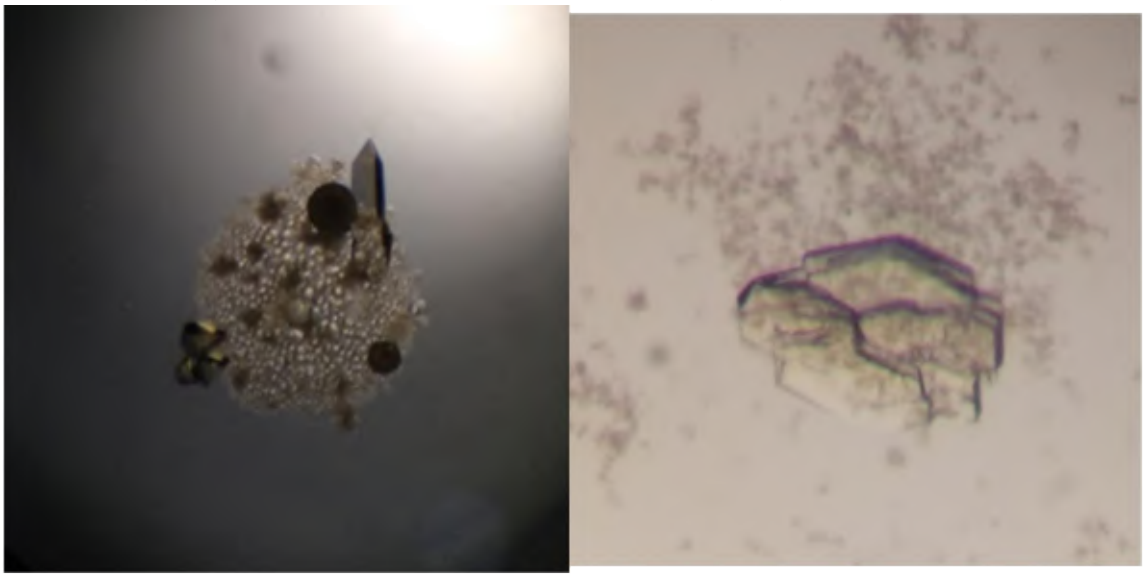

晶體名稱	長晶條件
PaSSB: (10-1)	**18 % PEG 8000、100 mM HEPES,pH7.5、200mM Sodium acetate**
PaSSB: (10-2)	**10% PEG4000、100 mM MES ,pH6.5、200 mM Magnesium chloride**
PaSSB: (10-3)	**18 % PEG 8000、100 mM HEPES,pH7.5 200mM Sodium acetate**
PaSSB: (10-4)	**30% PEG 4000、100 mM HEPES ,pH 7.5、200 mM Calcium chloride**

- **PaSSB+inhibitor 晶體成長 11**

PaSSB: (11-1) **PaSSB: (11-2)**

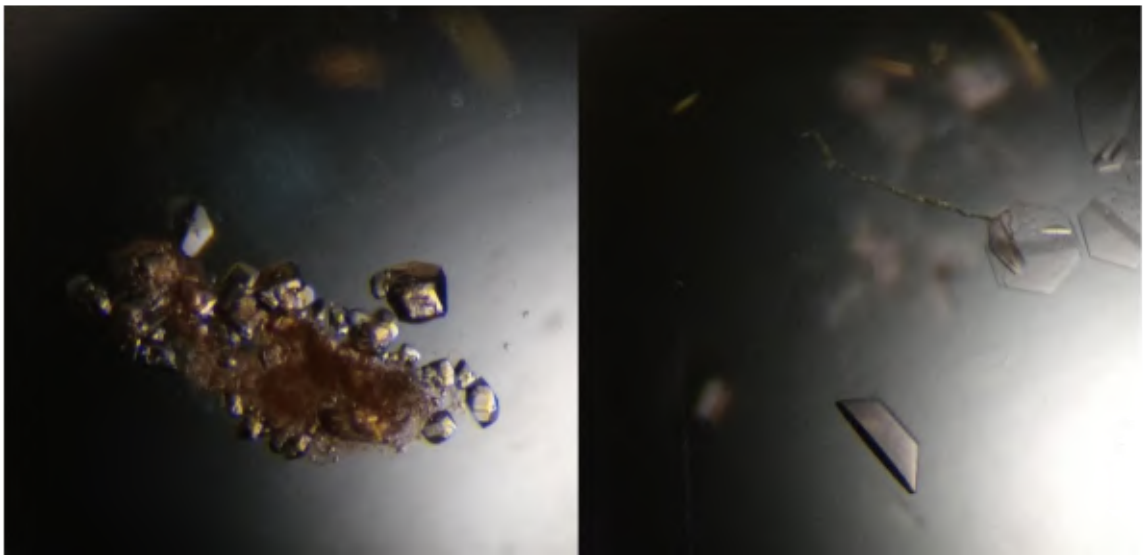

PaSSB: (11-3) **PaSSB: (11-4)**

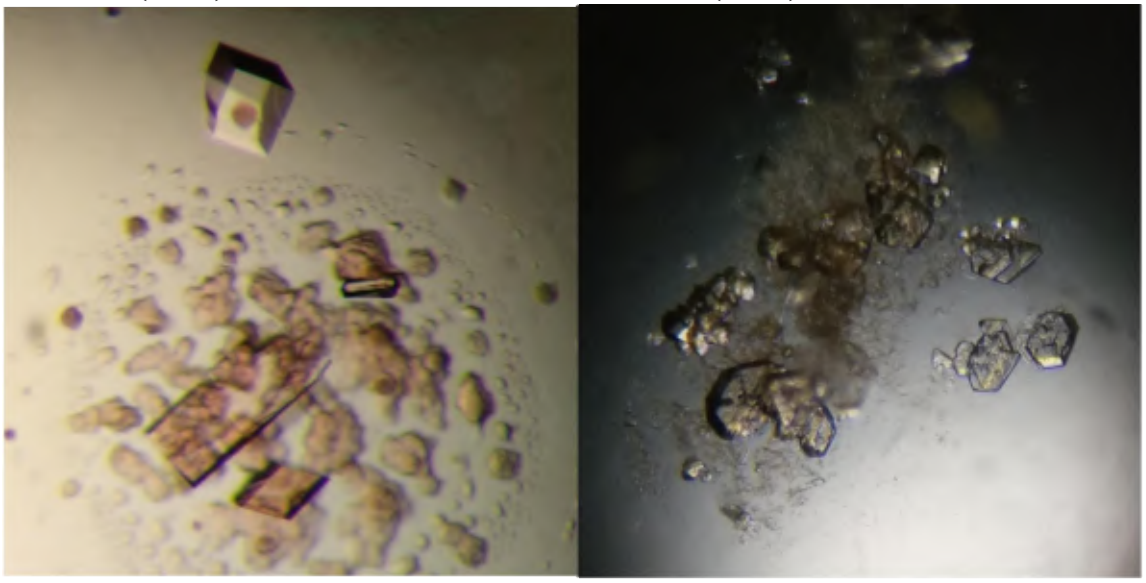

晶體名稱	長晶條件
PaSSB: (11-1)	**25% PEG 4000、 100 mM MES, pH 6.5、200 mM Magnesium chloride**
PaSSB: (11-2)	**3% PEG 6000、 100 mM Tris-HCL, pH 8.5、100 mM Potassium chloride**
PaSSB: (11-3)	**2M Sodium formate**
PaSSB: (11-4)	**25% PEG 4000、 100 mM MES, pH 6.5、200 mM Magnesium chloride**

- **PaSSB+inhibitor 晶體成長 12**

PaSSB: (12-1) **PaSSB: (12-2)**

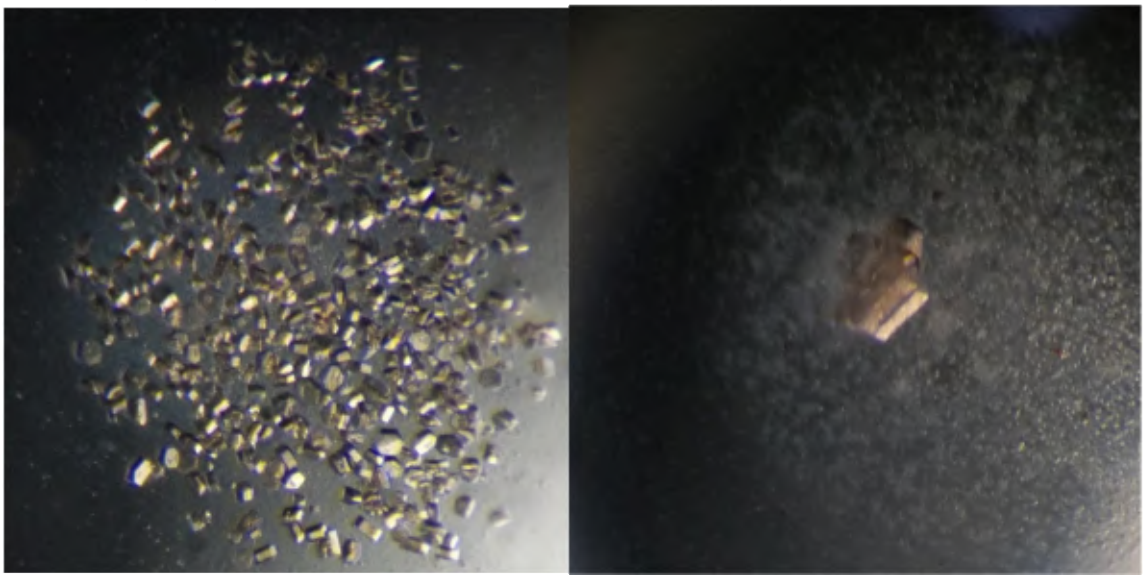

PaSSB: (12-3) **PaSSB: (12-4)**

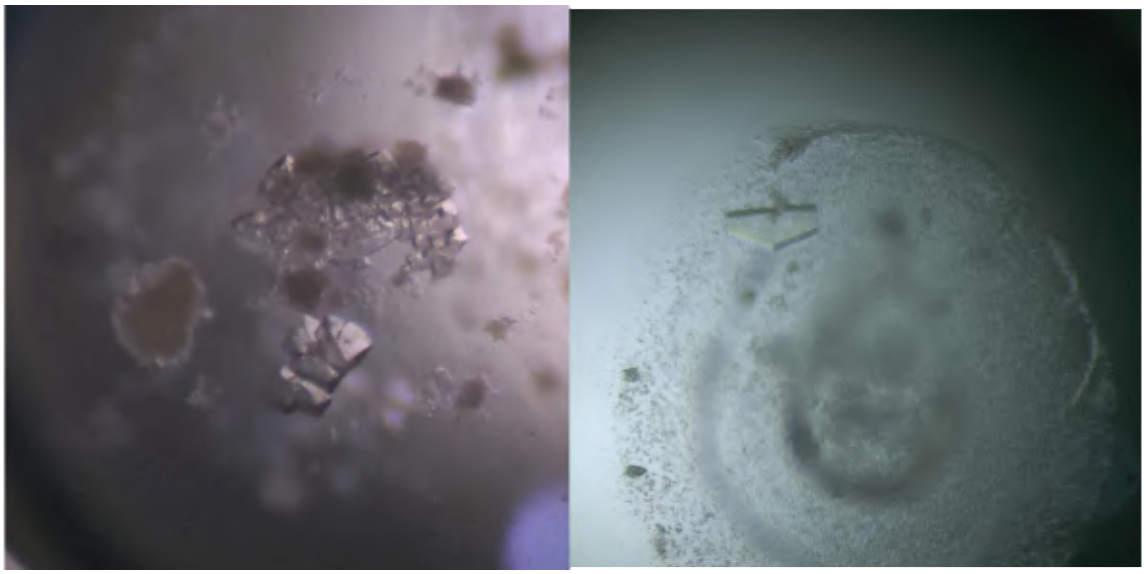

晶體名稱	長晶條件
PaSSB: (12-1)	**10% PEG 8000、10%PEG1000**
PaSSB: (12-2)	**10%PEG8000 、 200mM Magnesium acetate**
PaSSB: (12-3)	**16% PEG 4000、100 mM Tris-HCL ,pH 7.5、200 mM Ammonium sulfate、10% 2-Propanol**
PaSSB: (12-4)	**22%PEG4000、100 mM Sodium acetate、200 mM Ammonium sulfate**

3-1-3 PaSSB 結晶 X 光繞射相關數據

PaSSB + ssDNA（dT 15）

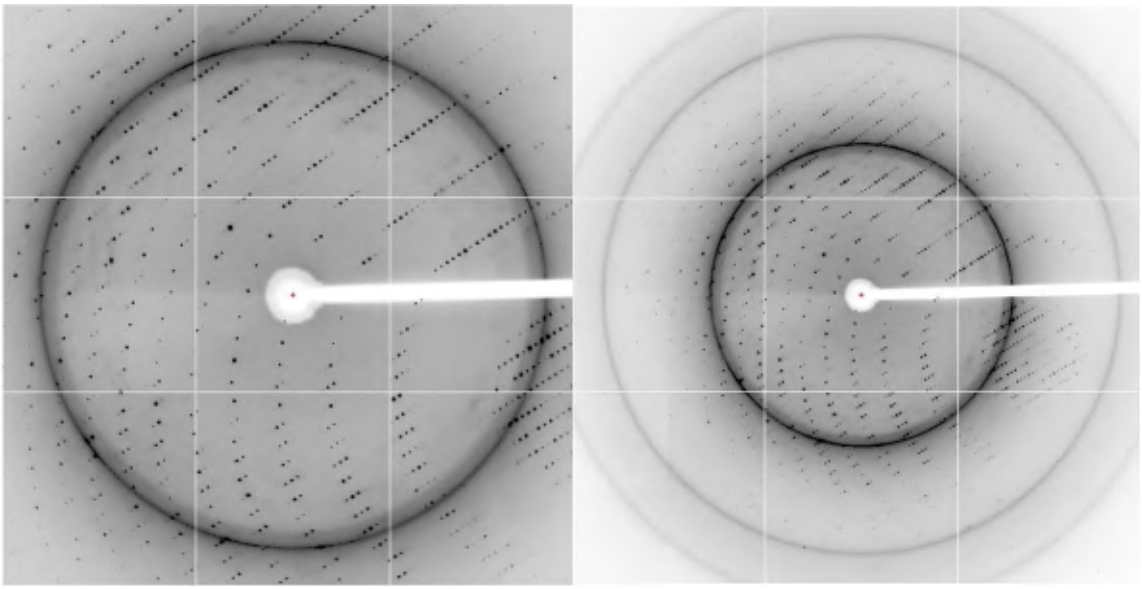

- **以下為綠膿桿菌 SSB（PaSSB）與 ssDNA（dT 15）透過共結晶(co-crystallization)獲得複合結晶，經由 X 光繞射實驗後所獲得的繞射圖相關資訊：**

晶體到 Detector 間的距離（Distance）	280 mm
X 光繞射之晶體曝光時間（Time）	8 s
數據收集之晶體繞射角度範圍（Phi）	130～220 deg
數據收集之晶體轉動幅度（Delta）	1 deg
數據收集之晶體繞射圖張數（Frame）	90
晶體解析度（Resolution）	30Å～1.92Å
晶體之晶格對稱性（Space group）	$P3_1$、$P3_2$

PaSSB + ssDNA（dT 20）

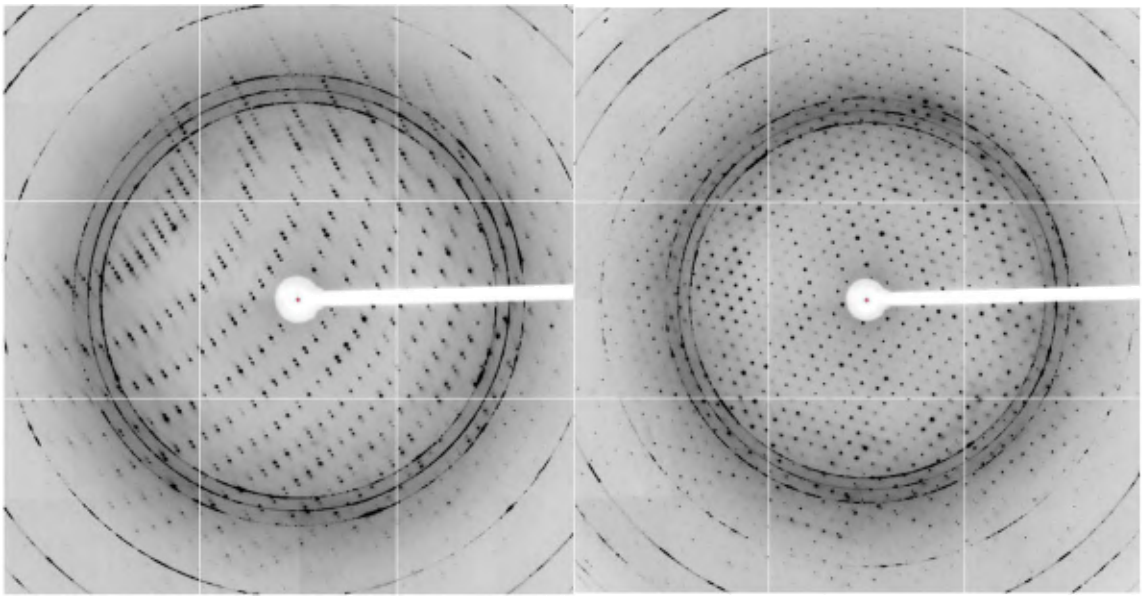

- **以下為綠膿桿菌 SSB（PaSSB）與 ssDNA（dT 20）透過共結晶(co-crystallization)獲得複合結晶，經由 X 光繞射實驗後所獲得的繞射圖相關資訊：**

晶體到 Detector 間的距離（Distance）	370 mm
X 光繞射之晶體曝光時間（Time）	4 s
數據收集之晶體繞射角度範圍（Phi）	65～170 deg
數據收集之晶體轉動幅度（Delta）	1 deg
數據收集之晶體繞射圖張數（Frame）	105
晶體解析度（Resolution）	30Å～2.44Å
晶體之晶格對稱性（Space group）	$P3_1$、$P3_2$

PaSSB + ssDNA（dT 25）

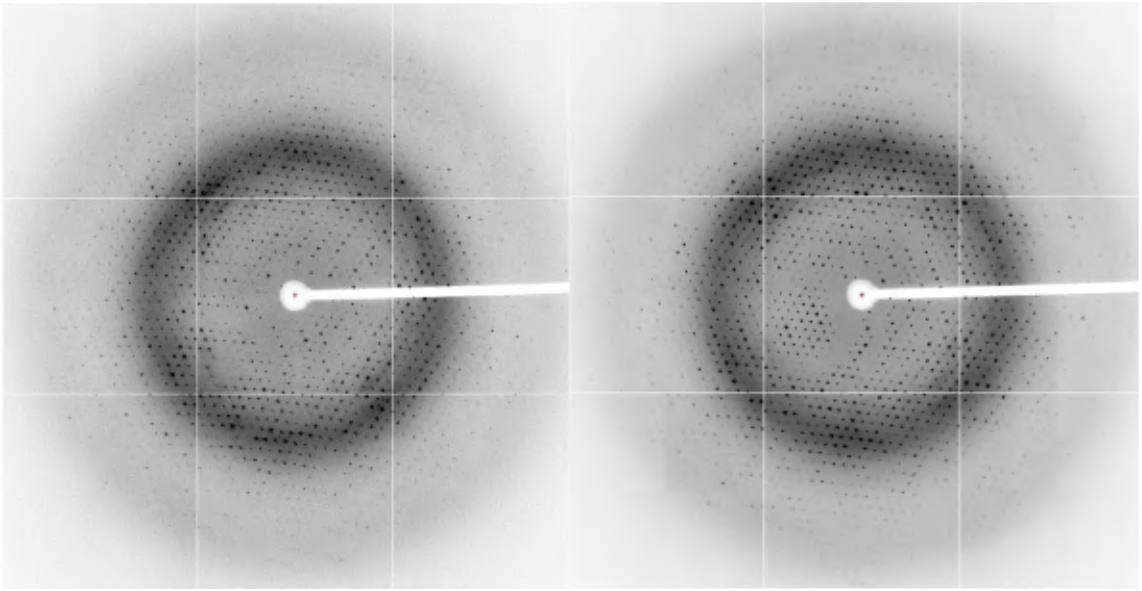

- **以下為綠膿桿菌 SSB（PaSSB）與 ssDNA（dT 25）透過共結晶(co-crystallization)獲得複合結晶，經由 X 光繞射實驗後所獲得的繞射圖相關資訊：**

晶體到 Detector 間的距離（Distance）	270 mm
X 光繞射之晶體曝光時間（Time）	4 s
數據收集之晶體繞射角度範圍（Phi）	0～130 deg
數據收集之晶體轉動幅度（Delta）	1 deg
數據收集之晶體繞射圖張數（Frame）	130
晶體解析度（Resolution）	30Å～2.3Å
晶體之晶格對稱性（Space group）	$P3_1$、$P3_2$

PaSSB + inhibitor（myc）

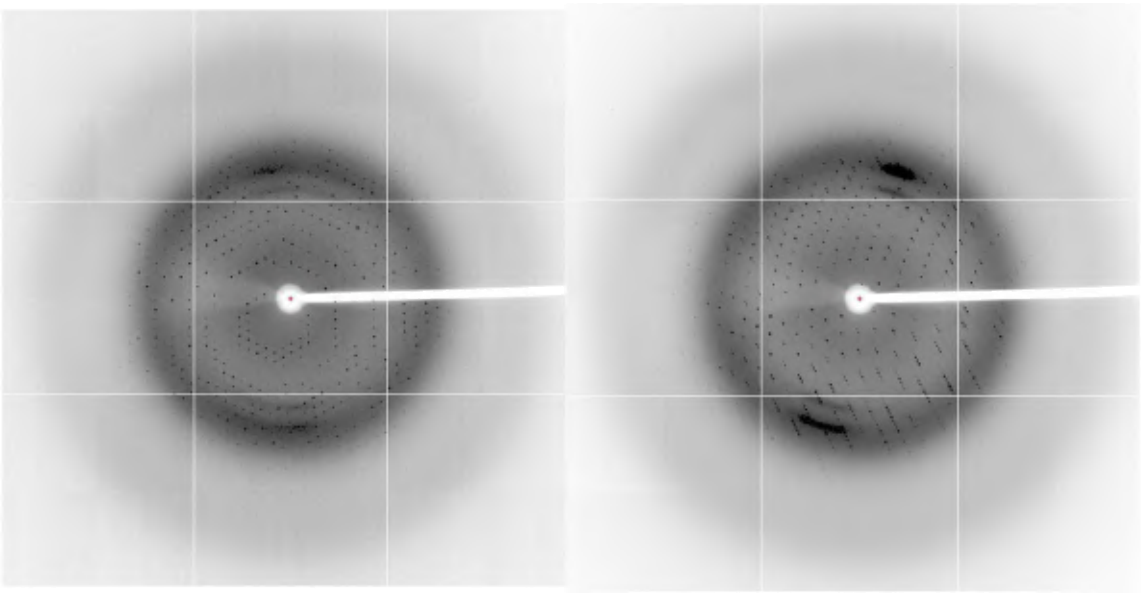

- **以下為綠膿桿菌 SSB（PaSSB）與 inhibitor（myc）透過共結晶(co-crystallization)獲得複合結晶，經由 X 光繞射實驗後所獲得的繞射圖相關資訊：**

晶體到 Detector 間的距離（Distance）	260 mm
X 光繞射之晶體曝光時間（Time）	10 s
數據收集之晶體繞射角度範圍（Phi）	123～226 deg
數據收集之晶體轉動幅度（Delta）	1 deg
數據收集之晶體繞射圖張數（Frame）	103
晶體解析度（Resolution）	30Å～2.38Å
晶體之晶格對稱性（Space group）	$P3_1$、$P3_2$

3-1-4 PaSSB 序列分析

- 綠膿桿菌 SSB（PaSSB）之序列分析，並與不同菌種如大腸桿菌（Ec）、克雷白氏菌（Kp）、傷寒沙門氏菌（St）之 SSB 序列進行比較。可以發現 N 端的 DNA 結合區與尾端的 DDDIPF 的蛋白質-蛋白質交互作用區(框起來處)是高度保留。

- 綠膿桿菌 SSB（PaSSB）與其他 300 多個細菌 SSB 之序列分析，其中顏色為酒紅色的是具高度保留性之胺基酸序列；另一顏色為青色則是較不具保留性（變異性較高）的氨基酸序列，因此可以

看出其 N 端多為高度保留性區域;而 C 端則在不同物種間的變異性較高。

3-1-5 PaSSB 結晶結構統計分析表

Data collection		
Crystal	PaSSB	
Wavelength (Å)	0.975	
Resolution (Å)	30–2.04	
Space group	C_12_1	
Cell dimension (Å)	$a = 102.2$	$\alpha = 90$
	$b = 64.1$	$\beta = 113.0$
	$c = 97.1$	$\gamma = 90$
Completeness (%)	98.2 (89.9)*	
$<I/\sigma I>$	31.36 (2.53)	
R_{sym} or R_{merge} (%)	0.038 (0.465)	
Redundancy	3.6 (3.1)	
Refinement		
Resolution (Å)	30–2.04	
No. reflections	34580	
R_{work}/R_{free}	0.21/0.27	
No. atoms		
Protein	422	
Water	180	
R.m.s deviation		
Bond lengths (Å)	0.0188	
Bond angles (°)	1.9949	
Ramachandran Plot		
In preferred regions	348 (93.89%)	
In allowed regions	17 (4.16%)	
Outliers	8 (1.96%)	
PDB entry	5YUO	

- 綠膿桿菌 SSB（PaSSB） 的結晶結構統計分析表，經過 X 光繞射實驗後，並透過 HKL2000 計算各個繞射圖中繞射點，可得知相關結構資訊，包括 Space group、Resolution、PDB entry 等資訊。

3-1-6 PaSSB 結晶結構

- 綠膿桿菌 SSB (PaSSB) 的結晶結構 (有四個次單元)。PaSSB 的四級結構為四套體，其單套體有 6 個 sheets 與 1 個 helix，此構型為著名的 OB fold (oligonucleotide/oligosaccharide-binding fold)，通常用於結合長鏈寡核甘酸或寡醣結構。

3-1-7 PaSSB 結晶結構（與 ssDNA 交互作用區）

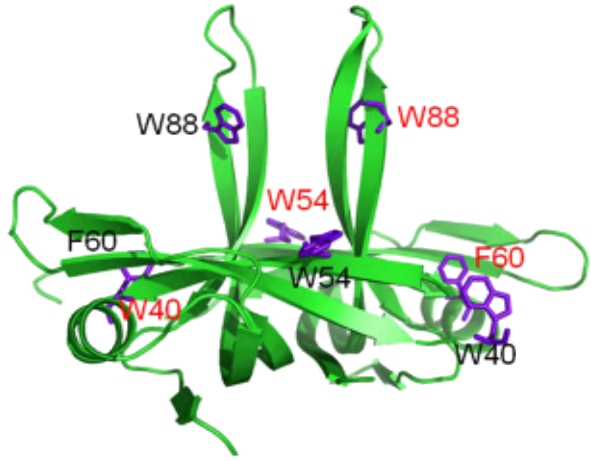

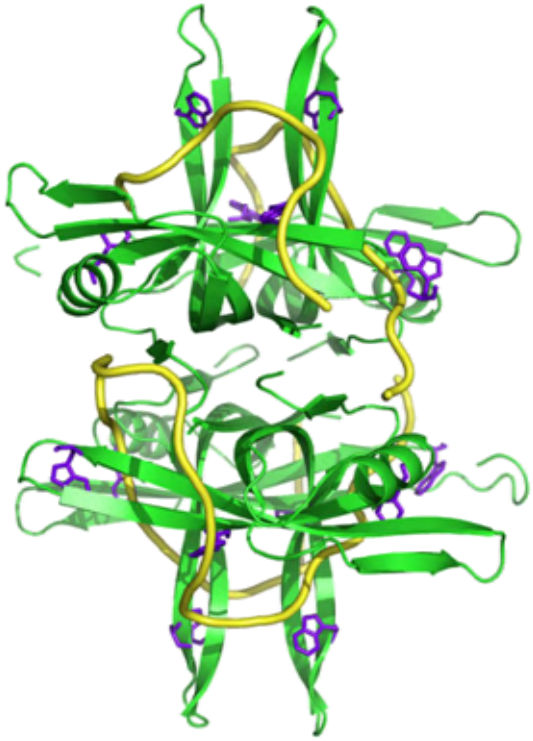

- 綠膿桿菌 SSB (PaSSB)中的 4 個極保留的芳香環胺基酸(W40、W54、F60、W88)參與了 SSB 與單股 DNA 的交互作用，並引導 DNA 在 SSB 上的纏繞。

3-1-8 PaSSB 定點突變（site-directed mutagenesis）分析

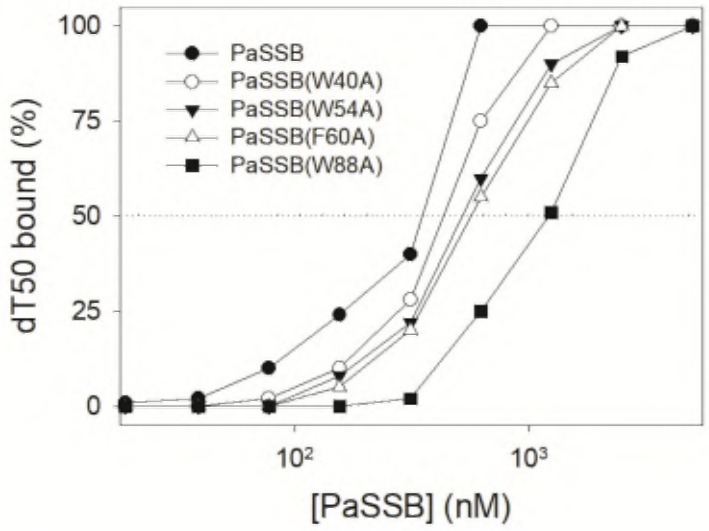

dT50	$[Protein]_{50}$ (nM)
PaSSB	355 ± 21
PaSSB(W40A)	434 ± 19
PaSSB(W54A)	522 ± 26
PaSSB(F60A)	569 ± 24
PaSSB(W88A)	1227 ± 61

- 由結晶結構得知綠膿桿菌 SSB（PaSSB）與 ssDNA 主要是透過四個芳香環的氨基酸(W40、W54、F60、W88)進行交互作用，並引導 DNA 在 SSB 上的纏繞，因此利用定點突變（site-directed mutagenesis），將此四個胺基酸突變成 alanine(側鏈為甲基)，來驗證 ssDNA 結合位與四個芳香環胺基酸之重要性。

3-1-9 PaSSB 與 ssDNA dT15＆dT20 複合體

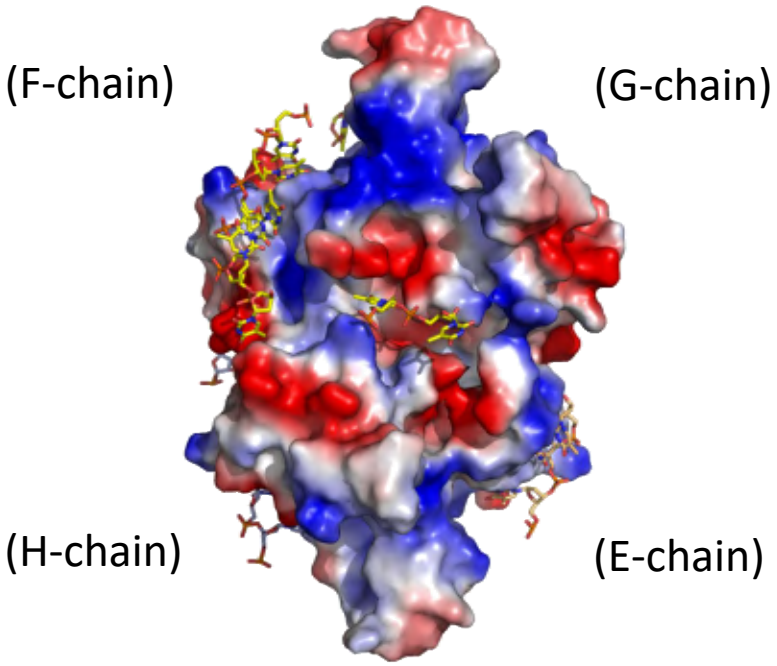

- 透過共結晶(co-crystallization)獲得綠膿桿菌 SSB（PaSSB）與 ssDNA 之複合結晶，此複合結晶結構為 PaSSB 與 dT15 複合體

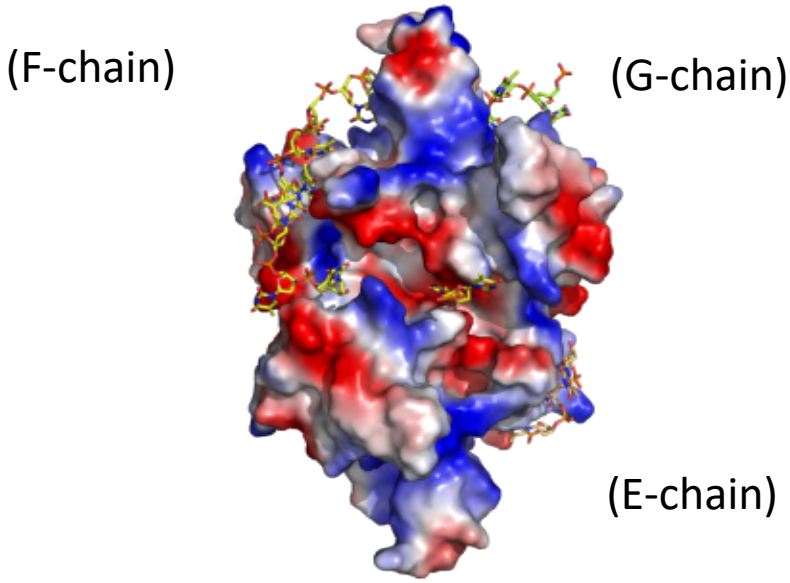

- 透過共結晶(co-crystallization)獲得綠膿桿菌 SSB（PaSSB）與 ssDNA 之複合結晶，此複合結晶結構為 PaSSB 與 dT20 複合體

3-1-10 PaSSB 與 ssDNA 交互作用之結構變化

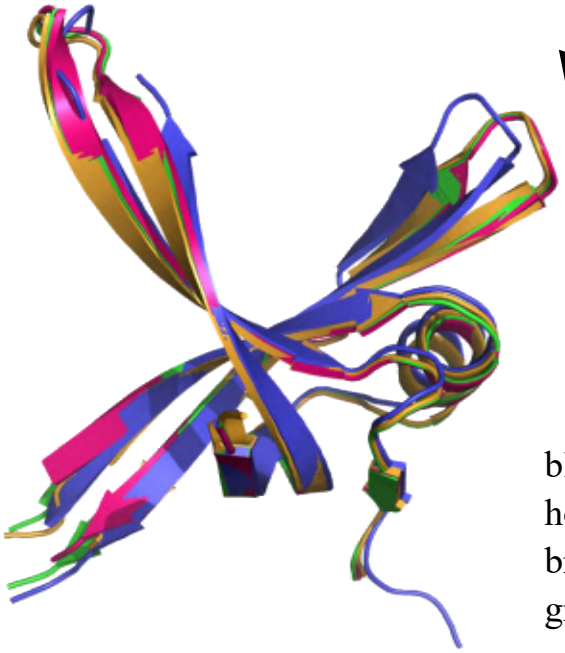

- 此為綠膿桿菌 SSB(PaSSB)以及其與不同長度之 ssDNA(dT15、dT20、dT25）的結晶結構，其中 PaSSB (5YUO)為藍色部分、PaSSB-dT15 (5ZBP)為桃紅色部分、PaSSB-dT20 (5ZDJ)為亮橘色、PaSSB-dT25 (5YX0)為綠色，將 PaSSB (5YUO)、PaSSB-dT15 (5ZBP)、PaSSB-dT20 (5ZDJ)、PaSSB-dT25 (5YX0)彼此交疊在一起後，可以發現 PaSSB 在與 ssDNA 交互作用結合時，會比原先的無 ssDNA 結合的狀態產生距離為 3.74 Å 與角度為 16.6° 的結構變化。

3-1-11 PaSSB 與 ssDNA dT25 之交互作用

一個 PaSSB 以χ型態結合兩條單股 DNA，而非四套體結合四條 DNA。

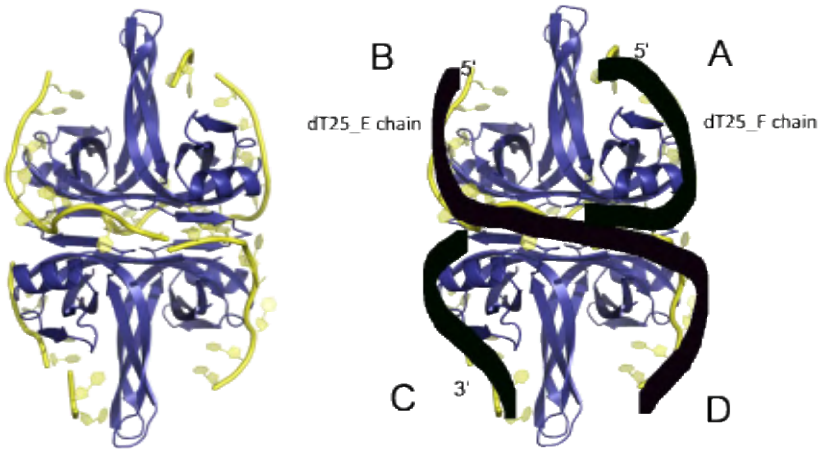

- 以上可以發現 DNA 長度會極大的影響 PaSSB 的結合模式。

3-1-12 PaSSB 與 DNA 的分子結合資訊

我們已整理出每一處 DNA 與蛋白質交互作用的距離與方式。例如此處列舉了部份 DNA 區域 (T1, T2, and T6-8)。

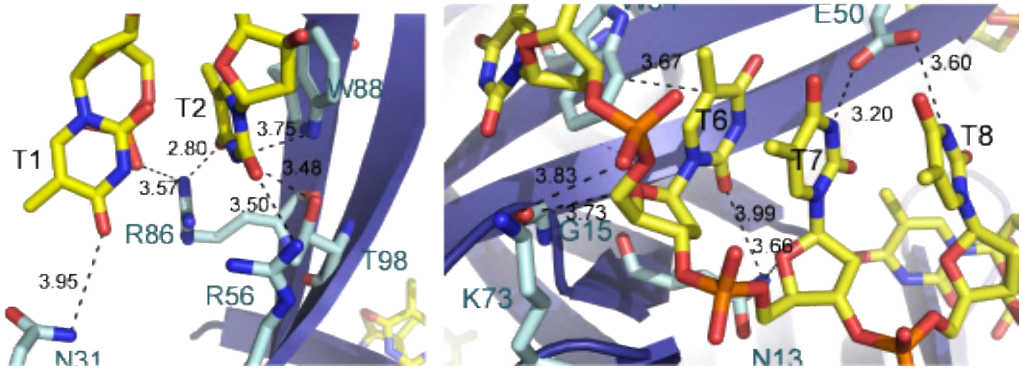

3-1-13 PaSSB 與 DNA dT25 的分子結合資訊示意圖

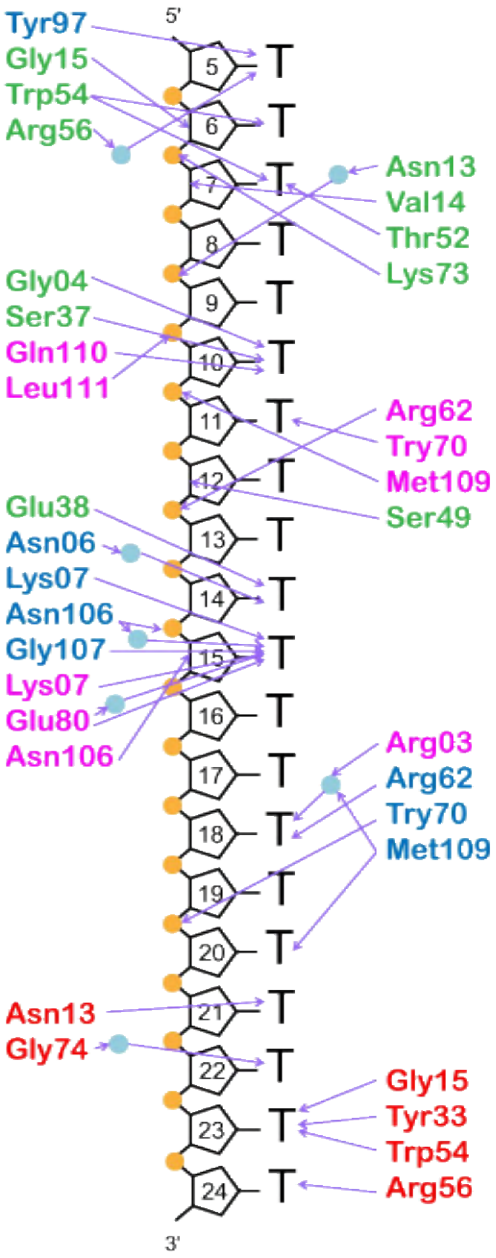

3-1-14 PaSSB 與 DNA dT25 的不對稱作用

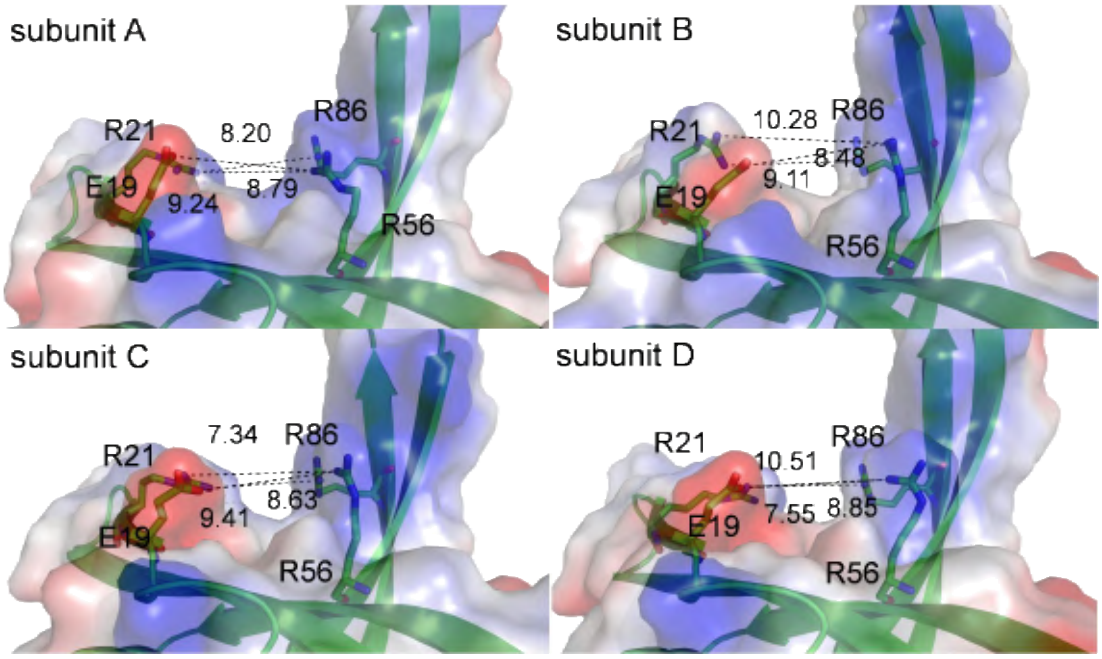

- 複合結晶結構顯示 SSB 四套體與 2 個 DNA 的結合作用並不一致，尤其是 R21/R56/R86 在結合凹洞處可能扮演共協同開關。

3-1-15 PaSSB 與 DNA dT15 以及抑制劑 myc 的三重結構

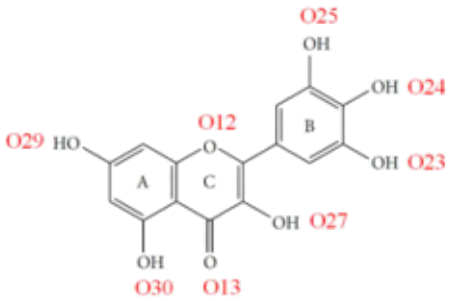

抑制劑 myc 結構

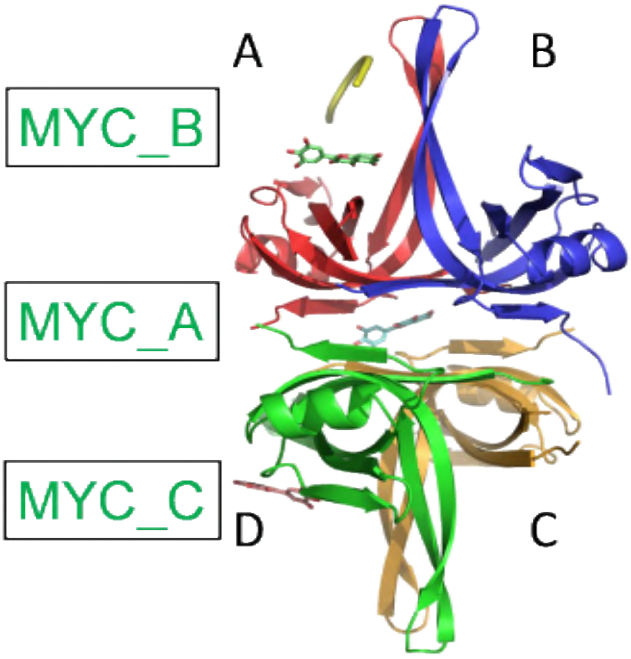

- 三重複合結晶結構顯示 SSB 四套體與 DNA 的結合凹洞開關(R21/R56/R86)被 myc B/C 占據致破壞，而 myc A 則卡住纏繞自身的二套體-二套體介面。DNA 無法纏繞 SSB，僅剩部分胺基酸能與 DNA 結合而致 SSB 失去強的結合能力。我們將據此結構持續優化藥物。

3-2 StyDnaT 84~179（DnaTc）相關實驗結果

3-2-1 StyDnaT 84~179（DnaTc）晶體形成（懸吊法）

StyDnaT 84~179: (1-1)

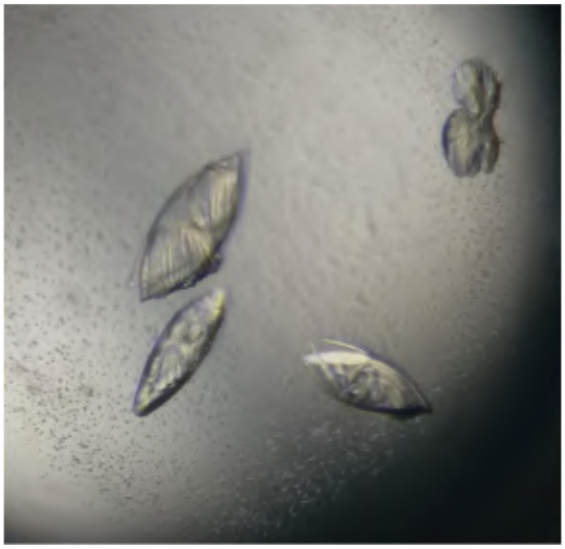

StyDnaT 84~179: (1-2)

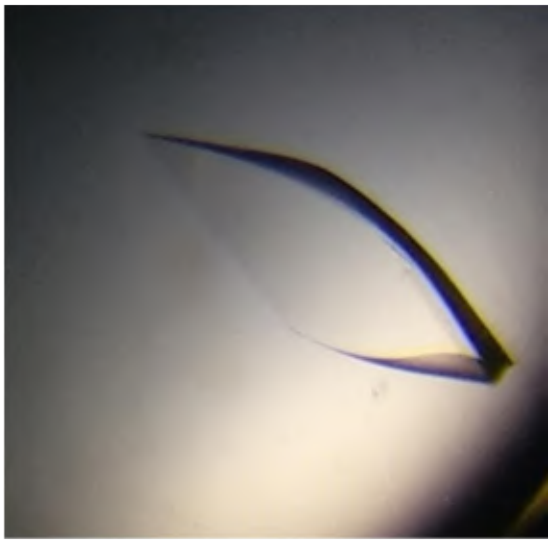

StyDnaT 84~179: (1-3)

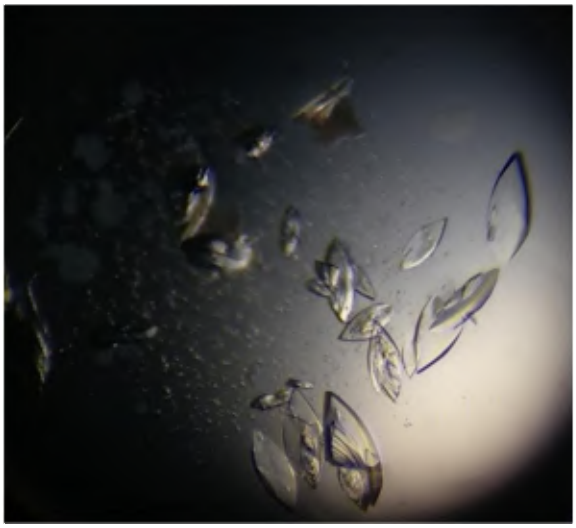

StyDnaT 84~179: (1-4)

晶體名稱	長晶條件
StyDnaT 84~179: (1-1)	1.6M Magnesium sulfate、 100 mM MES, pH 6.5
StyDnaT 84~179: (1-2)	1.6M Magnesium sulfate、 100 mM MES, pH 6.5
StyDnaT 84~179: (1-3)	1.6M Magnesium sulfate、 100 mM MES, pH 6.5
StyDnaT 84~179: (1-4)	1.6M Magnesium sulfate、 100 mM MES, pH 6.5

3-2-2 StyDnaT 84~179（DnaTc）結晶 X 光繞射相關數據

StyDnaT 84~179（DnaTc）

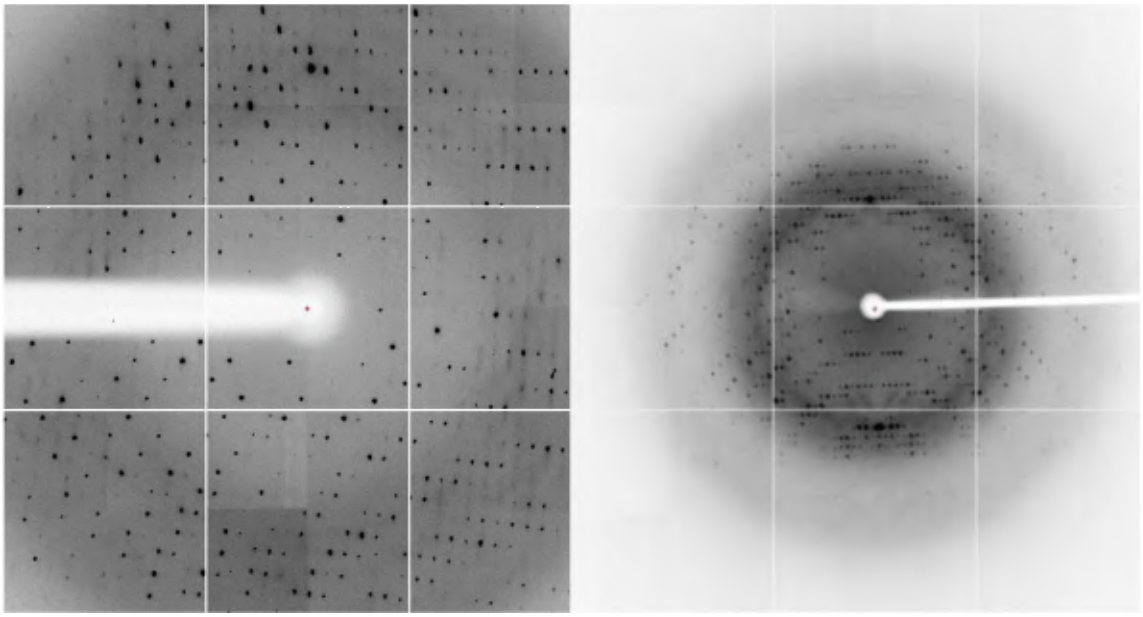

- **以下為傷寒沙門氏菌 StyDnaT 84~179（DnaTc）經過篩選多種條件後，獲得此蛋白質結晶，並經由 X 光繞射實驗後所獲得的繞射圖相關資訊：**

晶體到 Detector 間的距離（Distance）	220 mm
X 光繞射之晶體曝光時間（Time）	5 s
數據收集之晶體繞射角度範圍（Phi）	145～265 deg
數據收集之晶體轉動幅度（Delta）	1 deg
數據收集之晶體繞射圖張數（Frame）	120
晶體解析度（Resolution）	30Å～2.3Å
晶體之晶格對稱性（Space group）	$C222_1$

3-2-3 StyDnaT 84~179（DnaTc）結晶結構

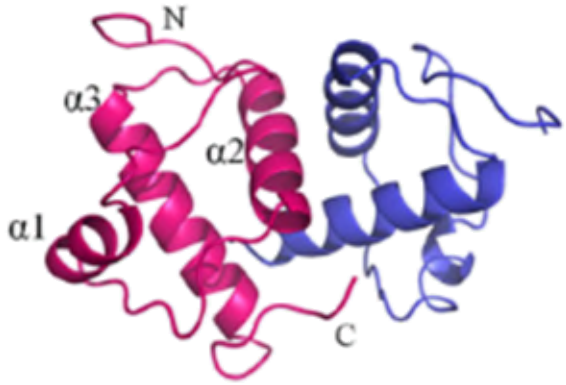

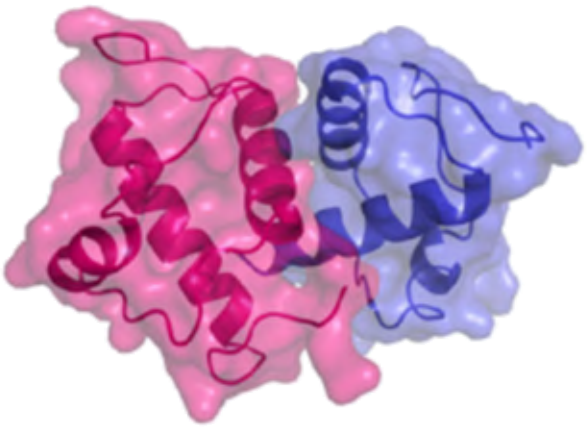

- 此為 StyDnaT 84~179(DnaTc)結晶結構，並有兩個單體(monomer)顯示於對稱性單元中，StyDnaT 84~179(DnaTc)具有三個 helix 在其 C 端區域，DnaTc 的三個 helix 分別位於第 101-108（α1）胺基酸、第 118-131 胺基酸（α2）和第 137-153 胺基酸（α3）中

3-2-4 StyDnaT 84~179（DnaTc）結晶結構統計分析表

Data collection	
Crystal	DnaTc
Wavelength (Å)	0.975
Resolution (Å)	30–2.30
Space group	$C222_1$
Cell parameters	
a, b, c (Å)	54.91, 92.32, 69.00
α, β, γ (°)	90, 90, 90
Completeness (%) [a]	98.4 (91.8)
<I/σI>	30.14 (4.58)
R_{sym} or R_{merge} (%) [b]	0.058 (0.320)
Redundancy	5.6 (5.0)
Refinement	
Resolution (Å)	21.48–2.30
No. reflections	8273
R_{work}/R_{free}	0.220/0.265
No. atoms	
Protein	151
Water	16
R.m.s deviation	
Bond lengths (Å)	0.009
Bond angles (°)	1.213
Ramachandran Plot	
In preferred regions	146 (99.32%)
In allowed regions	0 (0%)
Outliers	1 (0.68%)
PDB entry	6AEQ

- 傷寒沙門氏菌 DnaT 84~179（StyDnaT 84~179） 的結晶結構統計分析表，經過 X 光繞射實驗後，並透過 HKL2000 計算各個繞射圖中繞射點，可得知相關結構資訊，包括 Space group、Resolution、PDB entry 等資訊

3-2-5 StyDnaT 84~179（DnaTc）與 DnaT 84~153 比較

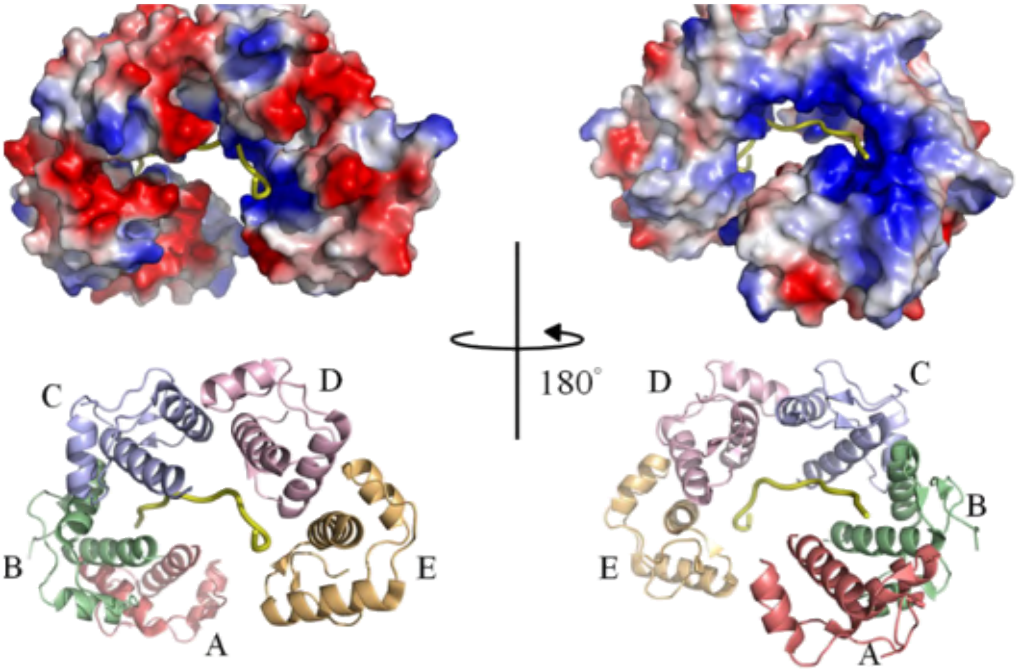

- 此為解析度 2.83 Å 之 DnaT 84~153 之結晶結構，此結晶結構顯示有 5 個 DnaT 84~153 互相結合於一條 ssDNA 上，表示其在與 ssDNA 作用時所形成的寡聚合現象會使其變成五聚體。

3-2-6 StyDnaT 84~179（DnaTc）與 DnaT 84~153 二級結構比較

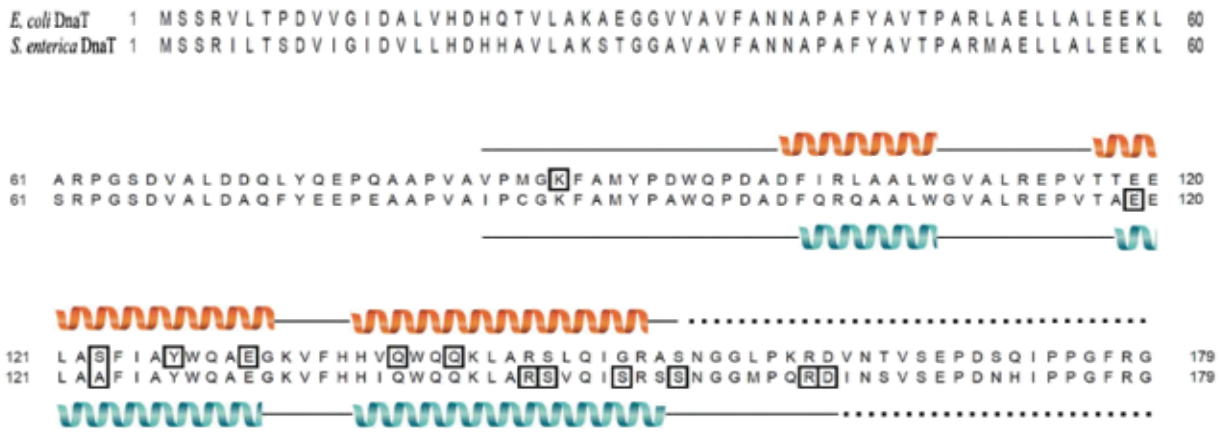

- 此為傷寒沙門氏菌 DnaT 84~179（*S. enterica* DnaT）的二級結構與大腸桿菌 DnaT84-153（*E. coli* DnaT）的二級結構，透過二級結構的序列比對分析，可以看出其二級結構是相似的，而參與寡聚化的胺基酸在這兩種結構之間則有顯著不同。

3-2-7 StyDnaT 84~179（DnaTc）二聚體型態

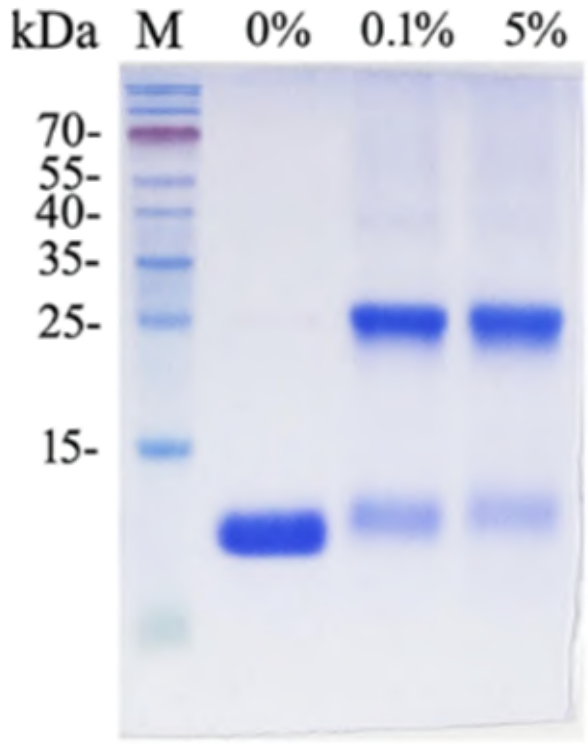

- 由上述 DnaTc 結構顯示由兩個單體（monomer）組成，為了進一步證實晶體結構的觀察結果，我們使用戊二醛（Glutaraldehyde）進行了 DnaTc 的化學性交聯反應，將 DnaTc（4μM）與濃度逐漸增加的戊二醛（0.1%和 5%）並在 4℃反應 20 分鐘，而在這些濃度下可以清楚地觀察到 DnaTc 的二聚體形式（24kDa），同時也發現了與其他聚合形式相對應的位置。此戊二醛化學性交聯結果顯示 DnaTc 主要在溶液中以二聚體形式出現，與晶體結構所顯示的一致。

3-2-8 StyDnaT 84~179（DnaTc）與 DnaT 84~153 二聚體組成之差異

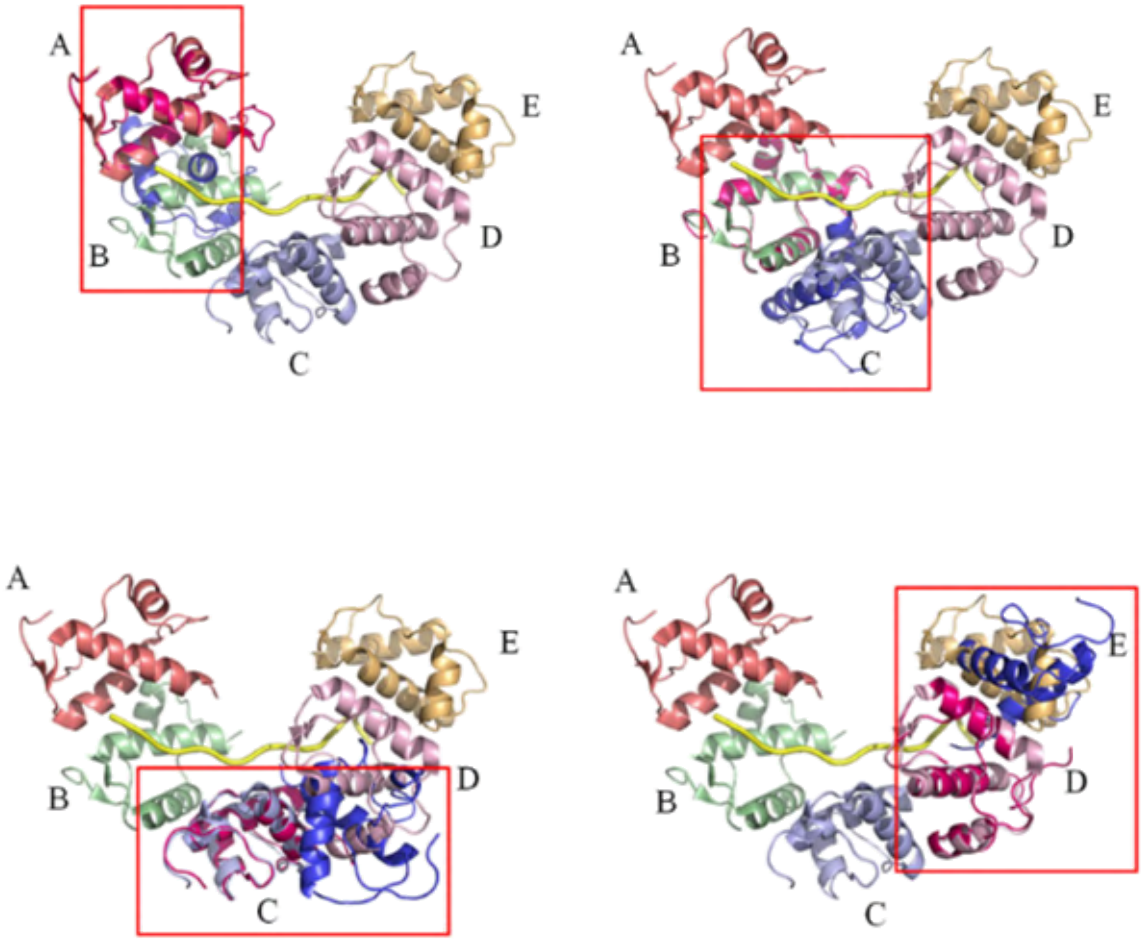

- 由此圖顯示五個 DnaT84-153 蛋白質分子透過每兩個單體相鄰之間的二聚體互相作用，其中具有 DnaTc 二聚體的次單元 A-B 次單元 B-C、次單元 C-D 和次單元 D-E 的結構重疊顯示 DnaTc 與五聚體 DnaT84-153 中的每個二聚體形成不同的二聚體結構，由此可知 DnaTc 二聚體不是五聚體 DnaT84-153 的一部分，並且不屬於五聚體 DnaT84-153 中所形成的任何二聚體。

3-2-9 StyDnaT 84~179（DnaTc）單體-單體（monomer-monomer）間作用

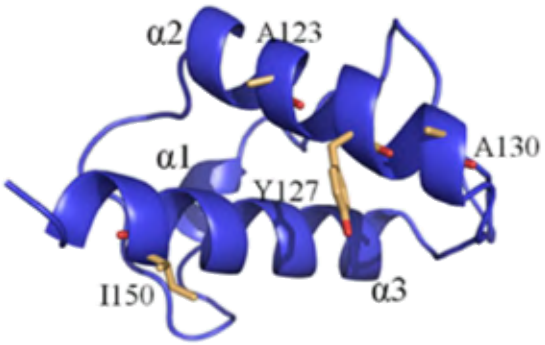

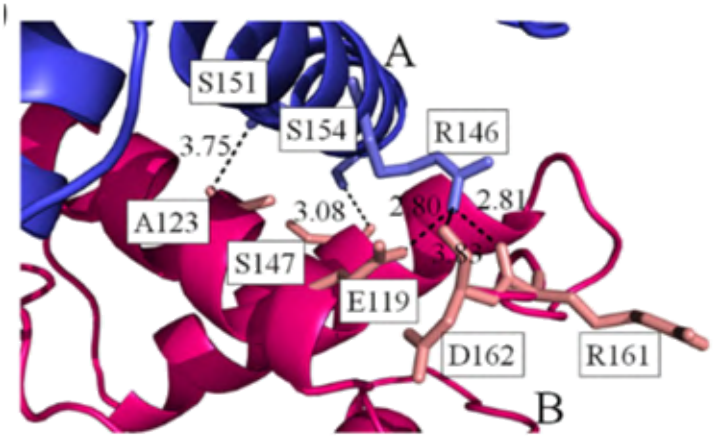

- DnaTc 單體（monomer）透過許多疏水性交互作用相互連接，如圖可以看出 DnaTc 的單體-單體（monomer-monomer）是由疏水性作用穩定其中心結構，即次單元 A 中的 A123(α2)，Y127(α2)，A130（α2）和 I150（α3），和 A122（ 次單元 B 中的 α2），A123-（α2），I125（α2），A126（α2），Y127（α2），A130（α2）-和 I150（α3），此外，還有 5 個氫鍵位在 DnaTc 的單體-單體（monomer-monomer）作用區的（R146-E119、R146-D162、R146-R161、S151-A123 和 S154-S147）。

3-2-10 StyDnaT 84~179（DnaTc）與 DnaT 84~153 氫鍵形成之差異

StyDnaT 84~179（DnaTc）

Hydrogen bonds			Salt bridges		
Subunit A	Subunit B	Dist. [Å]	Subunit A	Subunit B	Dist. [Å]
R146 [NH1]	E119 [OE1]	2.80	R146 [NH1]	E119 [OE1]	2.80
R146 [NH1]	D162 [O]	3.83	R146 [NH1]	E119 [OE2]	3.79
R146 [NH1]	R161 [O]	2.81	R146 [NH1]	D162 [O]	3.83
S151 [OG]	A123 [O]	3.75			
S154 [OG]	S147 [O]	3.08			

DnaT 84~153

Hydrogen bonds					
Subunit A	Subunit B	Subunit C	Subunit D	Subunit E	Dist. [Å]
		E131 [OE2]	K88 [NZ]		3.14
		Y127 [O]	Q139 [NE2]		3.29
		E131 [OE1]	Q139 [NE2]		3.16
		S123 [O]	Q142 [NE2]		2.80
		S123 [OG]	Q142 [NE2]		3.13
	S123 [O]	Q142 [NE2]			2.83
	S123 [OG]	Q142 [NE2]			3.26
	Y127 [O]	Q139 [NE2]			3.17
	E131 [OE1]	Q139 [NE2]			3.03
			E131 [OE2]	K88 [NZ]	2.98
			Y127 [O]	Q139 [NE2]	2.99
			E131 [OE1]	Q139 [NE2]	2.85
			S123 [O]	Q142 [NE2]	2.73
			S123 [OG]	Q142 [NE2]	3.12
S123 [O]	Q142 [NE2]				2.86
S123 [OG]	Q142 [NE2]				3.43
Y127 [O]	Q139 [NE2]				3.11
E131 [OE1]	Q139 [NE2]				2.80

- 由於 DnaT84-153 長度較短，因此不具有 R161 和 D162 與 R146 的氫鍵， DnaT84-153 中 R146 的側鏈向外突出，因此可與作用 ssDNA 結合，而不是二聚化，由於 DnaTc 長度較長，在 DnaT84-153 中未發現在 DnaTc 中形成的氫鍵 R146-E119，S151-A123 和 S154-S147。

3-2-11 StyDnaT 84~179（DnaTc）二聚化以及與 ssDNA 結合變化

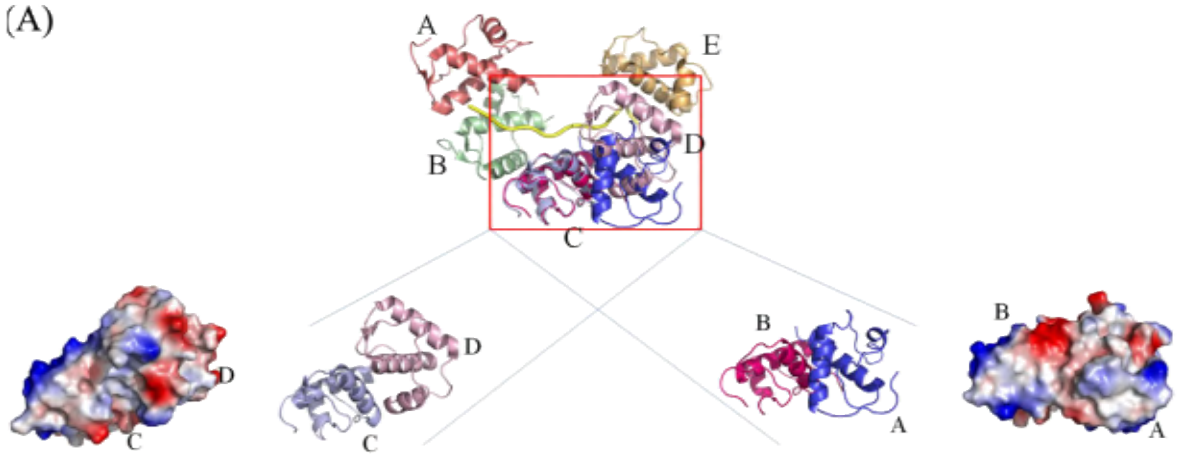

- DnaT84-153 中的 K133、K143 和 R146 是 ssDNA 結合的氨基酸，這些帶正電荷的氨基酸之間有助於形成用於與 ssDNA 相互作用的中心，R146A 突變體顯示，會明顯使得 ssDNA 結合能力下降。

3-2-12 StyDnaT 84~179（DnaTc）二聚化以及與 ssDNA 結合疊加顯示(superposition)

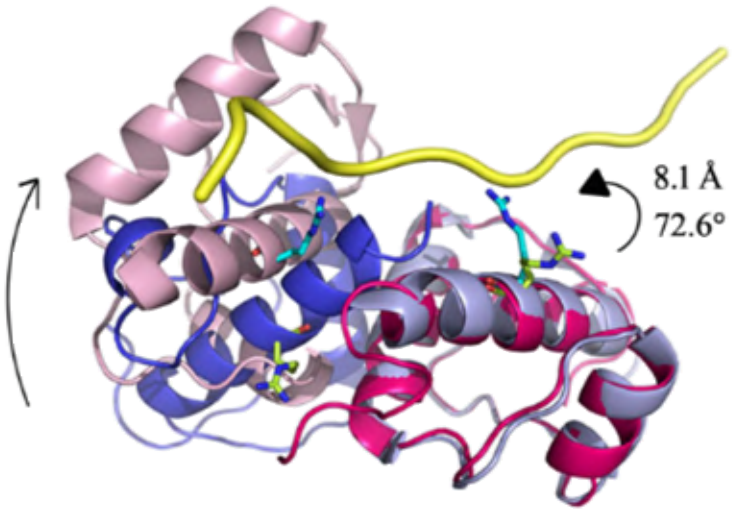

Superposition

- DnaTc 結構分析進一步揭示了 R146 在二聚化中的另一個作用，為了與 DnaT84-153 複合物中的 ssDNA 結合，DnaTc 會產生大幅度的構型變化使得 K133，K143 和 R146 暴露出來並去接觸 ssDNA。經過疊加分析進一步發現，如果與 DnaT84-153 複合物互相結合（疊合），則 DnaTc 的單體 B 中的 R146 必須移動 8.1 Å 的距離和 72.6°的角度，而 DnaTc 的單體 A 必須移開 7.5 Å 的距離和 170°的角度（y 軸）和 4.5°（z 軸）的角度才得以形成五聚體。

3-2-13 StyDnaT 84~179（DnaTc）與 ssDNA 作用之型態變化機制卡通示意圖

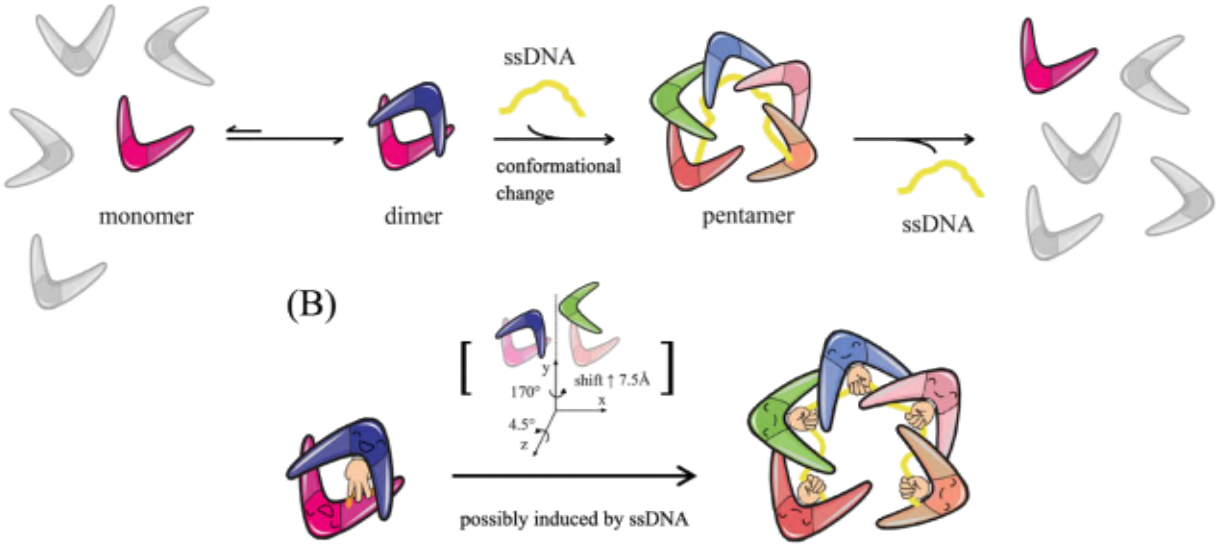

- DnaT 寡聚體的寡聚化和分解狀態的再組裝中是極為重要的，基於這些結果，我們提出了一個卡通模型，來顯示 DnaTc 單體（迴旋鏢）如何作為五聚體而產生寡聚化，這是一個可能由 ssDNA 結合誘導的過程，當存在 ssDNA 時，發生強烈的型態構型變化。R146 是 ssDNA 結合的關鍵胺基酸，並且不再位於 DnaTc 的單體-單體交互作用界面上，在 ssDNA 結合期間，最初用於 DnaTc 二聚化的氫鍵網絡將被重排以促進 DnaTc 寡聚化，作為高度有序的寡聚體如五聚體，而當 ssDNA 解離時，迴旋鏢 DnaTc 可透過在單體-單體交互作用界面處重建氫鍵網絡而形成二聚體。

3-3 SaSsbB 相關實驗結果

3-3-1 SaSsbB 純化（SDS-PAGE）

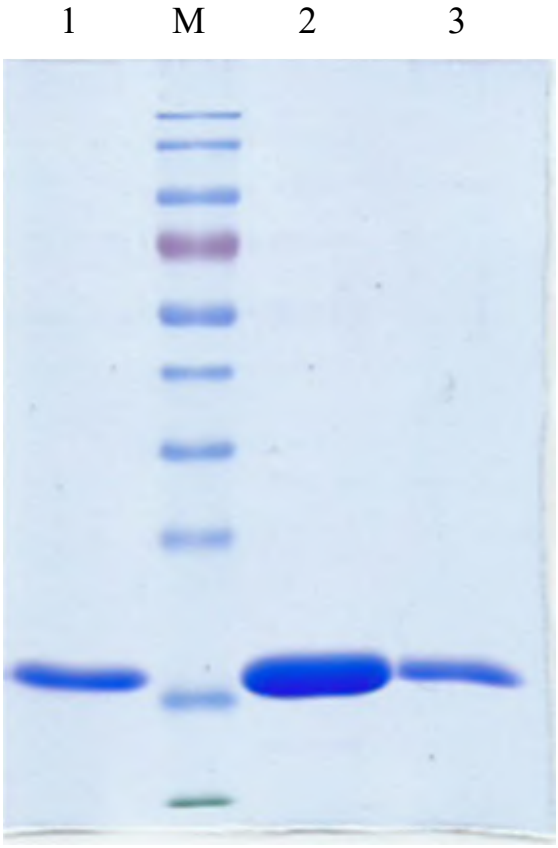

- 蛋白質表現與純化。利用轉型大腸桿菌來大量表達重組蛋白質，經由放大培養後，再透過IPTG 誘導表現目標蛋白，經過高速低溫離心、超音波破菌後，利用Ni-NTA column，透過金屬親和性管柱層析法進行蛋白質純化，我們利用內含200 mM imidazole, 500 mM NaCl, pH 7.4 溶液純化出金黃色葡萄球菌SSB（SaSsbB）(lane 2)，從SDS-PAGE可以得知綠膿桿菌SSB (PaSSB)分子量約為15 kDa。

3-3-2 SaSsbB 晶體形成（懸吊法）

SaSsbB: (1-1)

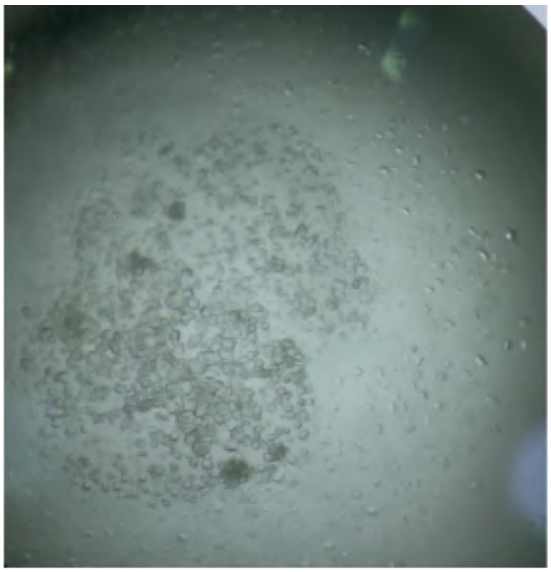

SaSsbB: (1-2)

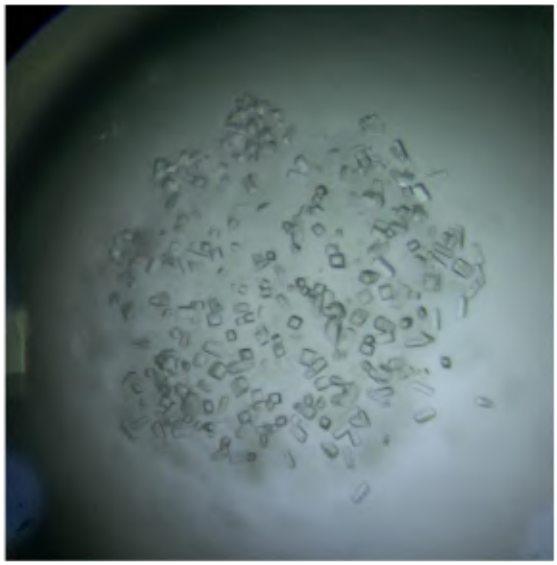

SaSsbB:(1-3)

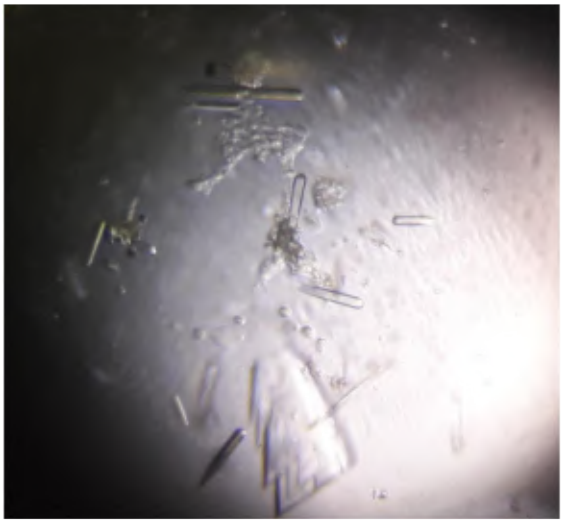

SaSsbB: (1-4)

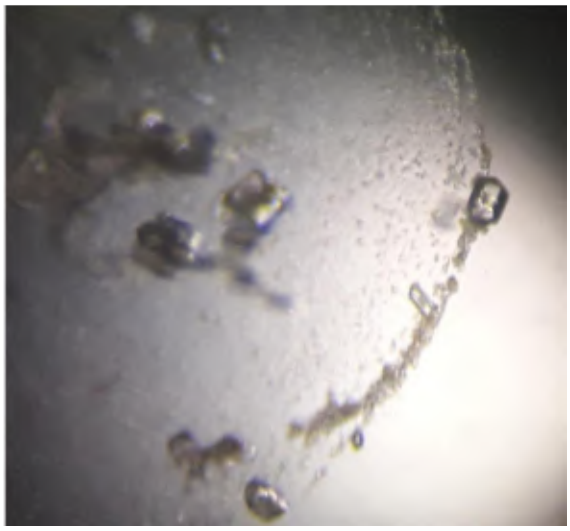

晶體名稱	長晶條件
SaSsbB: (1-1)	**20% PEG 10000、100 mM HEPES, pH 7.5**
SaSsbB: (1-2)	**30% PEG 10000、100 mM Tris-HCL, pH 8.5**
SaSsbB: (1-3)	**26% PEG 4000、100 mM Tris-HCL, pH 7.5、200 mM sodium acetate**
SaSsbB: (1-4)	**32% PEG 4000、100 mM Tris-HCL, pH 8.0、200 mM sodium acetate**

3-3-3 SaSsbB 結晶 X 光繞射相關數據

SaSsbB

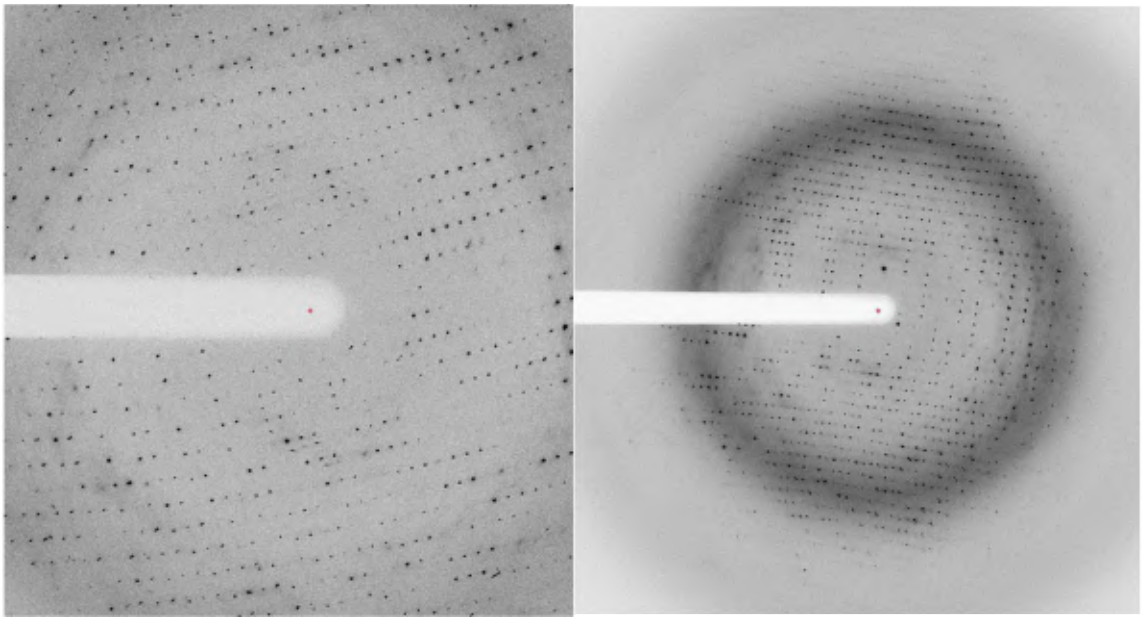

- **以下為金黃色葡萄球菌 SSB（SaSsbB）透過懸吊法（hanging drop method）獲得蛋白質結晶，經由 X 光繞射實驗後所獲得的繞射圖相關資訊：**

晶體到 Detector 間的距離（Distance）	300 mm
X 光繞射之晶體曝光時間（Time）	20 s
數據收集之晶體繞射角度範圍（Phi）	0～100 deg
數據收集之晶體轉動幅度（Delta）	1 deg
數據收集之晶體繞射圖張數（Frame）	100
晶體解析度（Resolution）	30Å～2.98Å
晶體之晶格對稱性（Space group）	$P2_12_12$

3-3-4 SaSsbB 結晶結構統計分析表

Data collection	
Crystal	SaSsbB
Wavelength (Å)	0.975
Resolution (Å)	30–2.98
Space group	$P2_12_12_1$
Cell dimension (Å)	$a = 63.99, \alpha = 90$ $b = 84.74, \beta = 90$ $c = 84.86, \gamma = 90$
Completeness (%)	99.8 (99.8)[a]
$\langle I/\sigma I \rangle$	13 (2.5)
R_{sym} or R_{merge} (%)[b]	0.125 (0.541)
Redundancy	3.8 (4.0)
Refinement	
Resolution (Å)	30–2.98
No. reflections	9334
R_{work}/R_{free}	0.2139/0.2995
No. atoms	
Protein	399
Water	16
R.m.s deviation	
Bond lengths (Å)	0.011
Bond angles (°)	1.385
Ramachandran plot	
In preferred regions	359 (93.25%)
In allowed regions	20 (5.19%)
Outliers	6 (1.56%)
PDB entry	5YYU

- 此為金黃色葡萄球菌 SSB（SaSsbB）的結晶結構統計分析表，經過 X 光繞射實驗後，並透過 HKL2000 計算各個繞射圖中繞射點，可得知相關結構資訊，包括 Space group、Resolution、PDB entry 等資訊

3-3-5 SaSsbB 結晶結構

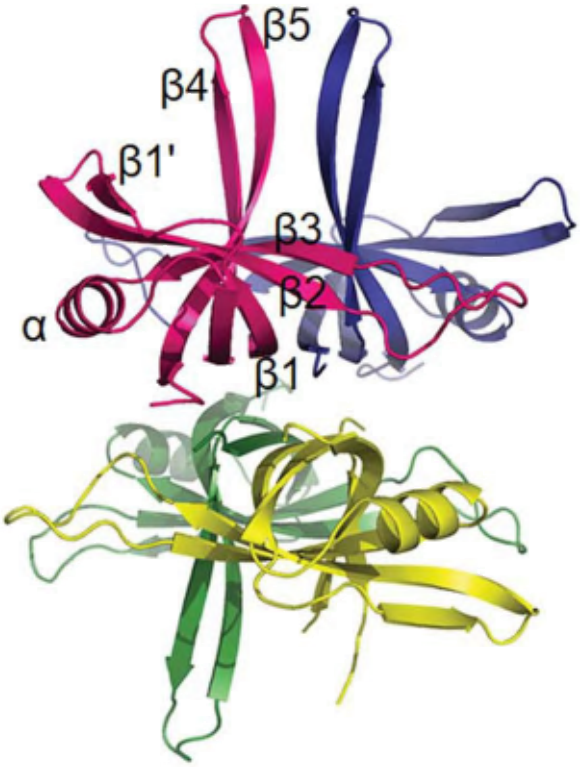

- 此為金黃色葡萄球菌 SSB（SaSsbB）之結晶結構圖，SaSsbB 由四個 OB-fold 之 monomer 組成四套體，其結晶結構皆顯示 N 端具有一明顯的 OB-fold domain 包含一個結構緊實的 β 桶型折疊(β-barrel)與一個內延伸的蓋頭 α 螺旋(α-helix)，而 SaSsbB 的結構中並沒有 β6

3-3-6 SaSsbB 結晶結構（與 ssDNA 交互作用區）

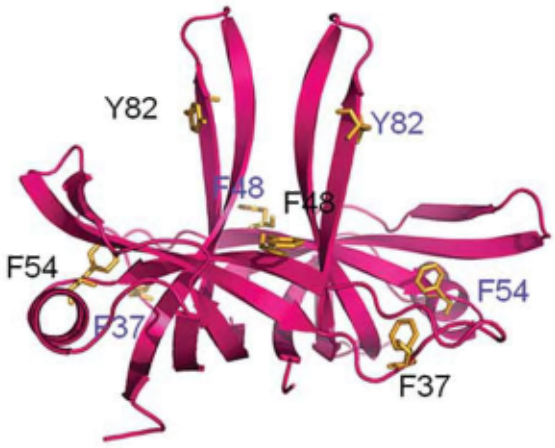

- 金黃色葡萄球菌 SSB（SaSsbB）中的 4 個極保留的芳香環胺基酸(Phe37 、Phe48 、Phe54、Tyr82)參與了 SSB 與單股 DNA 的交互作用，並引導 DNA 在 SSB 上的纏繞。

3-3-7 SaSsbB 定點突變（site-directed mutagenesis）分析

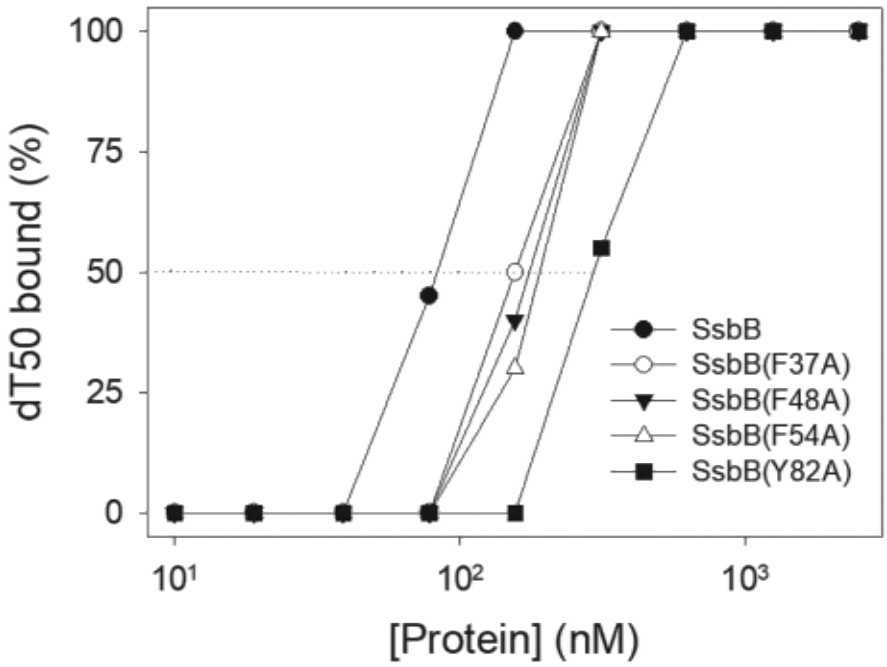

DNA	$[Protein]_{50}$ (nM)
dT15	> 2000
dT20	190 ± 8
dT30	164 ± 7
dT40	90 ± 4
dT40 (with 0.4 M NaCl)	382 ± 16

- 由結晶結構得知 SaSsbB 與 ssDNA 主要是透過四個芳香環的氨基酸 (Phe37 、Phe48 、Phe54、Tyr82) 進行交互作用，因此利用定點突變（Site-directed mutagenesis），將此四個胺基酸

突變成 alanine (側鏈為甲基)，來驗證 ssDNA 結合位與四個芳香環胺基酸之重要性。

3-3-8 SaSsbB 熱穩定性（Thermostability）分析

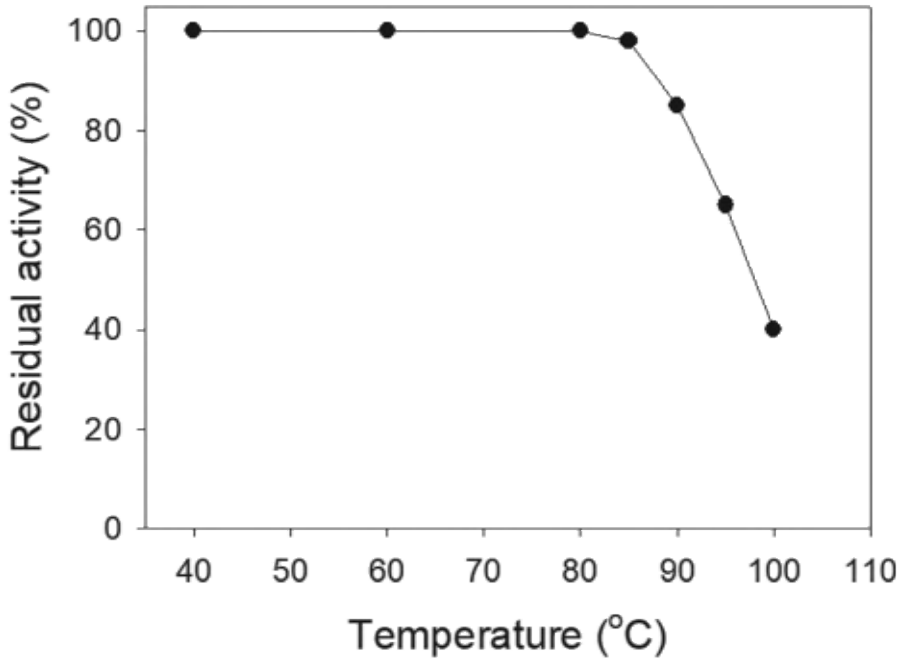

	The decreased activity (%)			
Temperature	SaSsbA	SaSsbB	SaSsbC	EcSSB
85 °C	2	2	2	
90 °C	15	15	20	
95 °C	35	35	40	50
100 °C	60	60	70	

- 此圖為金黃色葡萄球菌 SSB（SaSsbB）熱穩定性分析，我們發現了金黃色葡萄球菌 SSB 在 90-100 ℃ 下仍具高度活性，暗示 SSB 在生醫生技上有可能的應用性。

第四章：結論

在本計畫的執行下，經過篩選、不斷修飾多種結晶條件，再透過光學顯微鏡在不同時間來觀察晶體的生長情形後，已在不同條件中獲得金黃色葡萄球菌與綠膿桿菌的 SSB (SaSsbB 與 PaSSB) 結晶，其結晶結構的空間群 (space group) 分別為 $P2_12_12_1$ 與 C_12_1 而解析度分別是 2.98 Å 與 2.04 Å，兩者的結晶結構皆顯示 N 端具有一明顯的 OB-fold domain 包含一個結構緊實的 β 桶型折疊(β-barrel)與一個內延伸的蓋頭 α 螺旋(α-helix)。雖然兩者的 C 端序列大不相同，但因具高度空間活動性而無規則的結構可解析。結構為基礎的突變分析(structure-based mutational analysis)發現 4 個極保留的芳香環胺基酸參與了 SSB 與單股 DNA 的交互作用，並引導 DNA 在 SSB 上的纏繞。我們亦發現了金黃色葡萄球菌 SSB 在 90-100 ^oC 下仍具高度活性，暗示 SSB 在生醫生技上有可能的應用性。然而不同於大腸桿菌的模型，金黃色葡萄球菌 SSB 並無法刺激 PriA 解旋酶的活性，可能是 C 端序列的顯著差異所致。在抑制劑開發與機制研究方面，我們利用共結晶(co-crystallization)的技術亦在篩選數千種條件下得到綠膿桿菌 SSB 與抑制劑 myc (IC_{50} 為 3 μM) 以及 dT15 的三重的複合結晶(SSB-dT15-myc)，並順利解出相位角與結構。此複合結晶結構(complex structure)顯示 SSB 四套體與 3 個 myc 抑制劑以及 1 條 DNA

是以 4:3:1 的方式結合，其中 myc 卡在 SSB 的 DNA 結合槽中，並形成多個氫鍵，可能因此專一的抑制了 SSB 的活性，除了與 myc 抑制劑之複合結晶結構外，我們亦獲得了綠膿桿菌 SSB 與不同長度的 ssDNA（dT15、dT20、dT25）之複合結晶結構，以此更加了解綠膿桿菌 SSB 在不同長度的 ssDNA 作用後產生的變化，而能進一步探討不同的結合機制。而在 DnaT 方面，我們也獲得了其 C 端（DnaTc）之結晶結構，並探討了關於 DnaTc 在與 DNA 作用時如何產生寡聚化(oligomerization)而形成不同的寡聚體，也發現了 R146 是 ssDNA 結合的關鍵胺基酸。綜觀以上結果，本計畫所提出的計畫內容皆已完成預期目標，同時業已產出 2 篇 SCI 論文。所帶出下一階段的重點則包括需加以探討不同物種間之 SSB 以及 DnaT 等蛋白質的功能與特性，再來也需進一步針對 PaSSB 與長度更長的 ssDNA 以及不同的相關抑制劑進行結構上的探討，以更深入了解 SSB 與 DNA 的結合模式，並能找出有效抑制 SSB 之化合物，並能進一步優化、找出阻斷病原菌中 SSB 功能的有效途徑，提供醫療上實質的運用。

第五章：參考文獻

[1] D.N. Wilson, Ribosome-targeting antibiotics and mechanisms of bacterial resistance, Nat Rev Microbiol, 12 (2014) 35-48.

[2] D.K. Tempe, New Delhi metallo-beta-lactamase 1, Lancet Infect Dis, 10 (2010) 750-751; author reply 752-754.

[3] K. Bush, Alarming beta-lactamase-mediated resistance in multidrug-resistant Enterobacteriaceae, Curr Opin Microbiol, 13 (2010) 558-564.

[4] S. Stefani, S. Campana, L. Cariani, V. Carnovale, C. Colombo, M.M. Lleo, V.D. Iula, L. Minicucci, P. Morelli, G. Pizzamiglio, G. Taccetti, Relevance of multidrug-resistant Pseudomonas aeruginosa infections in cystic fibrosis, Int J Med Microbiol, 307 (2017) 353-362.

[5] J.W. Newman, R.V. Floyd, J.L. Fothergill, The contribution of Pseudomonas aeruginosa virulence factors and host factors in the establishment of urinary tract infections, FEMS Microbiol Lett, 364 (2017).

[6] W.H. Zhao, Z.Q. Hu, Beta-lactamases identified in clinical isolates of Pseudomonas aeruginosa, Crit Rev Microbiol, 36 (2010) 245-258.

[7] Y.H. Huang, C.Y. Huang, SAAV2152 is a single-stranded DNA binding protein: the third SSB in Staphylococcus aureus, Oncotarget, 9 (2018) 20239-20254.

[8] A.F. Voter, M.P. Killoran, G.E. Ananiev, S.A. Wildman, F.M. Hoffmann, J.L. Keck, A High-Throughput Screening Strategy to Identify Inhibitors of SSB Protein-Protein Interactions in an Academic Screening Facility, SLAS Discov, (2017) 2472555217712001.

[9] T.A. Windgassen, S.R. Wessel, B. Bhattacharyya, J.L. Keck, Mechanisms of bacterial DNA replication restart, Nucleic Acids Res, 46 (2018) 504-519.

[10] E. Antony, T.M. Lohman, Dynamics of E. coli single stranded DNA binding (SSB) protein-DNA complexes, Semin Cell Dev Biol, (2018).

[11] B. Michel, S.J. Sandler, Replication Restart in Bacteria, J Bacteriol, (2017).

[12] D. Zhang, M. O'Donnell, The Eukaryotic Replication Machine, Enzymes, 39 (2016) 191-229.

[13] L.V. Croft, E. Bolderson, M.N. Adams, S. El-Kamand, R. Kariawasam, L. Cubeddu, R. Gamsjaeger, D.J. Richard, Human single-stranded DNA binding protein 1 (hSSB1, OBFC2B), a critical component of the DNA damage response, Semin Cell Dev Biol, 86 (2019) 121-128.

[14] B.M. Byrne, G.G. Oakley, Replication protein A, the laxative that keeps DNA regular: The importance of RPA phosphorylation in maintaining genome stability, Semin Cell Dev Biol, (2018).

[15] R.D. Shereda, A.G. Kozlov, T.M. Lohman, M.M. Cox, J.L. Keck, SSB as an organizer/mobilizer of genome maintenance complexes, Crit Rev Biochem Mol Biol, 43 (2008) 289-318.

[16] P.R. Bianco, The tale of SSB, Prog Biophys Mol Biol, 127 (2017) 111-118.

[17] T.A. Windgassen, M. Leroux, K.A. Satyshur, S.J. Sandler, J.L. Keck, Structure-specific DNA replication-fork recognition directs helicase and replication restart activities of the PriA helicase, Proc Natl Acad Sci U S A, 115 (2018) E9075-e9084.

[18] C.J. Cadman, P. McGlynn, PriA helicase and SSB interact physically and functionally, Nucleic Acids Res, 32 (2004) 6378-6387.

[19] Y.H. Huang, M.J. Lin, C.Y. Huang, Yeast two-hybrid analysis of PriB-interacting proteins in replication restart primosome: a proposed PriB-SSB interaction model, Protein J, 32 (2013) 477-483.

[20] R.R. Meyer, P.S. Laine, The single-stranded DNA-binding protein of Escherichia coli, Microbiol Rev, 54 (1990) 342-380.

[21] T.M. Lohman, M.E. Ferrari, Escherichia coli single-stranded DNA-binding protein: multiple DNA-binding modes and cooperativities, Annu Rev Biochem, 63 (1994) 527-570.

[22] T.H. Dickey, S.E. Altschuler, D.S. Wuttke, Single-stranded DNA-binding proteins: multiple domains for multiple functions, Structure, 21 (2013) 1074-1084.

[23] A.G. Murzin, OB(oligonucleotide/oligosaccharide binding)-fold: common structural and functional solution for non-homologous sequences, EMBO J, 12 (1993) 861-867.

[24] S. Raghunathan, A.G. Kozlov, T.M. Lohman, G. Waksman, Structure of the DNA binding domain of E. coli SSB bound to ssDNA, Nat Struct Biol, 7 (2000) 648-652.

[25] C. Yang, U. Curth, C. Urbanke, C. Kang, Crystal structure of human mitochondrial single-stranded DNA binding protein at 2.4 A resolution, Nat Struct Biol, 4 (1997) 153-157.

[26] H.Y. Tan, L.A. Wilczek, S. Pottinger, M. Manosas, C. Yu, T. Nguyenduc, P.R. Bianco, The intrinsically disordered linker of E. coli SSB is critical for the release from single-stranded DNA, Protein Sci, 26 (2017) 700-717.

[27] P.R. Bianco, S. Pottinger, H.Y. Tan, T. Nguyenduc, K. Rex, U. Varshney, The IDL of E. coli SSB links ssDNA and protein binding by mediating protein-protein interactions, Protein Sci, 26 (2017) 227-241.

[28] P.R. Bianco, Y.L. Lyubchenko, SSB and the RecG DNA helicase: an intimate association to rescue a stalled replication fork, Protein Sci, 26 (2017) 638-649.

[29] M.M. Cox, M.F. Goodman, K.N. Kreuzer, D.J. Sherratt, S.J. Sandler, K.J. Marians, The importance of repairing stalled replication forks, Nature, 404 (2000) 37-41.

[30] Y.H. Huang, C.Y. Huang, Structural insight into the DNA-binding mode of the primosomal proteins PriA, PriB, and DnaT, Biomed Res Int, 2014 (2014) 195162.

[31] S.J. Sandler, K.J. Marians, Role of PriA in replication fork reactivation in Escherichia coli, J Bacteriol, 182 (2000) 9-13.

[32] K.J. Marians, PriA-directed replication fork restart in Escherichia coli, Trends Biochem Sci, 25 (2000) 185-189.

[33] C.C. Huang, C.Y. Huang, DnaT is a PriC-binding protein, Biochem Biophys Res Commun, 477 (2016) 988-992.

[34] Y.H. Huang, M.J. Lin, C.Y. Huang, DnaT is a single-stranded DNA binding protein, Genes Cells, 18 (2013) 1007-1019.

[35] M. Lopper, R. Boonsombat, S.J. Sandler, J.L. Keck, A hand-off mechanism for primosome assembly in replication restart, Mol Cell, 26 (2007) 781-793.

[36] Y.H. Huang, H.H. Guan, C.J. Chen, C.Y. Huang, Staphylococcus aureus single-stranded DNA-binding protein SsbA can bind but cannot stimulate PriA helicase, PLoS One, 12 (2017) e0182060.

[37] Y.H. Huang, Y. Lien, C.C. Huang, C.Y. Huang, Characterization of *Staphylococcus aureus* primosomal DnaD protein: highly conserved C-terminal region is crucial for ssDNA and PriA helicase binding but not for DnaA protein-binding and self-tetramerization, PLoS One, 11 (2016) e0157593.

[38] Y.H. Huang, Huang, C.Y., The glycine-rich flexible region in SSB is crucial for PriA stimulation, RSC Adv., 8 (2018) 35280-35288.

[39] K.L. Chen, Cheng, J.H., Lin, C.Y., Huang, Y.H., Huang, C.Y., Characterization of single-stranded DNA-binding protein SsbB from Staphylococcus aureus: SsbB cannot stimulate PriA helicase, RSC Adv., 8 (2018) 28367-28375.

[40] R. Schekman, A. Weiner, A. Kornberg, Multienzyme systems of DNA replication, Science, 186 (1974) 987-993.

[41] J.Y. Ng, K.J. Marians, The ordered assembly of the phiX174-type primosome. II. Preservation of primosome composition from assembly through replication, J Biol Chem, 271 (1996) 15649-15655.

[42] J.Y. Ng, K.J. Marians, The ordered assembly of the phiX174-type primosome. I. Isolation and identification of intermediate protein-DNA complexes, J Biol Chem, 271 (1996) 15642-15648.

[43] J. Liu, P. Nurse, K.J. Marians, The ordered assembly of the phiX174-type primosome. III. PriB facilitates complex formation between PriA and DnaT, J Biol Chem, 271 (1996) 15656-15661.

[44] M.R. Szymanski, M.J. Jezewska, W. Bujalowski, Energetics of the Escherichia coli DnaT protein trimerization reaction, Biochemistry, 52 (2013) 1858-1873.

[45] Z. Liu, P. Chen, X. Wang, G. Cai, L. Niu, M. Teng, X. Li, Crystal structure of DnaT84-153-dT10 ssDNA complex reveals a novel single-stranded DNA binding mode, Nucleic Acids Res, 42 (2014) 9470-9483.

[46] S. Fujiyama, Y. Abe, M. Shiroishi, Y. Ikeda, T. Ueda, Insight into the interaction between PriB and DnaT on bacterial DNA replication restart: Significance of the residues on PriB dimer interface and highly acidic region on DnaT, Biochim Biophys Acta Proteins Proteom, 1867 (2019) 367-375.

[47] Y.H. Huang, Y.H. Lo, W. Huang, C.Y. Huang, Crystal structure and DNA-binding mode of *Klebsiella pneumoniae* primosomal PriB protein, Genes Cells, 17 (2012) 837-849.

[48] C.Y. Huang, C.H. Hsu, Y.J. Sun, H.N. Wu, C.D. Hsiao, Complexed crystal structure of replication restart primosome protein PriB reveals a novel single-stranded DNA-binding mode, Nucleic Acids Res, 34 (2006) 3878-3886.

[49] K.L. Chen, Y.H. Huang, J.F. Liao, W.C. Lee, C.Y. Huang, Crystal structure of the C-terminal domain of the primosomal DnaT protein: Insights into a new oligomerization mechanism, Biochem Biophys Res Commun, 511 (2019) 1-6.

[50] J.A. Marsh, H. Hernandez, Z. Hall, S.E. Ahnert, T. Perica, C.V. Robinson, S.A. Teichmann, Protein complexes are under evolutionary selection to assemble via ordered pathways, Cell, 153 (2013) 461-470.

[51] N. Unwin, A. Miyazawa, J. Li, Y. Fujiyoshi, Activation of the nicotinic acetylcholine receptor involves a switch in conformation of the alpha subunits, J Mol Biol, 319 (2002) 1165-1176.

[52] J.H. Cheng, C.C. Huang, Y.H. Huang, C.Y. Huang, Structural Basis for pH-Dependent Oligomerization of Dihydropyrimidinase from Pseudomonas aeruginosa PAO1, Bioinorg Chem Appl, 2018 (2018) 9564391.

[53] C.T. Tzeng, Y.H. Huang, C.Y. Huang, Crystal structure of dihydropyrimidinase from Pseudomonas aeruginosa PAO1: Insights into the molecular basis of formation of a dimer, Biochem Biophys Res Commun, 478 (2016) 1449-1455.

[54] M.R. Szymanski, M.J. Jezewska, W. Bujalowski, The Escherichia coli primosomal DnaT protein exists in solution as a monomer-trimer equilibrium system, Biochemistry, 52 (2013) 1845-1857.

第六章：附錄

其他與執行計畫有關之內容，然尚未成形足夠成為明顯結果部分我們將其整理成附錄，待未來持續研究。

StyDnaT84~179（DnaTc）純化（SDS-PAGE）

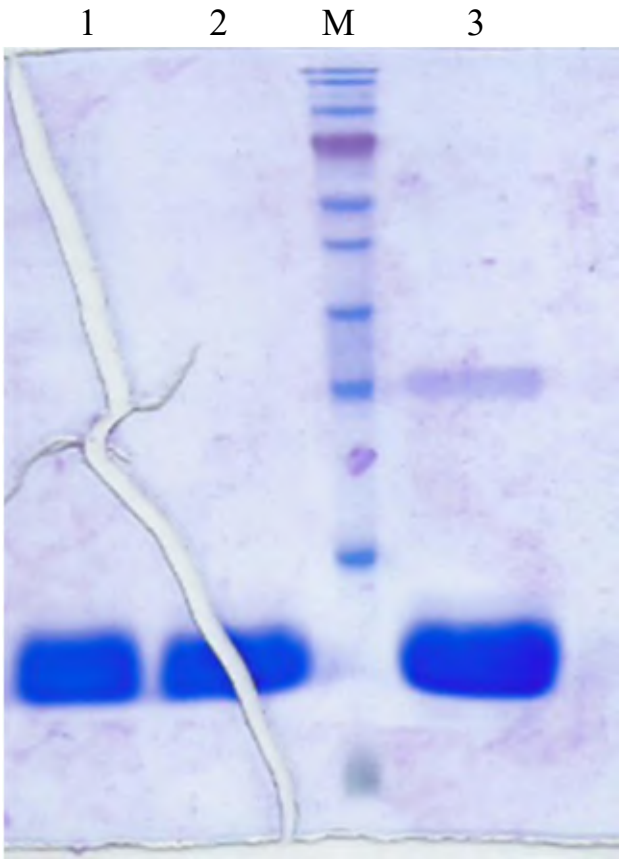

- 蛋白質表現與純化。利用轉型大腸桿菌來大量表達重組蛋白質，經由放大培養後，再透過IPTG 誘導表現目標蛋白，經過高速低溫離心、超音波破菌後，利用Ni-NTA column，透過金屬親和性管柱層析法進行蛋白質純化，我們利用內含 200 mM imidazole,

500 mM NaCl, pH 7.4 溶液純化出StyDnaT84~179（DnaTc） (lane 2)，從SDS-PAGE可以得知StyDnaT84~179（DnaTc）分子量約為 11kDa。

- **PaSSB（soaking glutaraldehyde）晶體成長**

PaSSB: (1-1)

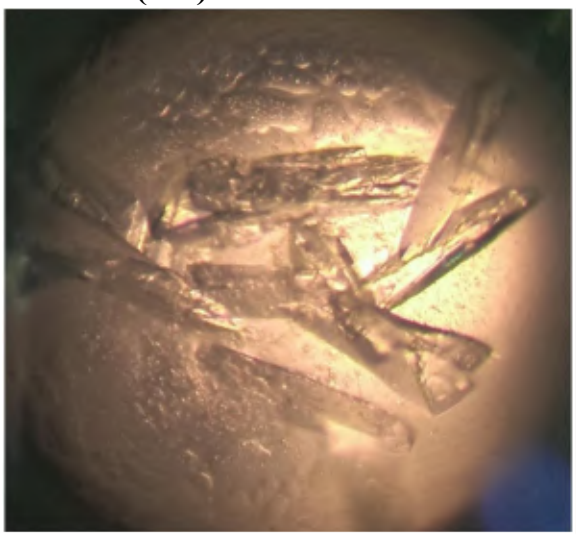

PaSSB: (1-2)

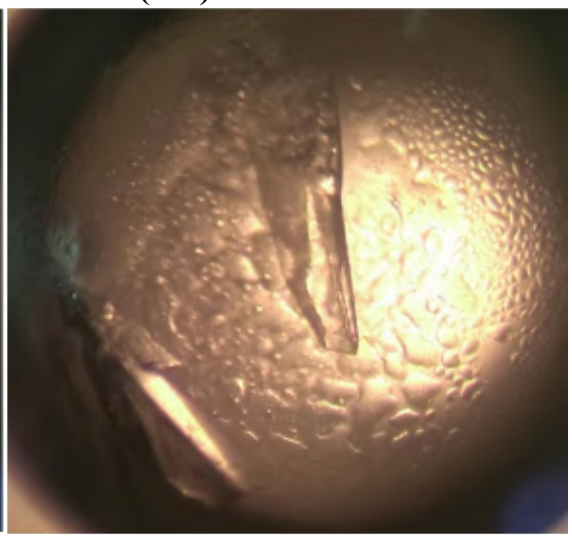

PaSSB: (1-3)

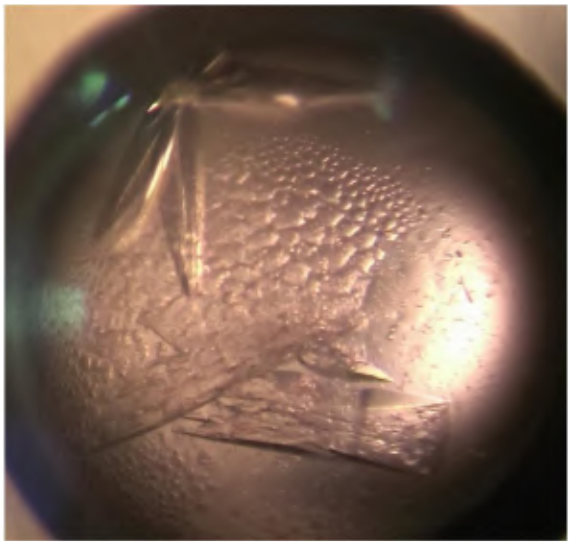

PaSSB: (1-4)

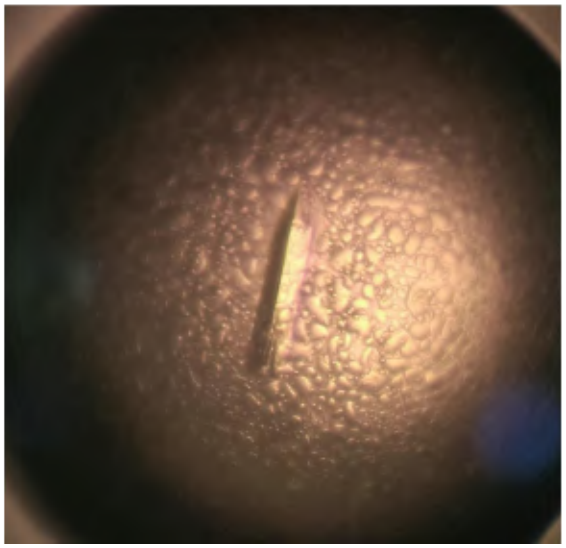

晶體名稱	長晶條件
PaSSB: (1-1)	**16%PEG4000 、 200 mM Lithium**

	Sulfate、100 mM Tris-HCL pH 8.5
PaSSB: (1-2)	16%PEG4000 、 200 mM Lithium Sulfate、100 mM Tris-HCL pH 8.5
PaSSB: (1-3)	8%PEG4000 、 800 mM Lithium Chloride、100 mM Tris-HCL pH 8.5
PaSSB: (1-4)	8%PEG4000 、 800 mM Lithium Chloride、100 mM Tris-HCL pH 8.5

- **KpDnaT+ssDNA 晶體成長**

KpDnaT+ssDNA: (2-1)

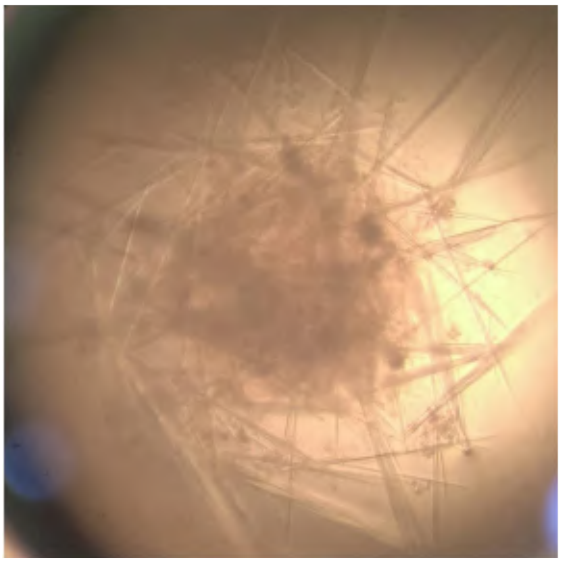

KpDnaT+ssDNA: (2-2)

KpDnaT+ssDNA: (2-3)

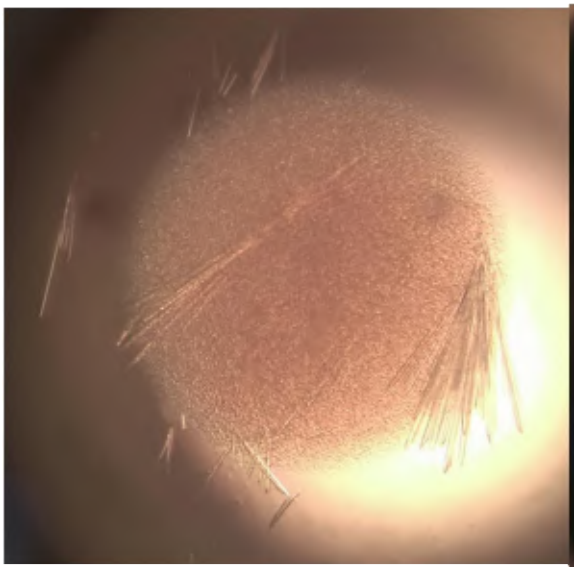

KpDnaT+ssDNA: (2-4)

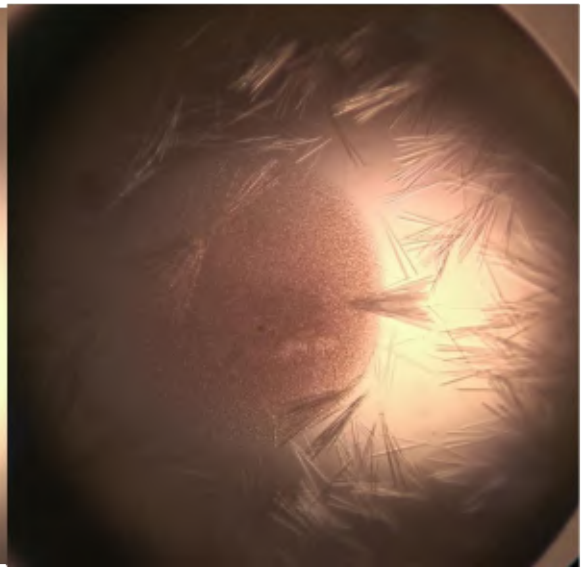

晶體名稱	長晶條件
KpDnaT+ssDNA: (2-1)	16%PEG4000 、 200 mM Lithium Sulfate、100 mM Tris-HCL pH 8.5
KpDnaT+ssDNA: (2-2)	16%PEG4000 、 200 mM Lithium Sulfate、100 mM Tris-HCL pH 8.5
KpDnaT+ssDNA: (2-3)	8%PEG4000 、 800 mM Lithium Chloride、100 mM Tris-HCL pH 8.5
KpDnaT+ssDNA: (2-4)	8%PEG4000 、 800 mM Lithium Chloride、100 mM Tris-HCL pH 8.5

- **KpDnaT+ssDNA 晶體成長**

KpDnaT+ssDNA: (3-1)

KpDnaT+ssDNA: (3-2)

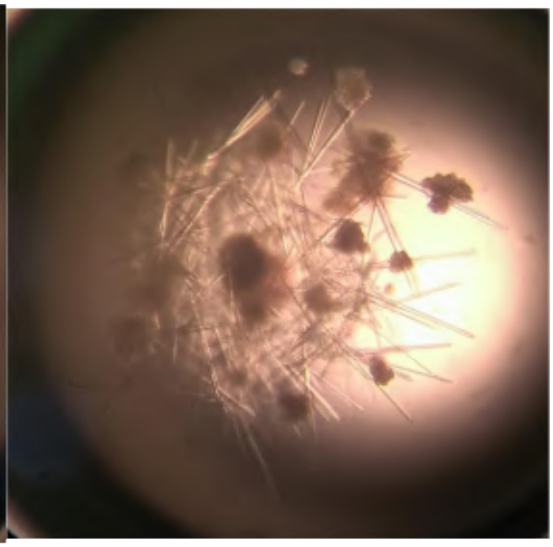

KpDnaT+ssDNA: (3-3)

KpDnaT+ssDNA: (3-4)

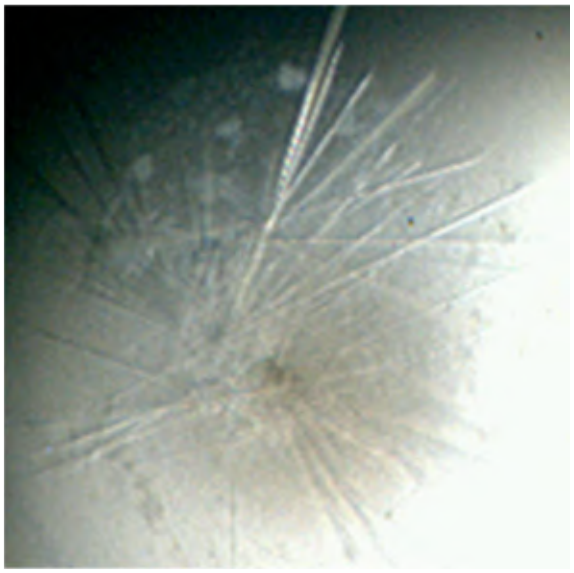

晶體名稱	長晶條件
KpDnaT+ssDNA: (3-1)	25%PEG 5000 MME、200 mM Lithium Sulfate、100 mM Tris-HCL pH 8.5
KpDnaT+ssDNA: (3-2)	25%PEG 5000 MME、200 mM Lithium Sulfate、100 mM Tris-HCL pH 8.5
KpDnaT+ssDNA:(3-3)	25%PEG 5000 MME、200 mM Lithium Sulfate、100 mM Tris-HCL pH 8.5
KpDnaT+ssDNA: (3-4)	20%PEG3000 、 200 mM Sodium Acetate 、100 mM HEPES ,pH 7.5

- **KpDnaT+ssDNA 晶體成長**

KpDnaT+ssDNA: (4-1)

KpDnaT+ssDNA: (4-2)

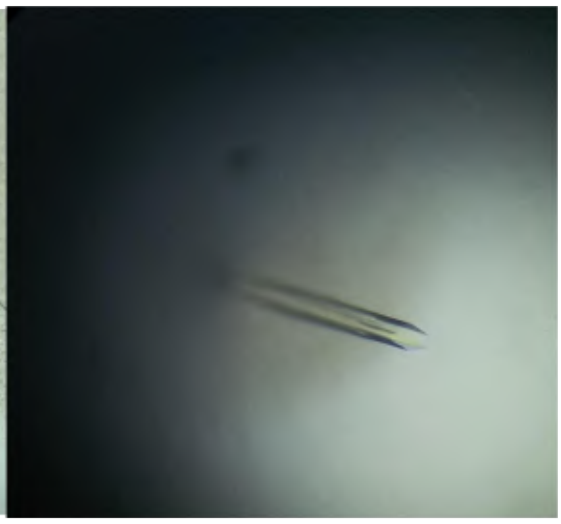

KpDnaT+ssDNA: (4-3)

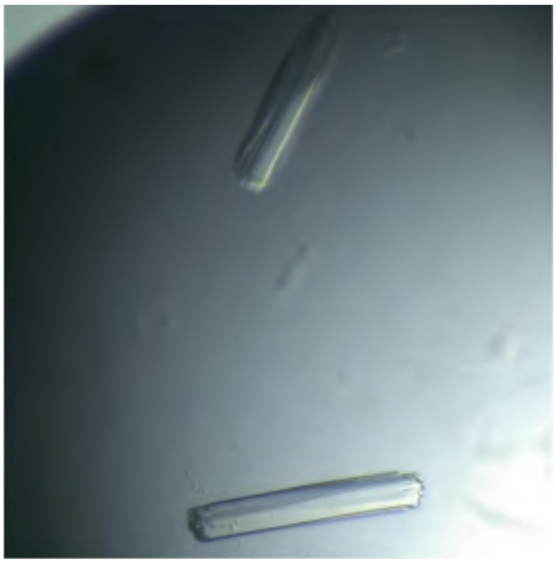

KpDnaT+ssDNA: (4-4)

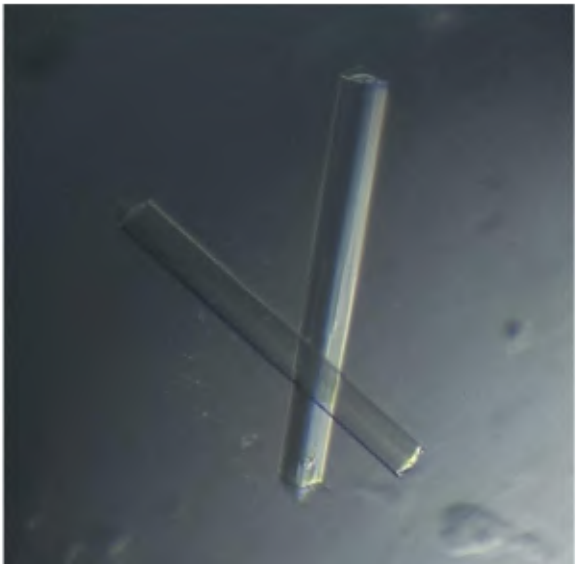

晶體名稱	長晶條件
KpDnaT+ssDNA: (4-1)	1M Ammonium sulfate、100 mM Tris-HCL ,pH 8.5
KpDnaT+ssDNA: (4-2)	1M Ammonium sulfate、100 mM Tris-HCL ,pH 8.5
KpDnaT+ssDNA:(4-3)	700 mM Lithium sulfate、100 mM Tris-HCL ,pH 8.5
KpDnaT+ssDNA: (4-4)	700 mM Lithium sulfate、100 mM Tris-HCL ,pH 8.5

- **KpDnaT+ssDNA 晶體成長**

KpDnaT+ssDNA: (5-1)

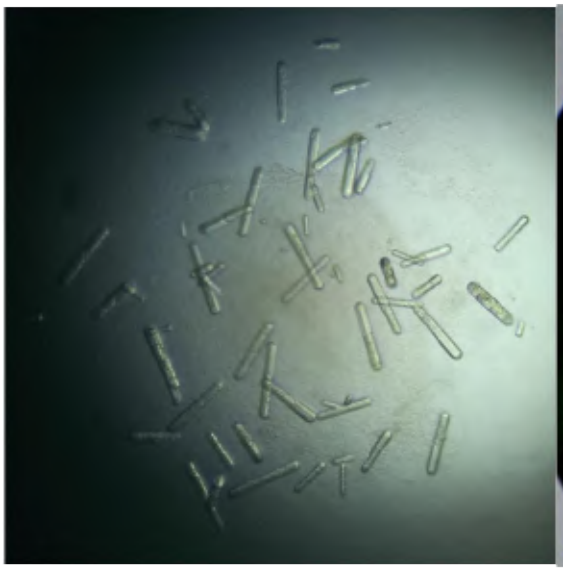

KpDnaT+ssDNA: (5-2)

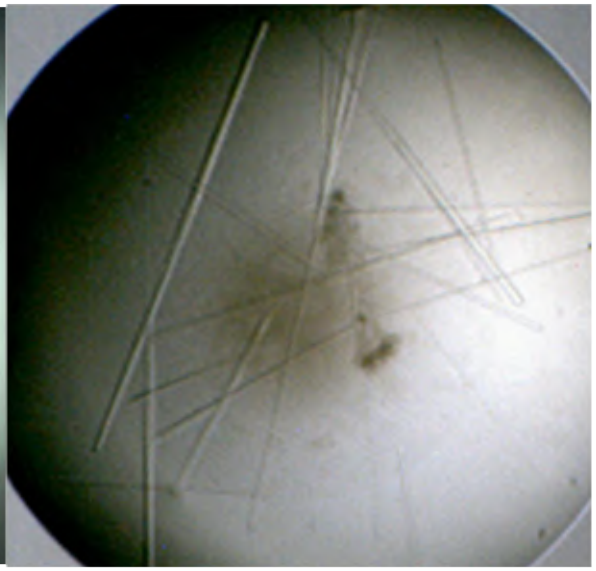

KpDnaT+ssDNA: (5-3)

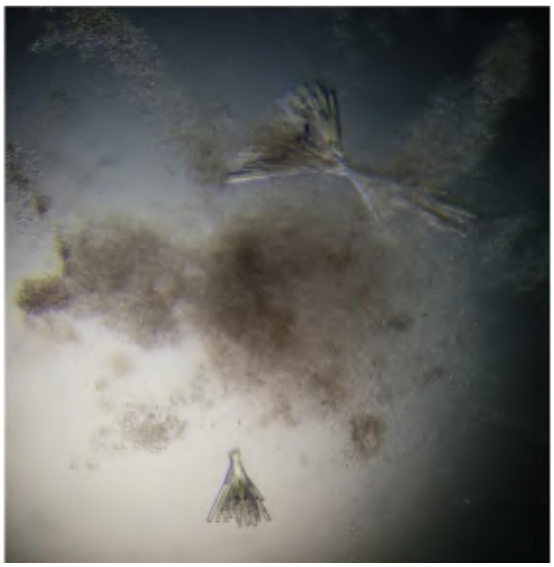

KpDnaT+ssDNA: (5-4)

晶體名稱	長晶條件
KpDnaT+ssDNA: (5-1)	1.6 M Magnesium sulfate、 100 mM MES ,pH 6.5
KpDnaT+ssDNA: (5-2)	22%PEG4000 、 100 mM Sodium Acetate、100 mM HEPES pH 7.5
KpDnaT+ssDNA:(5-3)	1.2M Magnesium sulfate、 100 mM MES, pH 6.0
KpDnaT+ssDNA: (5-4)	700 mM Lithium sulfate 、100 mM Tris-HCL ,pH 8.5

- **KpPriB-SSBc+KpDnaT＆ KpPriA + KpDnaT 晶體成長**

KpPriB-SSBc+KpDnaT: (6-1)

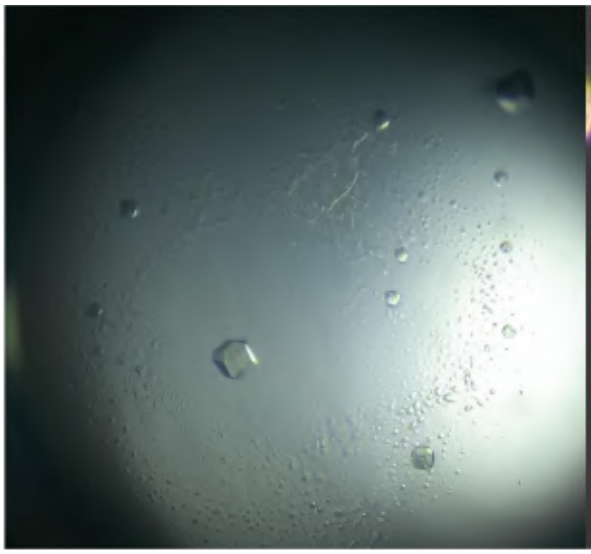

KpPriB-SSBc+KpDnaT: (6-2)

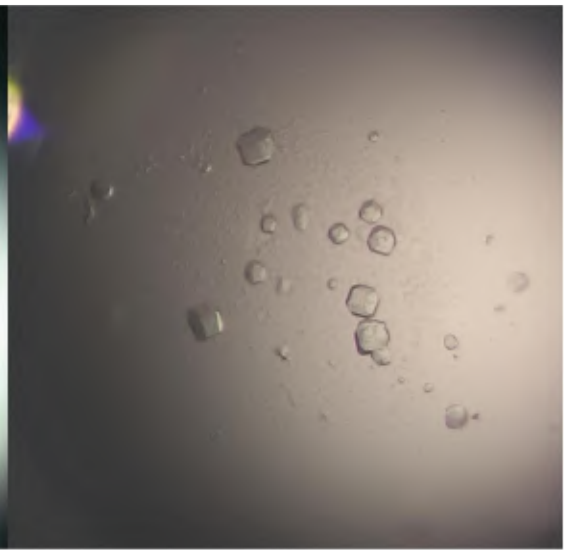

KpPriA + KpDnaT: (6-3)

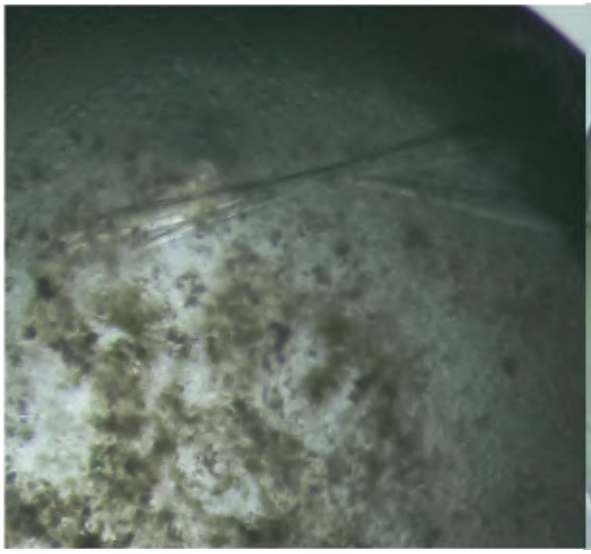

KpPriA + KpDnaT: (6-4)

晶體名稱	長晶條件
KpPriB-SSBc+KpDnaT: (6-1)	30% PEG 400、100 mM MES ,pH 6.5 、100 mM Sodium acetate
KpPriB-SSBc+KpDnaT: (6-2)	30% PEG 400、100 mM MES ,pH 6.5 、100 mM Sodium acetate
KpPriA + KpDnaT:(6-3)	2% PEG 1000、100 mM HEPES ,pH 6.5、1.4M Ammonium sulfate
KpPriA + KpDnaT:(6-4)	2% PEG 1000、100 mM HEPES ,pH 7.5、1.6M Ammonium sulfate

- **KpPriA + KpDnaT 晶體成長**

KpPriA + KpDnaT: (7-1)

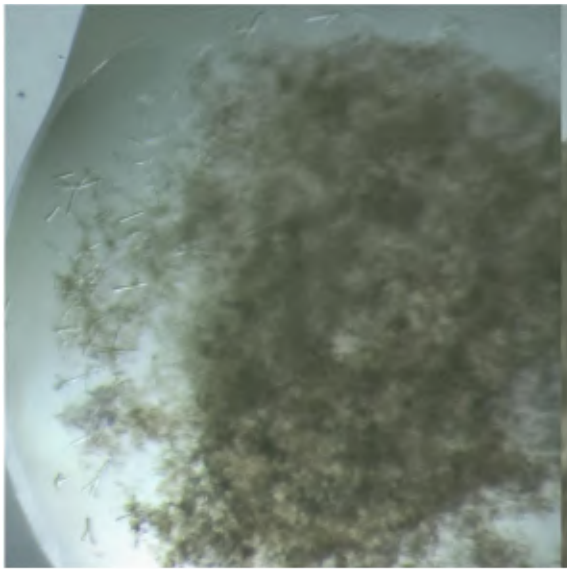

KpPriA + KpDnaT: (7-2)

KpPriA + KpDnaT: (7-3)

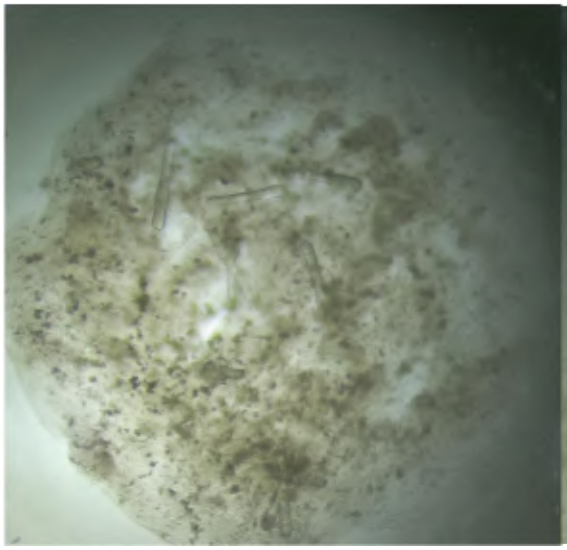

KpPriA + KpDnaT: (7-4)

晶體名稱	長晶條件
KpPriA + KpDnaT: (7-1)	**1% PEG 1000、100 mM HEPES ,pH 7.5、2.0M Ammonium sulfate**
KpPriA + KpDnaT: (7-2)	**1% PEG 1000、100 mM HEPES ,pH 7.5、1.8M Ammonium sulfate**
KpPriA + KpDnaT:(7-3)	**1% PEG 1000、100 mM HEPES ,pH 7.5、1.4M Ammonium sulfate**
KpPriA + KpDnaT:(7-4)	**1% PEG 1000、100 mM HEPES ,pH 7.5、1.6M Ammonium sulfate**

- 蛋白質結晶 X 光繞射相關數據

PaSSB + inhibitor（9-Me）

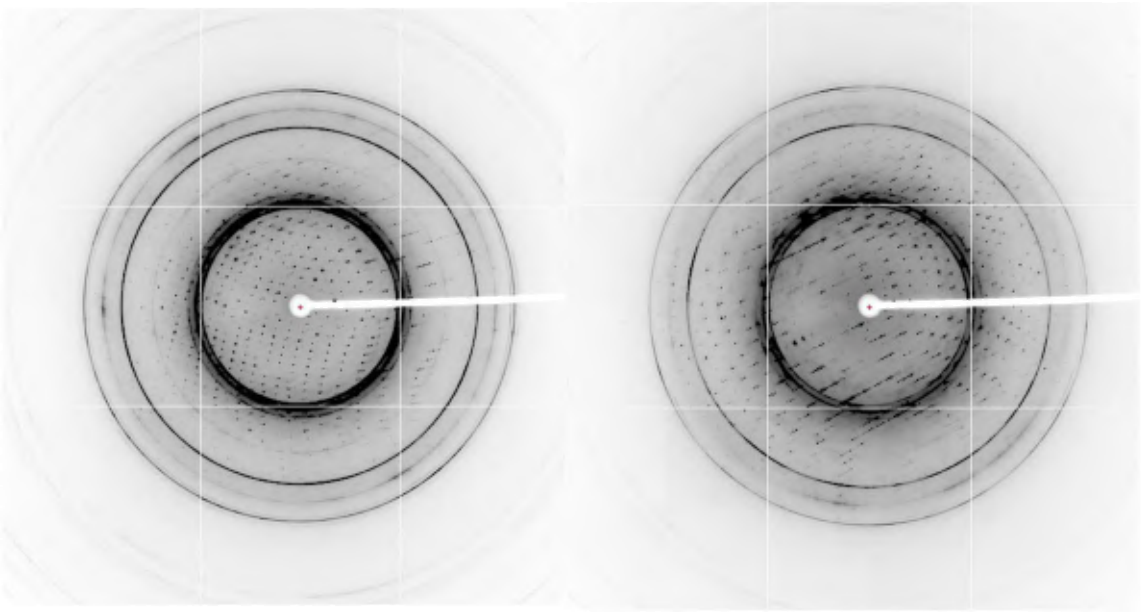

- **以下為綠膿桿菌 SSB（PaSSB）與 inhibitor（9-Me）透過共結晶(co-crystallization)獲得複合結晶，經由 X 光繞射實驗後所獲得的繞射圖相關資訊：**

晶體到 Detector 間的距離（Distance）	200 mm
X 光繞射之晶體曝光時間（Time）	5 s
數據收集之晶體繞射角度範圍（Phi）	165～245 deg
數據收集之晶體轉動幅度（Delta）	1 deg
數據收集之晶體繞射圖張數（Frame）	80
晶體解析度（Resolution）	30Å～2.23Å
晶體之晶格對稱性（Space group）	$P3_1$、$P3_2$

PaSSB + ssDNA（dT 35）

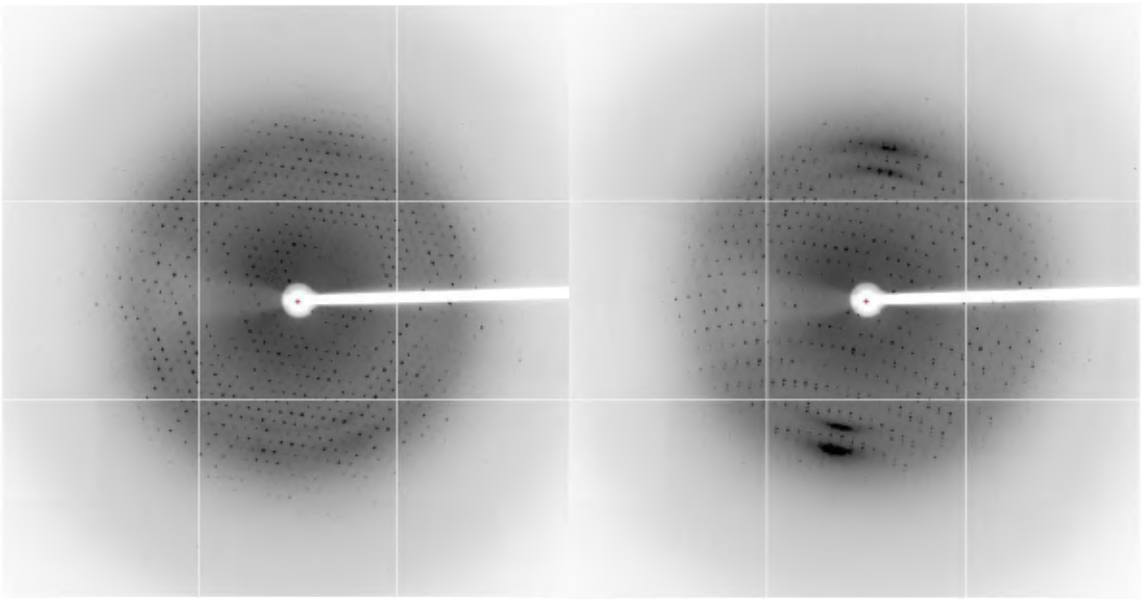

- **以下為綠膿桿菌 SSB（PaSSB）與 ssDNA（dT 35）透過共結晶(co-crystallization)獲得複合結晶，經由 X 光繞射實驗後所獲得的繞射圖相關資訊：**

晶體到 Detector 間的距離（Distance）	300 mm
X 光繞射之晶體曝光時間（Time）	20 s
數據收集之晶體繞射角度範圍（Phi）	65～170 deg
數據收集之晶體轉動幅度（Delta）	0.5 deg
數據收集之晶體繞射圖張數（Frame）	210
晶體解析度（Resolution）	30Å～2.26Å
晶體之晶格對稱性（Space group）	$P3_12_1$、$P3_22_1$

PaSSB + inhibitor（soaking myc）

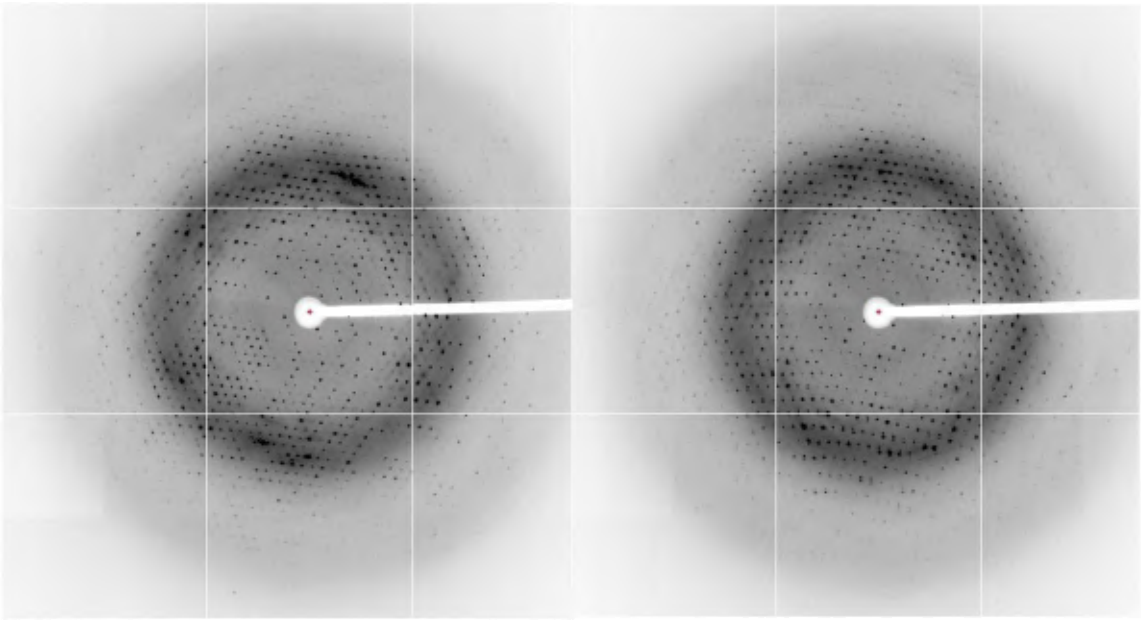

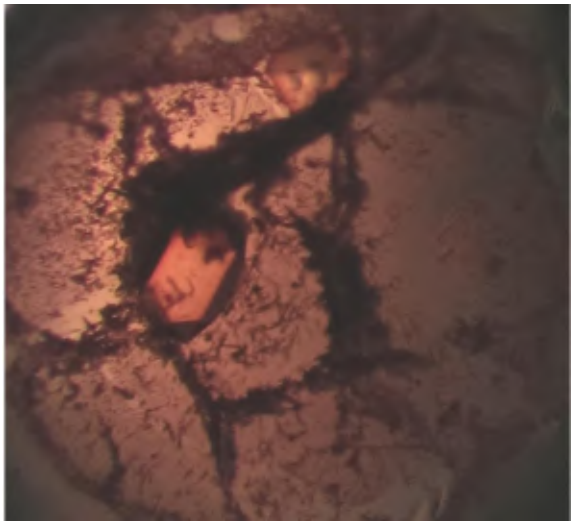

- **以下為綠膿桿菌 SSB（PaSSB）與 inhibitor（myc）透過浸泡法(soaking)在晶體形成後，再加入抑制劑至晶體周圍溶液環境中獲得複合結晶，經由 X 光繞射實驗後所獲得的繞射圖相關資訊：**

晶體到 Detector 間的距離（Distance）	260 mm
X 光繞射之晶體曝光時間（Time）	5 s
數據收集之晶體繞射角度範圍（Phi）	135～240 deg
數據收集之晶體轉動幅度（Delta）	0.5 deg
數據收集之晶體繞射圖張數（Frame）	210
晶體解析度（Resolution）	30Å～1.9Å
晶體之晶格對稱性（Space group）	$P3_1$、$P3_2$

PaSSB + inhibitor（soaking kae）

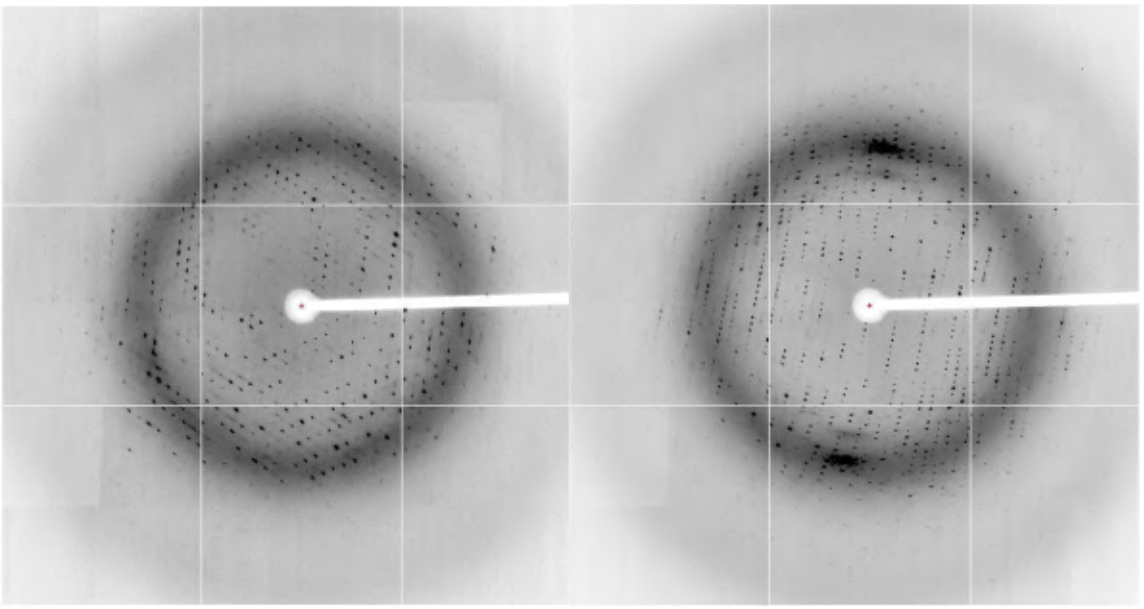

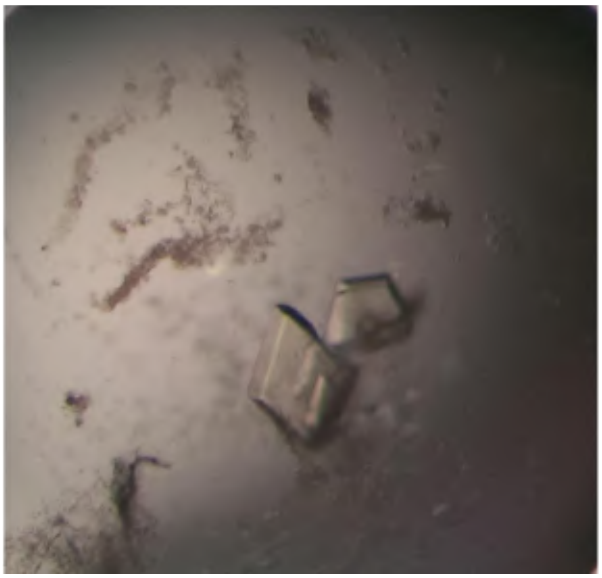

- **以下為綠膿桿菌 SSB（PaSSB）與 inhibitor（kae）透過浸泡法(soaking)在晶體形成後，再加入抑制劑至晶體周圍溶液環境中獲得複合結晶，經由 X 光繞射實驗後所獲得的繞射圖相關資訊：**

晶體到 Detector 間的距離（Distance）	270 mm
X 光繞射之晶體曝光時間（Time）	5 s

數據收集之晶體繞射角度範圍（Phi）	95～280 deg
數據收集之晶體轉動幅度（Delta）	1 deg
數據收集之晶體繞射圖張數（Frame）	185
晶體解析度（Resolution）	30Å～2.1Å
晶體之晶格對稱性（Space group）	C_12_1

已發表之著作

RSC Advances

PAPER

Cite this: *RSC Adv.*, 2018, **8**, 28367

Characterization of single-stranded DNA-binding protein SsbB from *Staphylococcus aureus*: SsbB cannot stimulate PriA helicase

Kuan-Lin Chen,[a] Jen-Hao Cheng,[a] Chih-Yang Lin,[ab] Yen-Hua Huang[a] and Cheng-Yang Huang *[ac]

Single-stranded DNA-binding proteins (SSBs) are essential to cells as they participate in DNA metabolic processes, such as DNA replication, repair, and recombination. The functions of SSBs have been studied extensively in *Escherichia coli*. Unlike *E. coli*, which contains only one type of SSB (EcSSB), some bacteria have more than one paralogous SSB. In *Staphylococcus aureus*, three SSBs are found, namely, SsbA, SaSsbB, and SsbC. While EcSSB can significantly stimulate EcPriA helicase, SaSsbA does not affect the SaPriA activity. It remains unclear whether SsbBs can participate in the PriA-directed DNA replication restart process. In this study, we characterized the properties of SaSsbBs through structural and functional analyses. Crystal structure of SaSsbB determined at 2.9 Å resolution (PDB entry 5YYU) revealed four OB folds in the N-terminal DNA-binding domain. DNA binding analysis using EMSA showed that SaSsbB binds to ssDNA with greater affinity than SaSsbA does. Gene map analysis demonstrated that *SAAV0835* encoding SaSsbB is flanked by unknown genes encoding hypothetical proteins, namely, putative Sipho_Gp157, ERF, and HNHc_6 gene products. Structure-based mutational analysis indicated that the four aromatic residues (Phe37, Phe48, Phe54, and Tyr82) in SaSsbB are at positions that structurally correspond to the important residues of EcSSB for binding to ssDNA and are also critical for SaSsbB to bind ssDNA. Similar to EcSSB and other SSBs such as SaSsbA and SaSsbC, SaSsbB also exhibited high thermostability. However, unlike EcSSB, which can stimulate EcPriA, SaSsbB did not affect the activity of SaPriA. Based on results in this study and previous works, we therefore established that SsbA and SsbB, as well as SsbC, do not stimulate PriA activity.

Received 23rd May 2018
Accepted 28th July 2018

DOI: 10.1039/c8ra04392b

rsc.li/rsc-advances

Introduction

Single-stranded DNA-binding proteins (SSBs) play crucial roles in DNA metabolic processes, such as DNA replication, repair, and recombination in prokaryotes and eukaryotes.[1,2] During these reactions, SSB is necessary to maintain the transient unwinding of duplex DNA in a single-stranded state.[3] SSB binds to ssDNA with high affinity in a sequence-independent manner. Bacterial SSBs are typically homotetramers, in which four oligonucleotide/oligosaccharide-binding folds (OB fold) form a DNA-binding domain. In additional to ssDNA, SSB also binds to many DNA metabolism proteins that constitute the SSB interactome.[4,5] The C-terminal acidic tail (DDDIPF) and the intrinsically disordered linker (IDL) of SSB are necessary to mediate protein–protein interactions.[4] The entire C-terminal domain of SSB is disordered even in the presence of ssDNA.[6]

The structure, DNA binding properties, and functions of SSB have been studied extensively in *Escherichia coli* (EcSSB).[7,8] EcSSB has three distinct DNA binding modes that are dependent on protein and salt concentrations in a solution.[9] ssDNA unwrapping analysis shows that EcSSB can diffuse along ssDNA in the different binding modes, indicating a highly dynamic complex.[10]

Several bacteria have two paralogous SSBs, namely, SsbA and SsbB.[11] Based on the sequence identity and the DNA binding properties, the third SSB (SsbC) is also identified in *Staphylococcus aureus*.[12] *S. aureus*, a Gram-positive pathogen, causes serious problems to public health worldwide.[13] Some SSB inhibitors as broad-spectrum antibacterial agents targeting *S. aureus* and other pathogens have been discovered.[12,14]

SsbA is referred to as a counterpart of EcSSB. SsbA and SsbB are essential for genome maintenance and transformational recombination, respectively.[15–18] Significant differences for SsbBs are found in their C-terminal sequences and DNA binding properties. In *Bacillus subtilis*, SsbB binds to ssDNA with lesser affinity than BsSsbA does.[17] However, *Streptomyces*

[a]*School of Biomedical Sciences, Chung Shan Medical University, No. 110, Sec. 1, Chien-Kuo N. Rd., Taichung City, Taiwan. E-mail: cyhuang@csmu.edu.tw; Tel: +886-4-24730022 ext. 11472*

[b]*School of Medicine, College of Medicine, Chung Shan Medical University, No. 110, Sec. 1, Chien-Kuo N. Rd., Taichung City, Taiwan*

[c]*Department of Medical Research, Chung Shan Medical University Hospital, No. 110, Sec. 1, Chien-Kuo N. Rd., Taichung City, Taiwan*

coelicolor SsbB (ScSsbB) exhibits greater DNA-binding affinity than ScSsbA does.[18] Unlike *Streptococcus pneumonia* SsbB (SpSsbB), BsSsbB and ScSsbB lack the C-terminal acidic tail of SSB for protein–protein interactions.[16–18] Thus, SsbBs from different organisms exhibit different protein–DNA and protein–protein interaction specificities.

PriA is a DEXH-type helicase used for replication restart in bacteria.[19–22] PriA is a poor helicase and needs some specific loading proteins to reload the replicative DnaB helicase back onto the chromosome. In *E. coli*, accessory proteins PriB and SSB are known to stimulate PriA helicase activity.[23,24] However, SaSsbA, a counterpart of EcSSB, does not trigger SaPriA.[25] Instead, SaDnaD is found to enhance the ATPase activity of SaPriA.[26] The manner by which SaSsbA and SaSsbB participate in SaPriA-directed primosome assembly and in DNA replication restart remains unclear.

SSB has mainly been studied in Gram-negative *E. coli*, and, to a lesser extent, in Gram-positive bacteria. Little is known about the fundamental function of SsbB for the assembly of the replication restart primosome. For instance, nothing is known whether or not SsbB can stimulate PriA helicase. Because of lacking experimental evidences, whether SsbB is thermostable and whether SsbB has the typical C-terminal acidic tail of SSB for protein–protein interactions also remain unclear. Whether PriB, an EcSSB-like ssDNA-binding protein lacking the C-terminal domain of SSB,[27–29] is a counterpart of SsbB still needs to be further elucidated.

In this study, we have cloned, expressed, purified, and biochemically characterized SaSsbB. We also have crystallized SaSsbB and determined its molecular structure. Unlike EcSSB, SsbB could not enhance PriA activity. Thus, we established that these three EcSSB-like proteins in *S. aureus* (SsbA, SsbB, and SsbC) do not stimulate PriA activity.

Experimental

Construction of plasmids for SaSsbA, SaSsbB, SaDnaD, and SaPriA expression

SaSsbA,[25] SaDnaD,[26] and SaPriA[30] expression plasmids have been constructed in other studies. *SAAV0835*, the gene encoding a putative SaSsbB, was amplified through PCR by using the genomic DNA of *S. aureus* subsp. *aureus* ED98 as a template. The primers used for the construction of the pET21-SaSsbB plasmid are summarized in Table 1.

Protein expression and purification

Recombinant SaSsbA,[25] SaDnaD,[26] and SaPriA[30] have been purified in other studies. Recombinant SaSsbB was expressed and purified in accordance with a previously described protocol for PriB.[27,28] In brief, *E. coli* BL21(DE3) cells were transformed with the expression vector, and the overexpression of the plasmids was induced by incubating with 1 mM isopropyl thio-galactopyranoside. The protein was purified from a soluble supernatant through Ni^{2+} affinity chromatography (HiTrap HP; GE Healthcare Bio-Sciences), eluted with Buffer A (20 mM Tris–HCl, 250 mM imidazole, and 0.5 M NaCl, pH 7.9) and dialyzed against a dialysis buffer (20 mM HEPES and 100 mM NaCl, pH 7.0; Buffer B). Protein purity remained at >97% as determined by SDS-PAGE (Mini-PROTEAN Tetra System; Bio-Rad, CA, USA).

Preparation of dsDNA substrate

The double-stranded DNA substrate (dsDNA) PS4/PS3-dT30 for ATPase assay was prepared at a 1 : 1 concentration ratio.[25,26] PS4/PS3-dT30 was formed in 20 mM HEPES (pH 7.0) and 100 mM NaCl by briefly heating at 95 °C for 5 min and by slowly cooling to room temperature overnight.

Electrophoretic mobility shift assay (EMSA)

EMSA for SaSsbB was conducted in accordance with a previously described protocol for SSB.[31] In brief, various lengths of ssDNA oligonucleotides were radiolabeled with [γ^{32}P] ATP (6000 Ci/mmol; PerkinElmer Life Sciences, Waltham, MA) and T4 polynucleotide kinase (Promega, Madison, WI, USA). The protein (0, 0.01, 0.02, 0.039, 0.078, 0.1563, 0.3125, 0.625, 1.25, and 2.5 μM; tetramer) was incubated for 30 min at 25 °C with 1.7 nM DNA substrates in a total volume of 10 μL in 20 mM Tris–HCl (pH 8.0) and 100 mM NaCl. Aliquots (5 μL) were removed from each of the reaction solutions and added to 2 μL of gel-loading solution (0.25% bromophenol blue and 40% sucrose). The resulting samples were resolved on 8% native polyacrylamide gel at 4 °C in TBE buffer (89 mM Tris borate and

Table 1 Primers used for construction of plasmids[a]

Oligonucleotide	Primer
SaSsbB-NdeI-N	GGGCATATGTTAAACAGAGTAGTTTTAGTA
SaSsbB-XhoI-C	GGGCTCGAGGAACGGGAGGTCTGAAAAATC
SaSsbB(F37A)-N	ACATTAGCAGTAAACAGAACAGCCACGAATGCTCAA
SaSsbB(F37A)-C	CTCGCCTTGAGCATTCGTGGCTGTTCTGTTTACTGC
SaSsbB(F48A)-N	GGCGAGCGTGAAGCAGAGCTTATAAACGTAGTAGTGTTC
SaSsbB(F48A)-C	GAACACTACTACGTTTATAAGCTCTGCTTCACGCTCGCC
SaSsbB(F54A)-N	TTTATAAACGTAGTAGTGGCCAAAAAACAAGCTGAAAAC
SaSsbB(F54A)-C	TTCAGCTTGTTTTTTGGCCACTACTACGTTTATAAAATC
SaSsbB(Y82A)-N	CGACTACAAACACGTAACGCCGAAAACAAAGACGGGCAA
SaSsbB(Y82A)-C	TTGCCCGTCTTTGTTTTCGGCGTTACGTGTTTGTAGTCG

[a] These plasmids were verified by DNA sequencing. Underlined nucleotides indicate the designated site for the restriction site or the mutation site.

1 mM EDTA) for 1 h at 100 V and visualized through phosphorimaging. A phosphor storage plate was scanned, and data regarding complex and free DNA bands were digitized for quantitative analysis. The ssDNA binding ability of the protein was estimated through linear interpolation from the concentration of the protein that bound 50% of the input DNA.

ATPase assay

SaPriA ATPase assay[25,26] was performed with 0.4 mM [γ-^{32}P] ATP and 0.12 μM SaPriA in a reaction buffer containing 40 mM Tris (pH 8.0), 10 mM NaCl, 2 mM DTT, 2.5 mM $MgCl_2$, and 0.1 μM PS4/PS3-dT30 DNA substrate. Aliquots (5 μL) were taken and spotted onto a polyethyleneimine cellulose thin-layer chromatography plate, which was subsequently developed in 0.5 M formic acid and 0.25 M LiCl for 30 min. Reaction products were visualized by autoradiography and quantified with a phosphorimager.

Site-directed mutagenesis

SaSsbB mutants were generated with a QuikChange Site-Directed Mutagenesis kit in accordance with the manufacturer's protocol (Stratagene, LaJolla, CA, USA) by using the primers (Table 1) and the wild-type plasmid pET21b-SaSsbB as the template. The presence of mutation was verified through DNA sequencing.

Bioinformatics

The amino acid sequences of 150 sequenced SSB homologs were aligned using ConSurf,[32] and the structures were visualized by using PyMol.

Crystallography

Before crystallization was performed, SaSsbB was concentrated to 15 mg mL^{-1} in Buffer B. Crystals were grown at room temperature through hanging drop vapor diffusion in 30% PEG 4000, 100 mM Tris, and 200 mM sodium acetate at pH 8.5. Data were collected with an ADSC Quantum-315r CCD area detector at SPXF beamline BL13C1 at NSRRC (Taiwan, ROC). Data were integrated and scaled with HKL-2000.[33] Four SaSsbB monomers per asymmetric unit were present. The crystal structure of SaSsbB was determined at 2.98 Å resolution with the molecular replacement software Phaser-MR[34] by using SaSsbA as a model (PDB entry 5XGT).[25] A model was built and refined with PHENIX[35] and Coot.[36] The final structure was refined to *R*-factor of 0.2139 and R_{free} of 0.2995. The atomic coordinates and related structure factors have been deposited in the PDB with the accession code 5YYU.

Results and discussion

Sequence analysis of SaSsbB

SAAV0835, which encodes SaSsbB of 141 aa, was found on the basis of the nucleotide sequence similar to BsSsbB and EcSSB. The amino acid sequence of SaSsbB shared 36% identity to that of SaSsbA. The ConSurf analysis reveals that the C-terminal region of SaSsbB was variable (Fig. 1). Like EcSSB, SaSsbB also had a long flexible region, but its flexible region was composed of few proline and glycine residues. SaSsbB (109–141 aa) had one Gly residue and two Pro residues (Fig. 1), which are significantly less than those of EcSSB (116–178 aa; 15 Gly residues and 10 Pro residues). In addition, SaSsbB did not have a C-terminal acidic peptide tail. The C-terminal acidic tail DDDIPF in EcSSB involved in protein–protein interactions was FSDLPF in SaSsbB.

Analysis of *ssb* (*SAAV0835*)

Fig. 2 shows the gene map of *S. aureus* chromosomal region with the *ssb* gene *SAAV0835*, which is flanked by unknown genes encoding hypothetical proteins with similarity to Sipho_Gp157, ERF, and HNHc_6. Unlike *E. coli*, which contains one type of SSB, *S. aureus* have three paralogous SSBs (SsbA, SsbB, and SsbC).[12] The gene map analyses of *ssb* show significant differences.[12,25] Unlike EcSSB located adjacent to *uvrA*, SaSsbA is flanked by *rpsF* and *rpsR*,[25] which encode the ribosomal proteins S6 and S18, respectively. SaSsbC is flanked by the putative *SceD*, the putative *YwpF*, and *fabZ* genes, which code for a transglycosylase, a hypothetical protein, and a β-hydroxyacyl-ACP dehydratase, respectively.[12] The gene regulation for SaSsbB is still unknown. Given that SsbB is essential for transformational recombination, these function-undetermined genes (Fig. 2) in *S. aureus* may be regulated with SaSsbB in a single signaling control and may be also involved in transformational recombination. However, this hypothesized relationship must be further confirmed by a detailed transcription analysis.

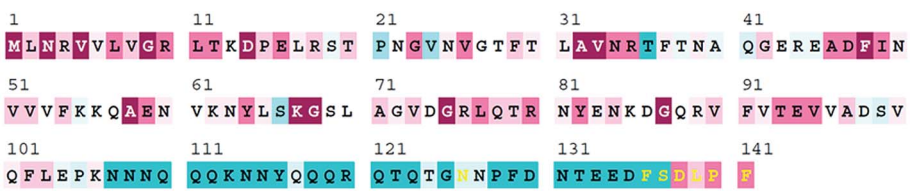

Fig. 1 Sequence analysis of SaSsbB. An alignment consensus of 150 sequenced SSB homologs by ConSurf reveals the degree of variability at each position along the primary sequence. Highly variable amino acid residues are colored teal, whereas highly conserved amino acid residues are burgundy. A consensus sequence was established by determining the most commonly found amino acid residue at each position relative to the primary sequence of SaSsbB.

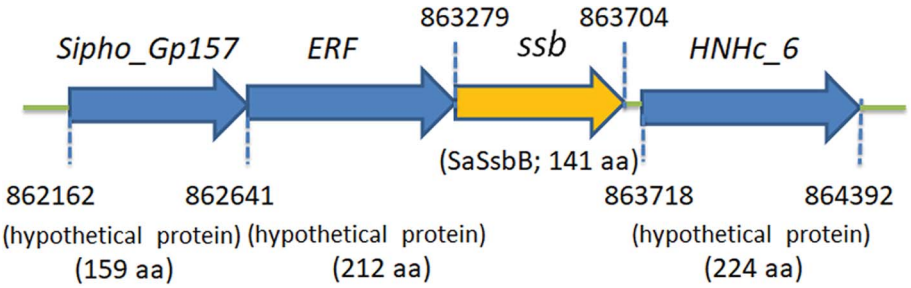

Fig. 2 Gene map of *S. aureus* chromosomal region with the *ssb* gene *SAAV0835*. The gene *SAAV0835* coding for SaSsbB maps from the 863279 to 863704 nt of the *S. aureus* genome. This *ssb* gene is flanked by unknown genes encoding hypothetical proteins, namely, the putative gene products similar to Sipho_Gp157, ERF, and HNHc_6.

SaSsbB bound to ssDNA

We studied the binding of purified SaSsbB (Fig. 3) to ssDNA (dT15-40) at various protein concentrations by using EMSA. To compare the DNA-binding abilities of SaSsbB, we quantified $[\text{Protein}]_{50}$ through linear interpolation from the protein concentration (Fig. 4 and Table 2). The binding ability of SaSsbB to dT40 in the presence of 0.4 M NaCl was also analyzed (Fig. 4). $[\text{SaSsbB}]_{50}$ of dT40 binding was 90 ± 4 nM, which was about fourfold lower than that in the presence of 0.4 M NaCl (382 ± 16 nM). Thus, the binding ability of SaSsbB to ssDNA is salt-dependent. Under the condition, only one band shift was found for dT20-60 (Fig. 5).

Stimulation of the ATPase activity of SaPriA by SaSsbB

To date, it remains unclear whether SsbB can stimulate the activity of the primosomal protein PriA. To investigate the possible effect of SaSsbB, we performed an ATPase assay for SaPriA. SaDnaD,[26] which stimulates the SaPriA activity, was used as a positive control. In contrast to SaDnaD,[26] we found that the ATPase activity of SaPriA in the presence of SaSsbB was not changed (Fig. 6). Given that the C-terminal domain of SsbB did not contain the acidic tail (Fig. 1), SsbB may not bind to PriA. Thus, no stimulation occurred (Fig. 6).

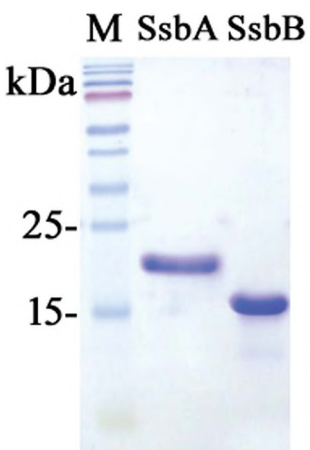

Fig. 3 Coomassie Blue-stained SDS-PAGE (15%) of the purified SaSsbA, SaSsbB, and molecular mass standards. The sizes of the standard proteins, from the top down, are as follows: 170, 130, 100, 70, 55, 40, 35, 25, and 15 kDa.

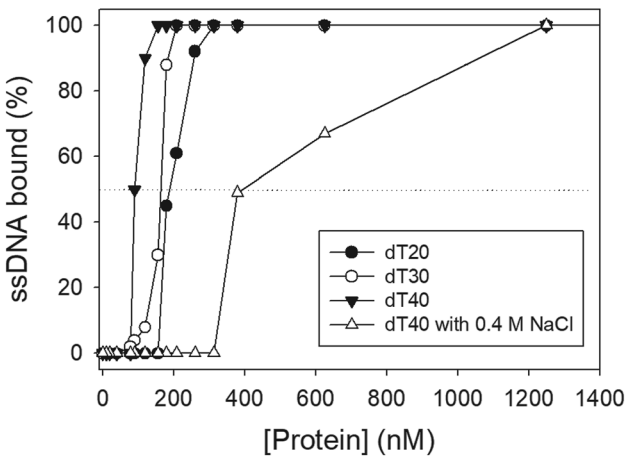

Fig. 4 ssDNA binding of SaSsbB. Protein was incubated at 25 °C for 30 min with ssDNA in a total volume of 10 μL in 20 mM Tris–HCl (pH 8.0) and 100 mM NaCl. The $[\text{Protein}]_{50}$ values of SaSsbB as a function of the length of the ssDNA were determined using EMSA.

Crystal structure of SaSsbB

In this study, we have shown that unlike EcSSB, SaSsbB did not contain the C-terminal acidic peptide and could not stimulate SaPriA helicase. To deeply understand the structure–function relationship of SaSsbB, we crystallized SaSsbB through hanging

Table 2 The $[\text{Protein}]_{50}$ values of SaSsbB as analyzed by EMSA[a]

DNA	$[\text{Protein}]_{50}$ (nM)
dT15	>2000
dT20	190 ± 8
dT30	164 ± 7
dT40	90 ± 4
dT40 (with 0.4 M NaCl)	382 ± 16

[a] $[\text{Protein}]_{50}$ was calculated from the titration curves of EMSA by determining the concentration of the protein needed to achieve the midpoint value for input DNA binding. Errors are standard deviations determined by three independent titration experiments.

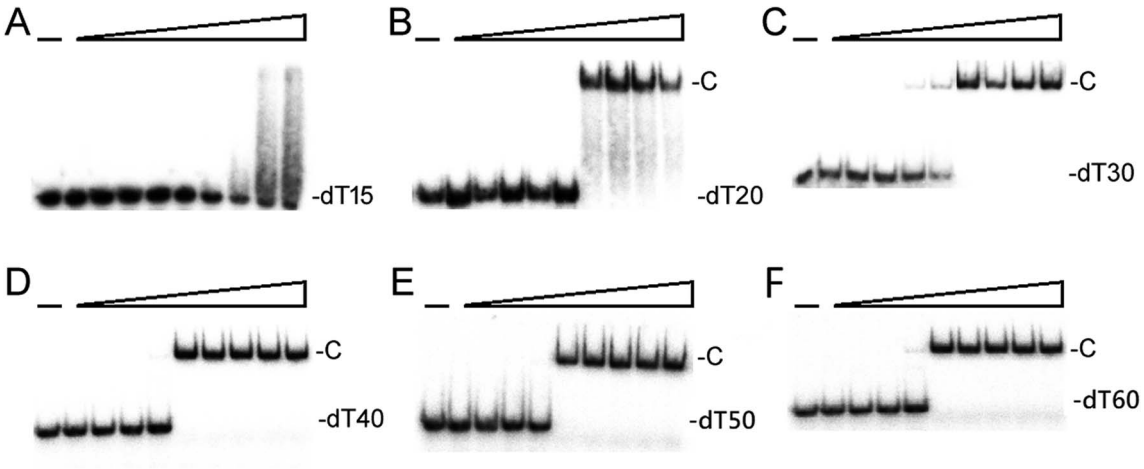

Fig. 5 EMSA of SaSsbB. Protein (0, 0.01, 0.02, 0.039, 0.078, 0.1563, 0.3125, 0.625, 1.25, and 2.5 μM; tetramer) was incubated at 25 °C for 30 min with 1.7 nM of (A) dT15, (B) dT20, (C) dT30, (D) dT40, (E) dT50, or (F) dT60 in a total volume of 10 μL in 20 mM Tris–HCl (pH 8.0) and 100 mM NaCl. Only one band shift was found for these ssDNAs.

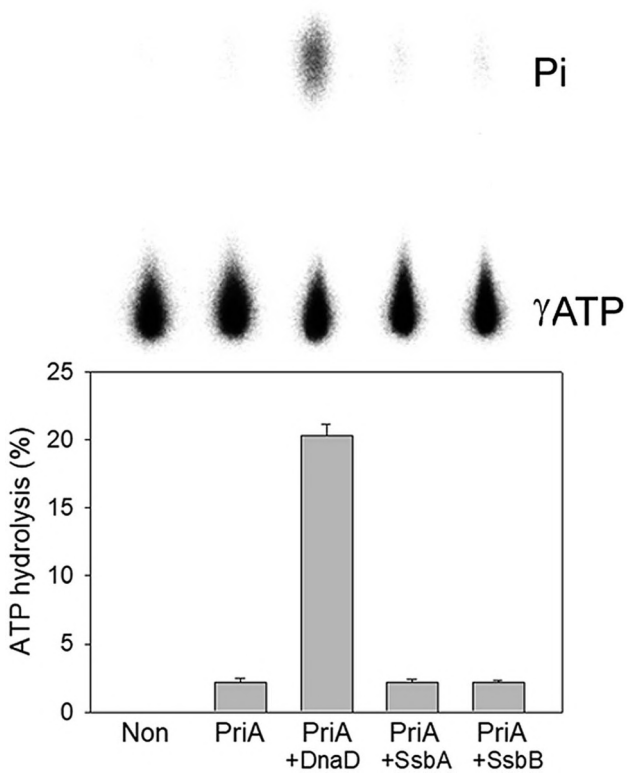

Fig. 6 The ATPase activity of SaPriA did not change when acting with SaSsbB. SaPriA ATPase assay was performed with 0.4 mM [γ-^{32}P] ATP, 0.12 μM of SaPriA, and 0.1 μM PS4/PS3-dT30 DNA substrate for 1 h. To study the effect, SaSsbA (10 μM), SaSsbB (10 μM), or SaDnaD (4 μM) was added into the assay solution. Reaction products were visualized by autoradiography and quantified with a phosphorimager.

Table 3 Data collection and refinement statistics

Data collection	
Crystal	SaSsbB
Wavelength (Å)	0.975
Resolution (Å)	30–2.98
Space group	$P2_12_12_1$
Cell dimension (Å)	$a = 63.99$, $\alpha = 90$ $b = 84.74$, $\beta = 90$ $c = 84.86$, $\gamma = 90$
Completeness (%)	99.8 (99.8)[a]
$\langle I/\sigma I \rangle$	13 (2.5)
R_{sym} or R_{merge} (%)[b]	0.125 (0.541)
Redundancy	3.8 (4.0)
Refinement	
Resolution (Å)	30–2.98
No. reflections	9334
R_{work}/R_{free}	0.2139/0.2995
No. atoms	
Protein	399
Water	16
R.m.s deviation	
Bond lengths (Å)	0.011
Bond angles (°)	1.385
Ramachandran plot	
In preferred regions	359 (93.25%)
In allowed regions	20 (5.19%)
Outliers	6 (1.56%)
PDB entry	5YYU

[a] Values in parentheses are for the highest resolution shell. [b] $R_{sym} = \Sigma|I - 'I'|/\Sigma I$, where I is the observed intensity, 'I' is the statistically weighted average intensity of multiple observations of symmetry-related reflections.

drop vapor diffusion and determined its structure at a resolution of 2.98 Å (Table 3). The secondary structural element of SaSsbB is similar to that of SaSsbA (Fig. 7A). The amino acids 107–141 in SaSsbB ternary structure were not observed. Consistent with the result from gel filtration analysis (data not shown), four monomers of SaSsbB per asymmetric unit were present (Fig. 7B). The SaSsbB monomer has an OB-fold domain similar to EcSSB, and the core of the OB-fold domain possesses a β-barrel capped with an α-helix. Unlike ScSSB, which contains

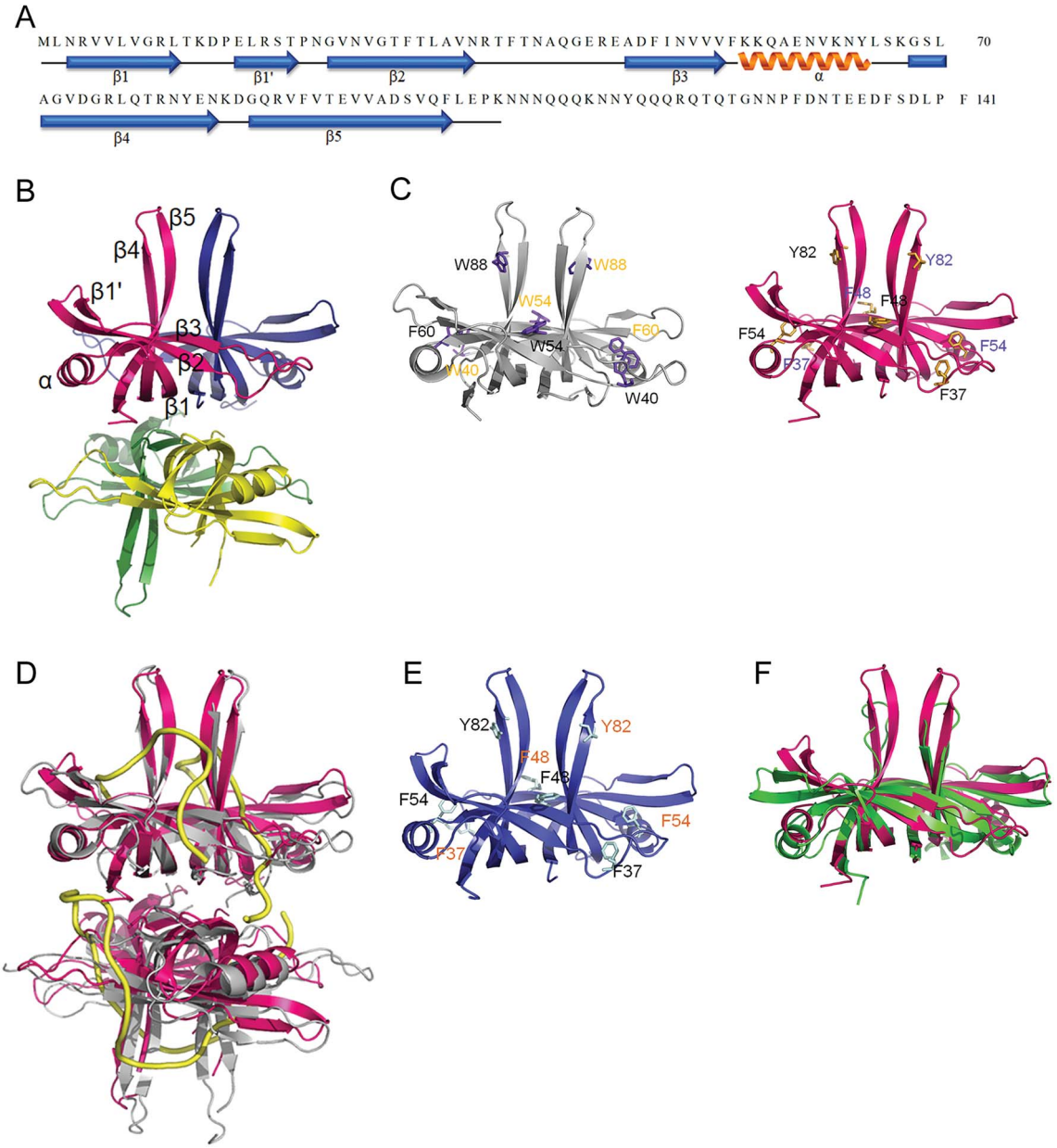

Fig. 7 Crystal structure of SaSsbB. (A) The secondary structural element of SaSsbB. The secondary structural element of SaSsbB is shown above its sequence. (B) Crystal structure of SaSsbB. Four monomers of SaSsbB per asymmetric unit were present. The entire C-terminal domain was disordered. (C) ssDNA-binding mode of SaSsbB. In the EcSSB–ssDNA complex (PDB entry 1EYG), Trp40, Trp54, Phe60, and Trp88 participated in ssDNA binding *via* stacking interactions. The corresponding residues in SaSsbB, namely, Phe37, Phe48, Phe54, and Tyr82, might play roles in ssDNA binding similar to those of EcSSB. For clarity, only a dimer of EcSSB and SaSsbB is shown. (D) Superposition of SaSsbB and EcSSB. The N-terminal domains of SaSsbB and EcSSB (gray) are similar. (E) Crystal structure of SaSsbA. The residues proposed for binding DNA in SaSsbB are also identical to those in SaSsbA. (F) Superposition of SaSsbB and KpPriB. The N-terminal domain of SaSsbB and KpPriB (PDB entry 4APV; green) are similar, in which the only significant difference is in the lengths of the β4 and β5 sheets.

an additional strand (β6),[18] SaSsbB does not contain β6. Additional β6 strands clamp two neighboring subunits together in a tetrameric SSB.[18] Thus, SsbBs from different organisms may exhibit different protein–DNA and protein–protein interaction specificities.

Trp40, Trp54, Phe60, and Trp88 in EcSSB participate in ssDNA binding *via* stacking interactions (Fig. 7C). Correspondingly, Phe37, Phe48, Phe54, and Tyr82 in SaSsbB might play roles in ssDNA binding (Fig. 7D). These residues proposed for binding DNA in SaSsbB were also identical to those in SaSsbA (Fig. 7E). SaSsbB structurally resembles PriB,[27,28] but significant differences in the lengths of β4- and β5-sheets were found (Fig. 7F).

Mutational analysis

According to crystal structure of SaSsbB, we speculated that Phe37, Phe48, Phe54, and Tyr82 in SaSsbB allow nucleic acids to

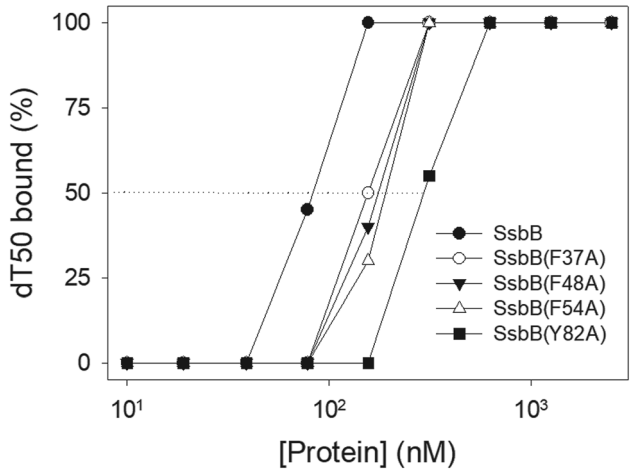

Fig. 8 Mutational analysis of SaSsbB for ssDNA binding. Binding of SaSsbB mutant protein (F37A, F48A, F54A, and Y82A) to dT50. The mutant protein was incubated with dT50. The phosphor storage plate was scanned, and the data for complex and free DNA bands were digitized for quantitative analysis.

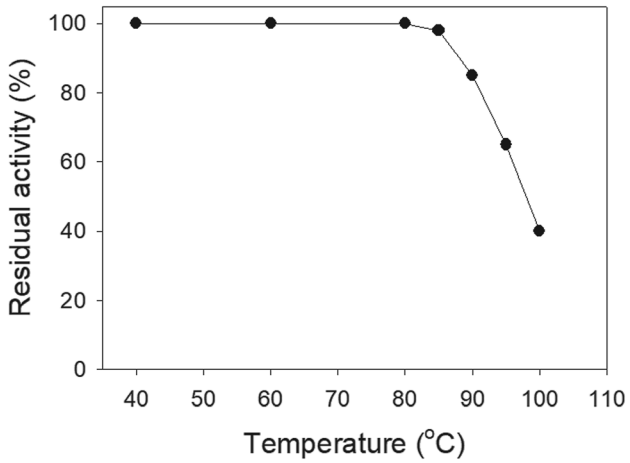

Fig. 9 The thermostability of SaSsbB. Protein (1 μM) was incubated at temperatures ranging from 40 °C to 100 °C for 30 min. The resultant protein solution was incubated at 25 °C for 30 min with dT30. The phosphor storage plate was scanned, and the data for complex and free DNA bands were digitized for quantitative analysis.

wrap around the whole SaSsbB. We constructed and analyzed alanine substitution mutants (*i.e.*, F37A, F48A, F54A, and Y82A) through EMSA (Fig. 8). Table 4 summarizes $[Protein]_{50}$ of the binding of these SaSsbB variants to dT50. These SaSsbB mutants have $[Protein]_{50}$ higher than that of the wild-type SaSsbB. The mutational effect on the ssDNA binding activity of SaSsbB followed the order Y82A > F54A > F48A > F37A. Structure-based mutational analysis indicated that SaSsbB might bind to ssDNA in a manner similar to that of EcSSB (Table 4).

Thermostability

SSB proteins have high thermostability.[37] SsbA and SsbC are highly thermostable.[12] It is still unknown whether SsbB has high thermostability. We performed indirect thermostability experiments (Fig. 9). The activity of SaSsbB incubated at 100 °C, 95 °C, 90 °C, and 85 °C for 30 min decreased by 60%, 35%, 15%, and 2%, respectively. Given that the activity of EcSSB decreased by 50% after 30 min incubation at 95 °C,[37] we determined that the thermostability of these SSBs followed the order SaSsbA = SaSsbB > SaSsbC > EcSSB (Table 5). Thus, SaSsbB also exhibited high thermostability.

SsbB is not a counterpart of PriB

PriB is a dimeric ssDNA-binding protein with two OB folds,[27–29] only found in some Gram-negative bacteria.[21,22] Our crystal structure reveals that the N-terminal DNA-binding domain of SaSsbB structurally resembles PriB, although they significantly differ in the lengths of β4- and β5-sheets (Fig. 7F). Like SaSsbB, PriB also lacks the acidic tail. Because *E. coli* has only one SSB, it may raise a question whether PriB is the second SSB in *E. coli* and plays a functional role that is similar to SsbB in *S. aureus*. Sequence comparisons and operon organization analyses also show that PriB evolves from the duplication of the SSB gene.[38] However, PriA activity can be significantly stimulated by PriB but not by SsbB (Fig. 6). Thus, SaSsbB and EcPriB have different functions, and PriB is not a counterpart of SsbB. Considering that the mechanisms of action of primosomes involved in DNA replication restart differ between *E. coli*[21,22] and Gram-positive

Table 4 The $[Protein]_{50}$ values of SaSsbB mutants as analyzed by EMSA[a]

dT50	$[Protein]_{50}$ (nM)
SaSsbB	83 ± 7
SaSsbB(F37A)	155 ± 12
SaSsbB(F48A)	176 ± 10
SaSsbB(F54A)	191 ± 16
SaSsbB(Y82A)	296 ± 18

[a] $[Protein]_{50}$ was calculated from the titration curves of EMSA by determining the concentration of the protein (tetramers) needed to achieve the midpoint value for input DNA binding. Errors are standard deviations determined by three independent titration experiments.

Table 5 Thermostability of SaSsbB[a]

	The decreased activity (%)			
Temperature	SaSsbA	SaSsbB	SaSsbC	EcSSB
85 °C	2	2	2	
90 °C	15	15	20	
95 °C	35	35	40	50
100 °C	60	60	70	

[a] Protein (1 μM) was incubated at temperatures ranging from 40 °C to 100 °C for 30 min. The resultant protein solution was incubated at 25 °C for 30 min with dT30. The phosphor storage plate was scanned, and the data for complex and free DNA bands were digitized for quantitative analysis. Results of SaSsbA,[12] SaSsbC,[12] and EcSSB[37] are adapted from previous works for comparison.

bacteria,[39] we should elucidate the process by which PriA can cooperate with various loading factors to reactivate the same stalled forks.

Recently, we have identified and characterized the third SSB (SsbC) in *S. aureus*.[12] The structure and ssDNA-binding mode of SaSsbA,[25] SaSsbB (this study), and SaSsbC[12] are similar. Further studies are still needed to understand why SSB in *S. aureus* is necessary to evolve three similar but different SSBs.

Conflicts of interest

There are no conflicts of interest to declare.

Acknowledgements

We thank the experimental facility and the technical services provided by the Synchrotron Radiation Protein Crystallography Facility of the National Core Facility Program for Biotechnology, Ministry of Science and Technology and the National Synchrotron Radiation Research Center, a national user facility supported by the Ministry of Science and Technology, Taiwan, ROC. This research was supported by a grant from the Ministry of Science and Technology, Taiwan (MOST 107-2320-B-040-014 to C. Y. Huang).

References

1 D. J. Richard, E. Bolderson and K. K. Khanna, *Crit. Rev. Biochem. Mol. Biol.*, 2009, **44**, 98–116.
2 E. Antony and T. M. Lohman, *Semin. Cell Dev. Biol.*, 2018, DOI: 10.1016/j.semcdb.2018.03.017.
3 R. R. Meyer and P. S. Laine, *Microbiol. Rev.*, 1990, **54**, 342–380.
4 P. R. Bianco, *Prog. Biophys. Mol. Biol.*, 2017, **127**, 111–118.
5 A. Costes, F. Lecointe, S. McGovern, S. Quevillon-Cheruel and P. Polard, *PLoS Genet.*, 2010, **6**, e1001238.
6 S. N. Savvides, S. Raghunathan, K. Futterer, A. G. Kozlov, T. M. Lohman and G. Waksman, *Protein Sci.*, 2004, **13**, 1942–1947.
7 T. H. Dickey, S. E. Altschuler and D. S. Wuttke, *Structure*, 2013, **21**, 1074–1084.
8 S. Raghunathan, A. G. Kozlov, T. M. Lohman and G. Waksman, *Nat. Struct. Biol.*, 2000, **7**, 648–652.
9 T. M. Lohman and M. E. Ferrari, *Annu. Rev. Biochem.*, 1994, **63**, 527–570.
10 S. Suksombat, R. Khafizov, A. G. Kozlov, T. M. Lohman and Y. R. Chemla, *eLife*, 2015, **4**, e08193.
11 C. Lindner, R. Nijland, M. van Hartskamp, S. Bron, L. W. Hamoen and O. P. Kuipers, *J. Bacteriol.*, 2004, **186**, 1097–1105.
12 Y. H. Huang and C. Y. Huang, *Oncotarget*, 2018, **9**, 20239–20254.
13 N. Koyama, J. Inokoshi and H. Tomoda, *Molecules*, 2012, **18**, 204–224.
14 J. G. Glanzer, J. L. Endres, B. M. Byrne, S. Liu, K. W. Bayles and G. G. Oakley, *J. Antimicrob. Chemother.*, 2016, **71**, 3432–3440.
15 S. Ayora, B. Carrasco, P. P. Cardenas, C. E. Cesar, C. Canas, T. Yadav, C. Marchisone and J. C. Alonso, *FEMS Microbiol. Rev.*, 2011, **35**, 1055–1081.
16 L. Attaiech, A. Olivier, I. Mortier-Barriere, A. L. Soulet, C. Granadel, B. Martin, P. Polard and J. P. Claverys, *PLoS Genet.*, 2011, **7**, e1002156.
17 T. Yadav, B. Carrasco, A. R. Myers, N. P. George, J. L. Keck and J. C. Alonso, *Nucleic Acids Res.*, 2012, **40**, 5546–5559.
18 T. Paradzik, N. Ivic, Z. Filic, B. A. Manjasetty, P. Herron, M. Luic and D. Vujaklija, *Nucleic Acids Res.*, 20, **41**, 3659–3672.
19 G. C. Allen Jr, N. E. Dixon and A. Kornberg, *Cell*, 1993, **74**, 713–722.
20 C. A. Ouzounis and B. J. Blencowe, *Nucleic Acids Res.*, 1991, **19**, 6953.
21 Y. H. Huang and C. Y. Huang, *BioMed Res. Int.*, 2014, **2014**, 195162.
22 T. A. Windgassen, S. R. Wessel, B. Bhattacharyya and J. L. Keck, *Nucleic Acids Res.*, 2018, **46**, 504–519.
23 C. J. Cadman, M. Lopper, P. B. Moon, J. L. Keck and P. McGlynn, *J. Biol. Chem.*, 2005, **280**, 39693–39700.
24 C. J. Cadman and P. McGlynn, *Nucleic Acids Res.*, 2004, **32**, 6378–6387.
25 Y. H. Huang, H. H. Guan, C. J. Chen and C. Y. Huang, *PLoS One*, 2017, **12**, e0182060.
26 Y. H. Huang, Y. Lien, C. C. Huang and C. Y. Huang, *PLoS One*, 2016, **11**, e0157593.
27 Y. H. Huang, Y. H. Lo, W. Huang and C. Y. Huang, *Genes Cells*, 2012, **17**, 837–849.
28 C. Y. Huang, C. H. Hsu, Y. J. Sun, H. N. Wu and C. D. Hsiao, *Nucleic Acids Res.*, 2006, **34**, 3878–3886.
29 J. H. Liu, T. W. Chang, C. Y. Huang, S. U. Chen, H. N. Wu, M. C. Chang and C. D. Hsiao, *J. Biol. Chem.*, 2004, **279**, 50465–50471.
30 Y. H. Huang, C. C. Huang, C. C. Chen, K. J. Yang and C. Y. Huang, *Protein J.*, 2015, **34**, 169–172.
31 C. Y. Huang, Determination of the binding site-size of the protein-DNA complex by use of the electrophoretic mobility shift assay, in *Stoichiometry and Research: The Importance of Quantity in Biomedicine*, ed. Innocenti A, InTech Press, Rijeka, Croatia, 2012, pp. 235–242.
32 M. Landau, I. Mayrose, Y. Rosenberg, F. Glaser, E. Martz, T. Pupko and N. Ben-Tal, *Nucleic Acids Res.*, 2005, **33**, W299–W302.
33 Z. Otwinowski and W. Minor, *Methods Enzymol.*, 1997, **276**, 307–326.
34 A. J. McCoy, R. W. Grosse-Kunstleve, P. D. Adams, M. D. Winn, L. C. Storoni and R. J. Read, *J. Appl. Crystallogr.*, 2007, **40**, 658–674.
35 J. J. Headd, N. Echols, P. V. Afonine, R. W. Grosse-Kunstleve, V. B. Chen, N. W. Moriarty, D. C. Richardson, J. S. Richardson and P. D. Adams, *Acta Crystallogr., Sect. D: Biol. Crystallogr.*, 2012, **68**, 381–390.
36 P. Emsley and K. Cowtan, *Acta Crystallogr., Sect. D: Biol. Crystallogr.*, 2004, **60**, 2126–2132.
37 M. Nowak, M. Olszewski, M. Spibida and J. Kur, *BMC Microbiol.*, 2014, **14**, 91.

38 V. A. Ponomarev, K. S. Makarova, L. Aravind and E. V. Koonin, *J. Mol. Microbiol. Biotechnol.*, 2003, **5**, 225–229.

39 M. Velten, S. McGovern, S. Marsin, S. D. Ehrlich, P. Noirot and P. Polard, *Mol. Cell*, 2003, **11**, 1009–1020.

Biochemical and Biophysical Research Communications 511 (2019) 1–6

Contents lists available at ScienceDirect

Biochemical and Biophysical Research Communications

journal homepage: www.elsevier.com/locate/ybbrc

Crystal structure of the C-terminal domain of the primosomal DnaT protein: Insights into a new oligomerization mechanism

Kuan-Lin Chen [a], Yen-Hua Huang [a], Jen-Fu liao [a], Wei-Chen Lee [a], Cheng-Yang Huang [a, b, *]

[a] School of Biomedical Sciences, Chung Shan Medical University, No.110, Sec.1, Chien-Kuo N. Rd., Taichung City, Taiwan
[b] Department of Medical Research, Chung Shan Medical University Hospital, No.110, Sec.1, Chien-Kuo N. Rd., Taichung City, Taiwan

ARTICLE INFO

Article history:
Received 31 January 2019
Received in revised form
3 February 2019
Accepted 5 February 2019
Available online 10 February 2019

Keywords:
DnaT
PriB
DNA replication restart
Oligomerization
Three-helix bundle
Primosome

ABSTRACT

DnaT is a replication restart primosomal protein required for re-initiating chromosomal DNA replication in bacteria. DnaT can be a monomer, dimer, trimer, tetramer, or pentamer. The oligomerization and disassembly of DnaT oligomers are critical in primosome assembly. Prior to this work, only the ssDNA-bound structure of the pentameric DnaT truncated protein (aa 84–153; DnaT84–153) was available. The mechanism by which DnaT oligomerizes as different states is unclear. In this paper, we report the crystal structure of the C-terminal domain of DnaT (aa 84–179; DnaTc) at 2.30 Å resolution (PDB entry 6AEQ). DnaTc forms a dimer both in the crystalline state and in solution. As compared with the ssDNA-bound structure of the pentameric DnaT84–153, their subunit–subunit interfaces significantly differ. The different oligomeric architecture suggests a strong conformational change possibly induced by ssDNA. Superposition analysis further indicated that the monomer of a DnaTc dimer shifted away by a distance of 7.5 Å and rotated by an angle of 170° for binding to ssDNA. Basing from these molecular evidence, we discussed and proposed a working model to explain how DnaTc oligomerizes through residue R146 mediation.

1. Introduction

The assembly of the primosome is a fundamental step for both normal chromosomal replication and the stalled replication fork restart [1–5]. In *Escherichia coli*, the PriA-directed primosome consists of PriA, PriB, DnaT, DnaB helicase, DnaC loader, and DnaG primase. The PriA-directed primosome preferentially binds three-way branched DNA structures with a leading strand [6–9]. Due to PriC–DnaT interactions, a putative link has been proposed between PriA- and PriC-mediated replication restart pathways [10,11].

DnaT, also known as protein i [12,13], is the third key protein to be assembled in the PriA-dependent primosome. The DnaT–PriA interaction is enhanced by PriB [14]. The *dnaT822* mutant showed UV sensitivity and an inability to properly partition nucleoids [15]. DnaT is a single-stranded DNA (ssDNA)-binding protein [16] of 179 amino acids (aa) with a molecular mass of approximately 20 kDa [13,16]. The C-terminal domain of DnaT (DnaTc; aa 84–179) is involved in ssDNA binding [16,17]. The N-terminal domain of DnaT (DnaTn; aa 1–83) interacts with PriB via the region Asp66–Glu76 [18] on the acidic linker [17,19]. Unlike PriB, which uses OB-fold to bind ssDNA [20–22], DnaT binds ssDNA via the three-helix bundle [23]. Although DnaT84–153 exists as a dimer, the pentameric DnaT84–153 forms upon ssDNA binding [23]. The crystal structure of DnaTc is not determined yet, and how DnaTc can form a dimer remains unclear.

Oligomerization is a common property of proteins, and at least 35% of all proteins are oligomeric in biological systems [24,25]. Some proteins form one specific active oligomeric state, such as the case with the acetylcholine receptor that is active only as a pentamer [26]. Some protein oligomerizations are pH-dependent [27,28]. Some other proteins are in dynamic oligomerization equilibria between several states with distinct activities [29]. DnaT can be a monomer, dimer, trimer, tetramer, or pentamer [13,30]. Although the role of DnaT [23] in the recruitment of DnaB helicase has been proposed as functioning a scaffold protein, the mechanism by which DnaT oligomerizes as different states remains unclear.

The oligomerization and disassembly of the DnaT oligomer(s) are critical in primosome assembly [31]. At present, only the pentameric structure of the truncated protein DnaT84–153 with one

* Corresponding author. School of Biomedical Sciences, Chung Shan Medical University, No.110, Sec.1, Chien-Kuo N. Rd., Taichung City, Taiwan.
E-mail address: cyhuang@csmu.edu.tw (C.-Y. Huang).

https://doi.org/10.1016/j.bbrc.2019.02.026
0006-291X/

bound ssDNA at 2.83 Å resolution is available [23]. Other forms of DnaT structure are still needed to formulate any oligomerization model of the mechanism of DnaT functioning in DNA replication restart. In this study, we report the crystal structure of DnaTc at 2.30 Å resolution (PDB entry 6AEQ). The monomer–monomer interfaces between these two structures are obviously different. The structural change, possibly induced by ssDNA, entails approximately 170° rotation of the DnaT monomer, which most likely acts as the trigger to form a pentamer and create a binding site of DnaT to ssDNA.

2. Materials and methods

2.1. Construction of the expression plasmid pET21b-DnaTc

The gene *STM4544* encoding DnaT was PCR-amplified from the genomic DNA of *Salmonella enterica* serovar Typhimurium LT2. The forward (5′-GCCGTCATATGATTCCCTGCGGAAAATTCG-3′) and the reverse (5′-AAATTCTCGAGCCCCCTAAAACCTGGTGGA-3′) primers were used. The insertion of the amplified fragment was ligated into the pET21b vector (Novagen Inc., Madison, WI, USA). The pET21b-DnaTc plasmid was verified by DNA sequencing.

2.2. Protein expression and purification

The recombinant DnaTc was expressed and purified using the protocol described previously for SSB [32,33]. The plasmid was transformed into *E. coli* BL21(DE3) cells. Cells were grown in Luria-Bertani medium that contained 100 μg/mL ampicillin and 1 mM isopropyl thiogalactopyranoside. The protein was purified from the soluble supernatant by Ni^{2+}-affinity chromatography, eluted with Buffer A (20 mM Tris-HCl, 250 mM imidazole, and 0.5 M NaCl, pH 7.9), and dialyzed against a dialysis buffer (20 mM HEPES and 100 mM NaCl, pH 7.0; Buffer B). Protein purity remained at >97% as determined by SDS-PAGE.

2.3. Chemical cross linking

The oligomerization state of DnaTc was analyzed by chemical cross linking using glutaraldehyde as described previously for SaSsbC [34]. DnaTc (4 μM) was incubated with increasing concentrations of glutaraldehyde (0.1%–5%) at 4 °C for 20 min. The reactions were stopped by adding SDS sample buffer and were fractionated on Coomassie Blue-stained SDS-PAGE.

2.4. Crystallography

DnaTc in Buffer B was concentrated to 18 mg/mL. Crystals were grown in 1.6 M magnesium sulfate, 100 mM MES, pH 6.5. Data were collected using an ADSC Quantum-315r CCD area detector at SPXF beamline BL13C1 at NSRRC, Taiwan. All data integration and scaling were carried out using HKL-2000 [35]. There were two DnaTc monomers per asymmetric unit. The crystal structure of DnaTc was solved at 2.30 Å resolution with the molecular replacement software Phaser-MR [36] using DnaT84–153 as model (PDB entry 4OU7) [23]. A model was built and refined with PHENIX [37] and Coot [38]. The final structure was refined to an *R*-factor of 0.220 and an R_{free} of 0.265. Atomic coordinates and related structure factors have been deposited in the PDB with accession code 6AEQ.

3. Results and discussion

3.1. Purification of the C-terminal domain of DnaT (DnaTc)

The recombinant DnaTc (aa 84–179) from *Salmonella enterica* serovar Typhimurium LT2 was expressed in *E. coli*. Pure protein was obtained in the single chromatographic step. Approximately >20 mg of purified protein was obtained from 1 L of a culture of *E. coli* cells.

3.2. Structure of DnaTc monomer

DnaT can exist as a monomer, dimer, trimer, tetramer, or pentamer [13]. Both the N- and C-terminal regions of DnaT are crucial for oligomerization [23,30]. We attempted to crystallize DnaT, but we did not obtain suitable crystals for structure determination. Rather, we obtained crystals of DnaTc successfully. The crystal structure of DnaTc was solved at a resolution of 2.30 Å (Table 1). Two monomers of DnaTc were found per asymmetric unit (Fig. 1A). Differently, the 2.83 Å DnaT84–153 structure showed a five-molecule assembly with one bound ssDNA in one asymmetry unit (Fig. 1B). The overall structure of each one DnaTc consists of three α-helices (Fig. 1A), revealing a three-helix bundle structure with a C-terminal tail. α-Helices of DnaTc are at residues 101–108 (α1), 118–131 (α2), and 137–153 (α3). The secondary structure of DnaTc is similar to that of DnaT84–153 (Fig. 1C); however, residues involved in oligomerization are significantly different between these two structures (boxed; see below). The majority of the electron density for DnaTc was of good quality, but the C-terminal region (residues 163–179) in this structure was not observed, suggesting that this region is dynamic.

3.3. DnaTc forms a dimer predominantly

Our DnaTc structure showed two protein molecules tightly associated. To further substantiate the observation from the crystal structure, we performed chemical cross-linking of DnaTc using glutaraldehyde (Fig. 1D). DnaTc (4 μM) was incubated with

Table 1
Data collection and refinement statistics.

Data collection	
Crystal	DnaTc
Wavelength (Å)	0.975
Resolution (Å)	30–2.30
Space group	$C222_1$
Cell parameters	
a, b, c (Å)	54.91, 92.32, 69.00
α, β, γ (°)	90, 90, 90
Completeness (%) [a]	98.4 (91.8)
<I/σI>	30.14 (4.58)
R_{sym} or R_{merge} (%) [b]	0.058 (0.320)
Redundancy	5.6 (5.0)
Refinement	
Resolution (Å)	21.48–2.30
No. reflections	8273
R_{work}/R_{free}	0.220/0.265
No. atoms	
Protein	151
Water	16
Mean B-factors	54.31
R.m.s deviation	
Bond lengths (Å)	0.009
Bond angles (°)	1.213
Ramachandran Plot	
In preferred regions	146 (99.32%)
In allowed regions	0 (0%)
Outliers	1 (0.68%)
PDB entry	6AEQ

[a] Values in parentheses are for the highest resolution shell.
[b] $R_{sym} = \Sigma|I - 'I'|/\Sigma I$, where I is the observed intensity, 'I' is the statistically weighted average intensity of multiple observations of symmetry-related reflections.

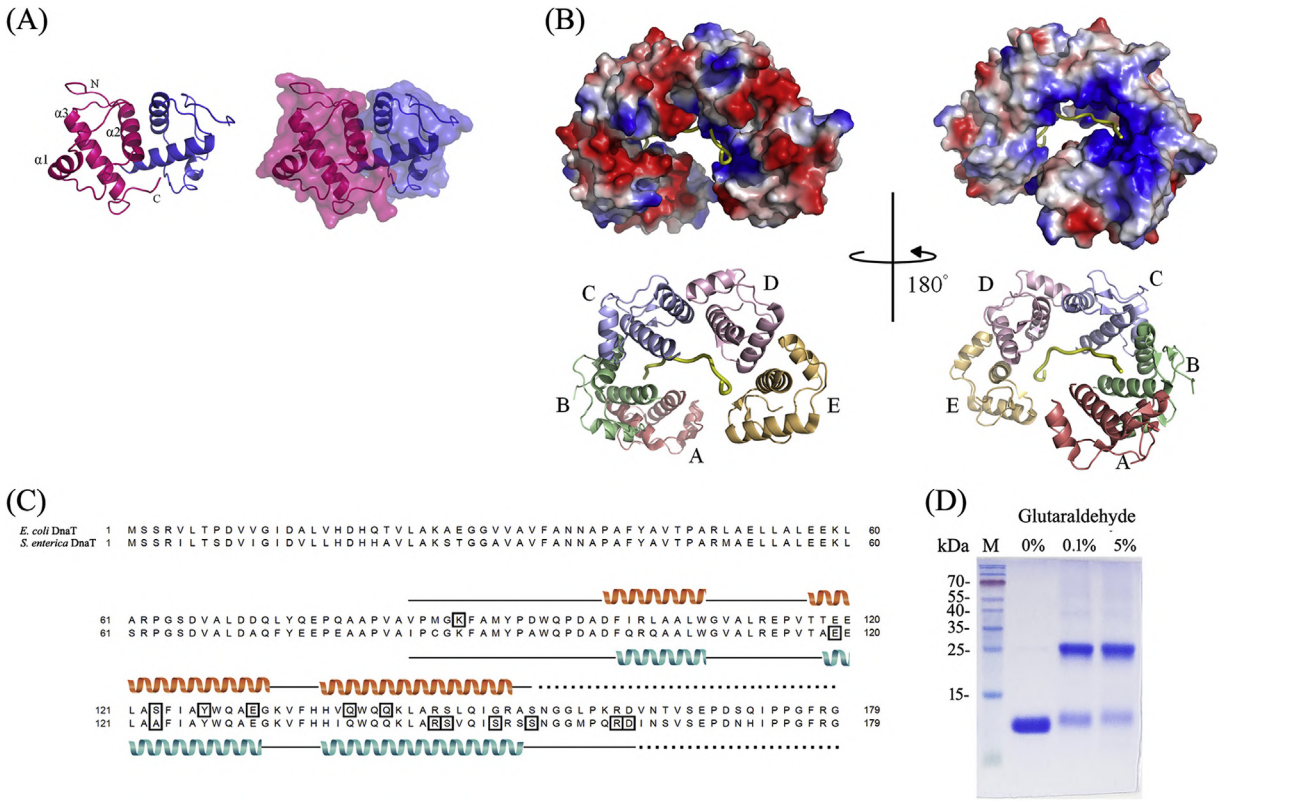

Fig. 1. Crystal structure of DnaTc. (A) Ribbon diagram of a DnaTc dimer. Each DnaTc monomer is color-coded. The overall structure of each one DnaTc monomer reveals a three-helix bundle structure with a C-terminal tail. (B) The crystal structure of DnaT84–153 in complex with ssDNA dT10. The structure of DnaT84–153 shows a five-molecule assembly with one bound ssDNA (gold). The positive charged residues (K133, K143, and R146) together contribute to generate a central cavity for ssDNA accommodation and interaction. The overall structure and electrostatic potential surface of the DnaT84–153 complex from different views are shown. (C) Structure-based sequence alignment of DnaT from *E. coli* and *S. enterica*. The labeled secondary structural elements derived from this and previous works are shown. The amino acids involved in monomer–monomer interface between these two DnaT structures are boxed. These two DnaT structures revealed that residues involved in DnaT oligomerization are significantly different. (D) Glutaraldehyde cross linking of DnaTc. DnaTc (4 μM) was incubated with increasing concentrations of glutaraldehyde (0.1% and 5%) at 4 °C for 20 min. Coomassie Blue-stained SDS-PAGE of the resulting samples and molecular mass standards are shown. At these concentrations, the dimeric form of DnaTc was observed. (For interpretation of the references to color in this figure legend, the reader is referred to the Web version of this article.)

increasing concentrations of glutaraldehyde (0.1% and 5%) at 4 °C for 20 min. At these concentrations, the dimeric form of DnaTc (24 kDa) was observed clearly. However, minor bands corresponding with the other aggregative forms were also found. Consequently, the glutaraldehyde cross-linking result showed that DnaTc mostly occurred as a dimer in solution, consistent with that analyzed using gel filtration chromatography [23] and the crystal structure (Fig. 1A).

3.4. Monomer–monomer interface of DnaTc

Although the complex crystal structure of DnaT84–153 shows five molecules (Fig. 1B) packed per asymmetric unit [23], DnaT84–153 exists as a dimer in solution [23]. The five DnaT84–153 molecules were mediated through dimeric interfaces between each two adjacent subunits. Structural superposition of subunits A–B, subunits B–C, subunits C–D, and subunits D–E with the DnaTc dimer indicated that DnaTc forms a different dimeric architecture from each dimer in the pentameric DnaT84–153 (Fig. 2A). The DnaTc dimer was not a part of the pentameric DnaT84–153 and did not belong to any dimer formed in the pentameric DnaT84–153.

DnaTc monomers are interconnected through many hydrophobic interactions. As shown in Fig. 2B, the monomer–monomer interface of DnaTc is stabilized by the hydrophobic core, namely, A123 (α2), Y127 (α2), A130 (α2), and I150 (α3) in subunit A, and A122 (α2), A123 (α2), I125 (α2), A126 (α2), Y127 (α2), A130 (α2), and I150 (α3) in subunit B. In addition, five hydrogen bonds (R146–E119, R146–D162, R146–R161, S151–A123, and S154–S147) at the monomer–monomer interface of DnaTc (Fig. 2C and Table 2) were found by using PISA (Protein Interfaces, Surfaces and Assemblies) analysis [39] (an automatic analytical tool for macromolecular assemblies in the crystalline state). The three contributing hydrogen bonds may render the R146 in DnaTc a key residue for dimerization.

3.5. Comparison of hydrogen bond formations in the monomer–monomer interface between the pentameric DnaT84–153 and dimeric DnaTc structures

In this study, we found that no similar monomer–monomer interface of DnaTc was present in the pentameric DnaT84–153 structure (Fig. 2A). The amino acid residues involved in forming hydrogen bonds at the monomer–monomer interface of DnaT84–153 and DnaTc are boxed in Fig. 1C; none of those is identical. Due to shorter length, DnaT84–153 does not have R161 and D162 to hydrogen bond to R146 as those in DnaTc (Tables 2 and 3). The side chain of R146 in DnaT84–153 protrudes outside to play a role for ssDNA binding rather for dimerization. Due to long distance, the hydrogen bonds R146–E119, S151–A123, and S154–S147 formed in DnaTc were not found in DnaT84–153. Taken together, all five possibly forming hydrogen bonds at the monomer–monomer

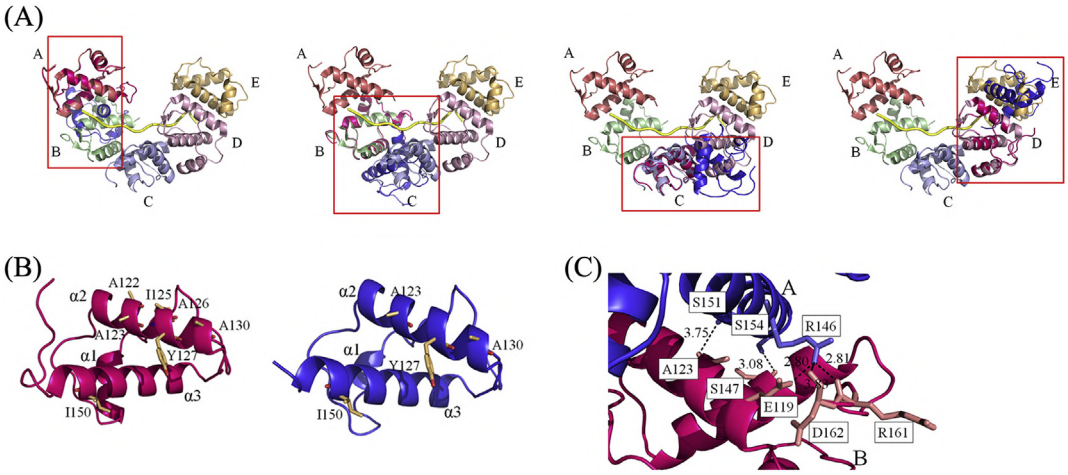

Fig. 2. Monomer–monomer interface of DnaTc. (A) Superposition of subunits A–B, subunits B – C, subunits C–D, and subunits D–E with the DnaTc dimer indicated that DnaTc forms a different dimeric architecture from each dimer in the pentameric DnaT84–153. (B) The hydrophobic core of DnaTc. The monomer–monomer interface of DnaTc is stabilized by A123 (α2), Y127 (α2), A130 (α2), and I150 (α3) in subunit A, and A122 (α2), A123 (α2), I125 (α2), A126 (α2), Y127 (α2), A130 (α2), and I150 (α3) in subunit B. (C) The hydrogen bond network. Five hydrogen bonds (R146–E119, R146–D162, R146–R161, S151–A123, and S154–S147) at the monomer–monomer interface of DnaTc were found by using PISA analysis. The distances (Å) of these hydrogen bonds are shown.

interface of DnaTc for being a dimer were not found in DnaT84–153.

3.6. Dual role of R146 in dimerization and ssDNA binding was proposed

K133, K143, and R146 in DnaT84–153 are important residues for ssDNA binding [23]. These positively charged residues together contribute to generate a central cavity for ssDNA accommodation and interaction. R146A mutant shows obviously impaired ssDNA binding ability [23]. DnaTc structural analysis further revealed another role of R146 in dimerization (Fig. 2C and Table 2). For binding to ssDNA as the DnaT84–153 complex, DnaTc should undergo a strong conformational change to expose K133, K143, and R146 to contact ssDNA (Fig. 3A). Superimposing analysis further indicated that if binding as the DnaT84–153 complex, R146 in the monomer B of DnaTc must be shifted by a distance of 8.1 Å and an angle of 72.6° (Fig. 3B). The monomer A of DnaTc must be shifted away by a distance of 7.5 Å and angles of 170° (*y*-axis) and 4.5° (*z*-axis) for forming a pentamer.

Table 2
The formation of hydrogen bonds at the monomer–monomer interface of DnaTc.

Hydrogen bonds		
Subunit A	Subunit B	Dist. [Å]
R146 [NH1]	E119 [OE1]	2.80
R146 [NH1]	D162 [O]	3.83
R146 [NH1]	R161 [O]	2.81
S151 [OG]	A123 [O]	3.75
S154 [OG]	S147 [O]	3.08

3.7. Structural insights into how DnaTc can bind ssDNA via the conformational change

The oligomerization and disassembly of the DnaT oligomer(s) are critical in primosome assembly [31]. Prior to this work, only the ssDNA-bound structure of the pentameric DnaT84–153 was

Table 3
The formation of hydrogen bonds at the monomer–monomer interface of DnaT84–153.

Hydrogen bonds					
Subunit A	Subunit B	Subunit C	Subunit D	Subunit E	Dist. [Å]
		E131 [OE2]	K88 [NZ]		3.14
		Y127 [O]	Q139 [NE2]		3.29
		E131 [OE1]	Q139 [NE2]		3.16
		S123 [O]	Q142 [NE2]		2.80
		S123 [OG]	Q142 [NE2]		3.13
	S123 [O]	Q142 [NE2]			2.83
	S123 [OG]	Q142 [NE2]			3.26
	Y127 [O]	Q139 [NE2]			3.17
	E131 [OE1]	Q139 [NE2]			3.03
			E131 [OE2]	K88 [NZ]	2.98
			Y127 [O]	Q139 [NE2]	2.99
			E131 [OE1]	Q139 [NE2]	2.85
			S123 [O]	Q142 [NE2]	2.73
			S123 [OG]	Q142 [NE2]	3.12
S123 [O]	Q142 [NE2]				2.86
S123 [OG]	Q142 [NE2]				3.43
Y127 [O]	Q139 [NE2]				3.11
E131 [OE1]	Q139 [NE2]				2.80

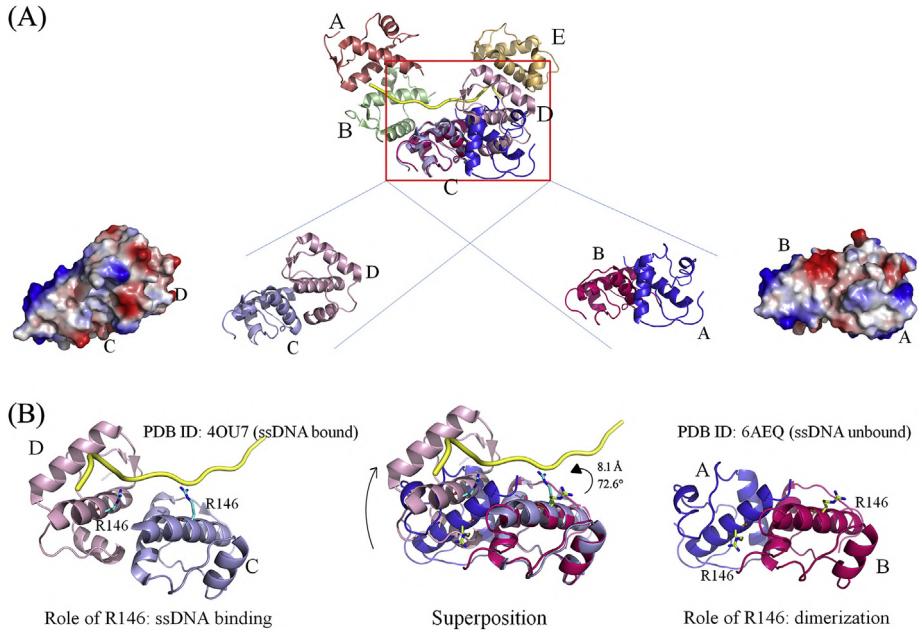

Fig. 3. Conformational changes suggested by the DnaTc structure. (A) The oligomerization mechanisms between these ssDNA-bound and ssDNA-unbound states of DnaT truncated variants are significantly distinct. Superimposing analysis indicated that the monomer A of DnaTc must be shifted away by a distance of 7.5 Å and angles of 170° (*y*-axis) and 4.5° (*z*-axis) for forming a pentamer. (B) Dual role of R146 in dimerization and ssDNA binding. R146 in DnaT84–153 are important residues for ssDNA binding. In this study, DnaTc structural analysis further revealed another role of R146 in dimerization. Superimposing analysis indicated that if binding as the DnaT84–153 complex, R146 in the monomer B of DnaTc must be shifted by a distance of 8.1 Å and an angle of 72.6°.

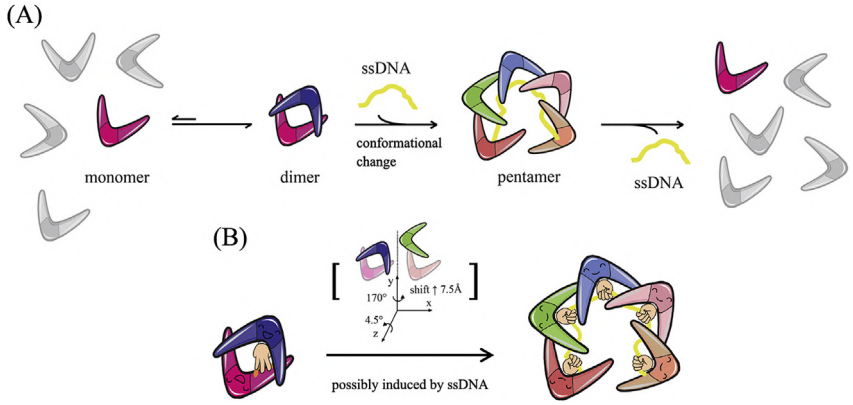

Fig. 4. A working model to explain how DnaTc oligomerizes. (A) The proposed boomerang mechanism. In this study, we identified DnaTc as a dimer both in the crystalline state and in solution. When ssDNA is present, strong conformational change in DnaTc (shown as boomerang) occurs. During ssDNA binding, the hydrogen bond network originally for dimerization of DnaTc will be rearranged to promote DnaTc oligomerization as a high-ordered oligomer, such as a pentamer. When ssDNA disassociates, the boomerang DnaTc may form the dimer back by rebuilding a hydrogen bond network at the interface. (B) The R146 mediation. Because of contributing three hydrogen bonds, R146 is a key residue for dimerization in DnaTc. However, the side chains of R146 in the pentameric DnaT84–153 protrude outside to play a role for ssDNA binding rather for dimerization. The conformational change in DnaTc may occur for binding to ssDNA via R146.

determined. In this study, we identified DnaTc as a dimer both in the crystalline state (Fig. 1) and in solution (Fig. 2). The oligomerization mechanisms between these ssDNA-bound and ssDNA-unbound states of DnaT truncated variants are significantly distinct (Tables 2 and 3). The different architecture present here may provide structural insights into how DnaT forms different oligomers. The conformational change suggested by our DnaTc structure (Fig. 3) might explain how DnaT can form the pentamer and bind ssDNA as a C-shaped helical assembly [23]. Basing from these results, we proposed a cartoon model to show how DnaTc monomers (boomerang) can oligomerize as a pentamer (Fig. 4), a process possibly induced by ssDNA binding. When ssDNA is present, strong conformational change occurs. R146, a crucial residue for ssDNA binding, is no longer at the monomer–monomer interface of DnaTc. During ssDNA binding, the hydrogen bond network originally for dimerization of DnaTc will be rearranged to promote DnaTc oligomerization as a high-ordered oligomer, such as a pentamer. When ssDNA disassociates, the boomerang DnaTc may form the dimer back by rebuilding a hydrogen bond network at the interface.

Disclosure statement

The author has no conflicts of interest.

Acknowledgments

We thank the experimental facility and the technical services

provided by the Synchrotron Radiation Protein Crystallography Facility of the National Core Facility Program for Biotechnology, Ministry of Science and Technology and the National Synchrotron Radiation Research Center, a national user facility supported by the Ministry of Science and Technology, Taiwan. This research was supported by a grant from the Ministry of Science and Technology, Taiwan (MOST 107-2320-B-040-014 to C.Y. Huang).

Transparency document

Transparency document related to this article can be found online at https://doi.org/10.1016/j.bbrc.2019.02.026.

References

[1] T.A. Windgassen, S.R. Wessel, B. Bhattacharyya, J.L. Keck, Mechanisms of bacterial DNA replication restart, Nucleic Acids Res. 46 (2018) 504–519.
[2] R.C. Heller, K.J. Marians, Replisome assembly and the direct restart of stalled replication forks, Nat. Rev. Mol. Cell Biol. 7 (2006) 932–943.
[3] P. McGlynn, R.G. Lloyd, Recombinational repair and restart of damaged replication forks, Nat. Rev. Mol. Cell Biol. 3 (2002) 859–870.
[4] H. Masai, T. Tanaka, D. Kohda, Stalled replication forks: making ends meet for recognition and stabilization, Bioessays 32 (2010) 687–697.
[5] M.M. Cox, M.F. Goodman, K.N. Kreuzer, D.J. Sherratt, S.J. Sandler, K.J. Marians, The importance of repairing stalled replication forks, Nature 404 (2000) 37–41.
[6] T. Tanaka, T. Mizukoshi, K. Sasaki, D. Kohda, H. Masai, *Escherichia coli* PriA protein, two modes of DNA binding and activation of ATP hydrolysis, J. Biol. Chem. 282 (2007) 19917–19927.
[7] K. Sasaki, T. Ose, N. Okamoto, K. Maenaka, T. Tanaka, H. Masai, M. Saito, T. Shirai, D. Kohda, Structural basis of the 3'-end recognition of a leading strand in stalled replication forks by PriA, EMBO J. 26 (2007) 2584–2593.
[8] T. Mizukoshi, T. Tanaka, K. Arai, D. Kohda, H. Masai, A critical role of the 3' terminus of nascent DNA chains in recognition of stalled replication forks, J. Biol. Chem. 278 (2003) 42234–42239.
[9] T. Tanaka, T. Mizukoshi, C. Taniyama, D. Kohda, K. Arai, H. Masai, DNA binding of PriA protein requires cooperation of the N-terminal D-loop/arrested-fork binding and C-terminal helicase domains, J. Biol. Chem. 277 (2002) 38062–38071.
[10] Y.H. Huang, C.Y. Huang, Structural insight into the DNA-binding mode of the primosomal proteins PriA, PriB, and DnaT, Biomed Res. Int. 2014 (2014) 195162.
[11] C.C. Huang, C.Y. Huang, DnaT is a PriC-binding protein, Biochem. Biophys. Res. Commun. 477 (2016) 988–992.
[12] H. Masai, M.W. Bond, K. Arai, Cloning of the *Escherichia coli* gene for primosomal protein i: the relationship to dnaT, essential for chromosomal DNA replication, Proc. Natl. Acad. Sci. U. S. A 83 (1986) 1256–1260.
[13] K. Arai, R. McMacken, S. Yasuda, A. Kornberg, Purification and properties of *Escherichia coli* protein i, a prepriming protein in phi X174 DNA replication, J. Biol. Chem. 256 (1981) 5281–5286.
[14] J. Liu, P. Nurse, K.J. Marians, The ordered assembly of the phiX174-type primosome. III. PriB facilitates complex formation between PriA and DnaT, J. Biol. Chem. 271 (1996) 15656–15661.
[15] J.D. McCool, C.C. Ford, S.J. Sandler, A *dnaT* mutant with phenotypes similar to those of a priA2::kan mutant in *Escherichia coli* K-12, Genetics 167 (2004) 569–578.
[16] Y.H. Huang, M.J. Lin, C.Y. Huang, DnaT is a single-stranded DNA binding protein, Genes Cells 18 (2013) 1007–1019.
[17] Y.H. Huang, C.Y. Huang, The N-terminal domain of DnaT, a primosomal DNA replication protein, is crucial for PriB binding and self-trimerization, Biochem. Biophys. Res. Commun. 442 (2013) 147–152.
[18] S. Fujiyama, Y. Abe, M. Shiroishi, Y. Ikeda, T. Ueda, Insight into the interaction between PriB and DnaT on bacterial DNA replication restart: significance of the residues on PriB dimer interface and highly acidic region on DnaT, Biochim. Biophys. Acta Protein Proteonomics 1867 (2019) 367–375.
[19] S. Fujiyama, Y. Abe, J. Tani, M. Urabe, K. Sato, T. Aramaki, T. Katayama, T. Ueda, Structure and mechanism of the primosome protein DnaT-functional structures for homotrimerization, dissociation of ssDNA from the PriB·ssDNA complex, and formation of the DnaT·ssDNA complex, FEBS J. 281 (2014) 5356–5370.
[20] Y.H. Huang, Y.H. Lo, W. Huang, C.Y. Huang, Crystal structure and DNA-binding mode of *Klebsiella pneumoniae* primosomal PriB protein, Genes Cells 17 (2012) 837–849.
[21] C.Y. Huang, C.H. Hsu, Y.J. Sun, H.N. Wu, C.D. Hsiao, Complexed crystal structure of replication restart primosome protein PriB reveals a novel single-stranded DNA-binding mode, Nucleic Acids Res. 34 (2006) 3878–3886.
[22] J.H. Liu, T.W. Chang, C.Y. Huang, S.U. Chen, H.N. Wu, M.C. Chang, C.D. Hsiao, Crystal structure of PriB, a primosomal DNA replication protein of *Escherichia coli*, J. Biol. Chem. 279 (2004) 50465–50471.
[23] Z. Liu, P. Chen, X. Wang, G. Cai, L. Niu, M. Teng, X. Li, Crystal structure of DnaT84-153-dT10 ssDNA complex reveals a novel single-stranded DNA binding mode, Nucleic Acids Res. 42 (2014) 9470–9483.
[24] D.S. Goodsell, A.J. Olson, Structural symmetry and protein function, Annu. Rev. Biophys. Biomol. Struct. 29 (2000) 105–153.
[25] S. Jones, J.M. Thornton, Principles of protein-protein interactions, Proc. Natl. Acad. Sci. U. S. A 93 (1996) 13–20.
[26] N. Unwin, A. Miyazawa, J. Li, Y. Fujiyoshi, Activation of the nicotinic acetylcholine receptor involves a switch in conformation of the alpha subunits, J. Mol. Biol. 319 (2002) 1165–1176.
[27] J.H. Cheng, C.C. Huang, Y.H. Huang, C.Y. Huang, Structural basis for pH-dependent oligomerization of dihydropyrimidinase from *Pseudomonas aeruginosa* PAO1, Bioinorgan. Chem. Appl. 2018 (2018) 9564391.
[28] C.T. Tzeng, Y.H. Huang, C.Y. Huang, Crystal structure of dihydropyrimidinase from *Pseudomonas aeruginosa* PAO1: insights into the molecular basis of formation of a dimer, Biochem. Biophys. Res. Commun. 478 (2016) 1449–1455.
[29] J.A. Marsh, H. Hernandez, Z. Hall, S.E. Ahnert, T. Perica, C.V. Robinson, S.A. Teichmann, Protein complexes are under evolutionary selection to assemble via ordered pathways, Cell 153 (2013) 461–470.
[30] M.R. Szymanski, M.J. Jezewska, W. Bujalowski, The *Escherichia coli* primosomal DnaT protein exists in solution as a monomer-trimer equilibrium system, Biochemistry 52 (2013) 1845–1857.
[31] J.Y. Ng, K.J. Marians, The ordered assembly of the phiX174-type primosome. II. Preservation of primosome composition from assembly through replication, J. Biol. Chem. 271 (1996) 15649–15655.
[32] Y.H. Huang, C.Y. Huang, The glycine-rich flexible region in SSB is crucial for PriA stimulation, RSC Adv. 8 (2018) 35280–35288.
[33] K.L. Chen, J.H. Cheng, C.Y. Lin, Y.H. Huang, C.Y. Huang, Characterization of single-stranded DNA-binding protein SsbB from *Staphylococcus aureus*: SsbB cannot stimulate PriA helicase, RSC Adv. 8 (2018) 28367–28375.
[34] Y.H. Huang, C.Y. Huang, SAAV2152 is a single-stranded DNA binding protein: the third SSB in *Staphylococcus aureus*, Oncotarget 9 (2018) 20239–20254.
[35] Z. Otwinowski, W. Minor, Processing of X-ray diffraction data collected in oscillation mode, Methods Enzymol. 276 (1997) 307–326.
[36] A.J. McCoy, R.W. Grosse-Kunstleve, P.D. Adams, M.D. Winn, L.C. Storoni, R.J. Read, Phaser crystallographic software, J. Appl. Crystallogr. 40 (2007) 658–674.
[37] J.J. Headd, N. Echols, P.V. Afonine, R.W. Grosse-Kunstleve, V.B. Chen, N.W. Moriarty, D.C. Richardson, J.S. Richardson, P.D. Adams, Use of knowledge-based restraints in phenix.refine to improve macromolecular refinement at low resolution, Acta Crystallogr. D Biol. Crystallogr. 68 (2012) 381–390.
[38] P. Emsley, K. Cowtan, Coot: model-building tools for molecular graphics, Acta Crystallogr. D Biol. Crystallogr. 60 (2004) 2126–2132.
[39] E. Krissinel, K. Henrick, Inference of macromolecular assemblies from crystalline state, J. Mol. Biol. 372 (2007) 774–797.